TRIBOLOGICAL EVALUATION OF TOTAL SHOULDER ARTHROPLASTY IMPLANTS: ADVANCED IN VITRO WEAR TESTING AND RETRIEVAL ANALYSIS

Israel Ramírez Martínez

A thesis submitted in partial fulfilment
of the requirements for the degree of
Doctor of Philosophy (PhD)

School of Engineering
Faculty of Science, Agriculture and Engineering (SAgE)
Newcastle University

Newcastle upon Tyne,
Tyne and Wear, United Kingdom

April 2021

Tribological evaluation of total shoulder arthroplasty implants.

The candidate confirms that the work submitted is his own and that appropriate credit has been given when reference has been made to the work of others. This research was carried out in the School of Engineering at Newcastle University in the United Kingdom, under the supervision of Prof. Tom J. Joyce and Dr. Simon L. Smith.

This page intentionally left blank

ACKNOWLEDGEMENTS

First and foremost, I would like to thank God Almighty for giving me the strength, knowledge, ability, and opportunity to undertake this research work and to persevere and complete it satisfactorily. Without His blessings, this achievement would not have been possible.

I would like to extend my sincere gratitude to my primary supervisor, Prof. Tom J. Joyce, for giving me the opportunity to do this Doctorate and more importantly for his friendship, trust, and support over the time we have known each other. I would also like to thank the insightful guidance of my co-supervisor, Dr. Simon L. Smith, for his constant source of support and guidance throughout my research.

I would like to acknowledge the financial support I have received, provided by The National Council of Science and Technology (CONACYT) of México and The Institute of Innovation and Technology Transfer (I2T2) of Nuevo León via the PhD scholarship to undertake this postgraduate study in the School of Engineering at Newcastle University.

I would also like to thank JRI Orthopaedics and Prof. Ian Trail (Wrightington Hospital) for supply the test specimens, and The Peter Jost Charitable Foundation for the economic support to attend and present part of this research work at International Society for Technology in Arthroplasty (ISTA) 31st and 32nd Annual Congress.

In the journey towards this degree, I had the opportunity to meet and work together with exceptional colleagues, Dr. Amin Dadgari, Dr. Kathryn Hughes, Dr. Rohan Bhalekar, and Dr. Shannen Soji whom I would also like to thank for their incredible friendship, insights, and constant support.

This thesis is dedicated to my beloved family, my parents Mrs. Griselda Martínez Moore & Mr. Gregorio Ramírez Tintos and my brother Abram Ramírez Martínez whom without their love, prayers, encouragement, strength, caring and sacrifices I could not have come this far.

Finally, my immense gratitude to my dearest wife, Kati Tikkanen, who is my eternal love and who has blessed my life with joy. ***Minä rakastan sinua!***

This page intentionally left blank

ABSTRACT

The glenohumeral joint is subject to dynamic and cyclic loading and motion during activities of daily life (ADLs), which can promote the wear of the articulating surfaces of shoulder joint replacements. The adverse reaction to the generated wear debris can influence the long-term survival of the implant and is considered an issue of contemporary concern.

Therefore, it is important to be able to measure the wear and surface characteristics of anatomical and reversed total shoulder replacements in order to understand the complex wear mechanisms that occurs *in vivo* and predict their performance. To date, there is no consensus in the literature regarding the methods to test the *in vitro* wear of shoulder replacements. Hence, the aim of this research was to develop a novel protocol based on the loading and motion of relevant ADLs. This protocol subjects the shoulder prosthesis to cyclic loading and intermittent motion in a multi-station shoulder wear simulator.

After five million cycles, the polymeric volumetric wear was 58.8 mm^3 for reverse shoulder components against metallic glenospheres. The three-dimensional surface roughness (S_a) values of the polyethylene humeral components fell from 692 ± 132 nm to 42 ± 29 nm. Comparison with an earlier wear tests revealed a non-statically significant difference in wear, suggesting that the addition of intermittent loading is unnecessary. This could help those wear testing shoulder implants in future. When an anatomic shoulder design consisting of a PyroCarbon humeral heads (ceramic-like alternative bearing material) and a polyethylene glenoid inserts were tested, the polyethylene wear was 90.6 mm^3. The surface roughness of the polyethylene components fell from 296 ± 28 nm to 32 ± 8 nm. Interestingly, PyroCarbon components did not exhibit a measurable loss in mass or change in the surface roughness.

Explant analysis can give key insights into how artificial joints have performed in the body. Therefore, and for the first time, the surface characteristics of retrieved metal–on–polyethylene reverse shoulder prostheses were assessed. From a heterogeneous cohort of thirteen explants with a mean time *in vivo* of 16 ± 11 months, results indicated

no correlation between the surface roughness and duration of implantation. However, tantalisingly among the metallic components available, low surface roughness values were found ($\rho = 0.032$) when the bearing material was inverted and used as a humeral component. If shown to be true in larger explant studies, this could suggest that such inverted materials could be associated with a superior tribological performance compared with a conventional arrangement.

Predominant surface damage modes observed on most of the *conventional* reverse total shoulder arthroplasty implants during the analysis of the surface topography were similar to those obtained from the *in vitro* wear test, and consistent with previous observations on retrieved components; the similitude between these results helped to validate the Newcastle Shoulder Wear Simulator.

The collection of results and findings obtained in this research at Newcastle University may help others who test artificial shoulder joints to validate the design of their simulators, improve mathematical wear model predictions, optimize the selection of bearing materials, and contribute to the ongoing efforts to produce the first international standard for *in vitro* wear testing of shoulder prostheses.

TABLE OF CONTENTS

LIST OF FIGURES

LIST OF TABLES

ABBREVIATIONS

AA.	*Abduction/adduction*
AAOS.	*American Academy of Orthopaedic Surgeons*
AC.	*Acromioclavicular joint*
ADL.	*Activities of daily living*
AISI.	*American Iron and Steel Institute*
AOA.	*Australian Orthopaedic Association*
ASTM.	*American Society for Testing and Materials*
aTSA.	*Anatomic total shoulder arthroplasty*
aTSR.	*Anatomic total shoulder replacement*
ATZ.	*Alumina-toughened zirconia*
CoCr.	*Cobalt-chromium alloy*
CoC.	*Ceramic–on–ceramic*
CoM.	*Ceramic–on–metal*
CoP.	*Ceramic–on–polyethylene*
CMM.	*Coordinate measuring machine*
CTPOD.	*Circularly translating pin-on-disk*
CVD.	*Chemical vapor deposition*
DoF.	*Degrees-of-freedom*
FDA.	*Food and Drug Administration*
FE.	*Flexion/extension*
GH.	*Glenohumeral joint*
HXLPE.	*Highly cross-linked polyethylene*
IE.	*Internal/external rotation*
L.	*Load*

MCP.	*Metacarpophalangeal joint*
Micro–CT.	*Micro-computed tomography*
MoM.	*Metal–on–metal*
MoP.	*Metal–on–polyethylene*
NAR.	*Norwegian Arthroplasty Register*
NJR.	*National Joint Registry for England, Wales, Northern Ireland and the Isle of Man*
NMHM.	*National Museum of Health and Medicine*
NZOA.	*New Zealand Orthopaedic Association*
PyC.	*PyroCarbon*
PyCoP.	*PyroCarbon–on–polyethylene*
rTSA.	*Reverse total shoulder arthroplasty*
rTSR.	*Reverse total shoulder replacement*
SC.	*Sternoclavicular joint*
SI.	*Superior-inferior translation*
SSAR.	*Swedish Shoulder Arthroplasty Registry*
ST.	*Scapulothoracic joint*
Ti-6Al-4V.	*Titanium-6Aluminum-4Vanadium alloy*
UHMWPE.	*Ultra-high molecular weight polyethylene*
UK.	*United Kingdom*
US.	*United States*
XLPE.	*Cross-linked polyethylene*
ZTA.	*Zirconia-toughened alumina*

NOMENCLATURE

2D	*Two-dimensional*
3D	*Three-dimensional*
BW	*Body weight*
E*	*Equivalent elastic modulus*
h_{min}	*Minimum film thickness*
NA	*Data not available*
R_a	*Two-dimensional average surface roughness*
R_x	*Equivalent radius*
S_a	*Three-dimensional average surface roughness*
SD	*Standard deviation*
S_q	*Root mean square height of the surface*
S_{sk}	*Surface skewness of height distribution*
λ	*Lambda ratio*

Chapter 1. INTRODUCTION

1.1 THESIS AIMS AND OBJECTIVES

This thesis is concerned with the engineering of shoulder joint replacement. The overall aim of this research was to develop a clinically relevant simulation method to investigate the wear performance of anatomic and reverse total shoulder joint replacements under adverse conditions. The research also aimed to measure the change of the surface topography of explanted reverse total shoulder replacements and to compare with the damage observed on *in vitro* wear-tested simulator components.

The aims of the research were achieved by completing the following objectives:

i. To develop a new realistic wear simulation protocol for testing shoulder joint replacements based on clinically relevant activities conducted by patients with shoulder joint replacements in daily life allowing a more physiologically representative test. To perform a five million cycles wear test on current commercially available reverse shoulder joint replacements using the newly developed protocol and compare the wear results with previous *in vitro* wear tests.

ii. To evaluate the *in vitro* wear behaviour of a novel PyroCarbon–on–polyethylene bearing materials combination in comparison with the traditional "metal–on–polyethylene" used in total shoulder replacements under the newly developed protocol.

iii. To assess and document the surface damage on *ex vivo* reverse total shoulder joint replacements and investigate any correlation with clinical data. To compare the articulating surfaces of these components with those tested in the shoulder simulator.

1.2 RESEARCH QUESTIONS

The research will contribute to the enhanced understanding of tribology of total shoulder arthroplasty by answering the following research questions. It should be appreciated that these questions have been raised as a result of notable gaps in the scientific literature:

i. How does the addition of an intermittent motion and cyclic loading during an *in vitro* wear test on reverse total shoulder replacements affect the wear behaviour of the bearing components?
ii. Can the use of a ceramic-like humeral head typically used in shoulder hemi-arthroplasty (against cortical bone), lead to reduced polyethylene wear in an anatomic total shoulder replacement?
iii. How does the articulating surface roughness of reverse total shoulder replacements change in the body?

1.3 THESIS ORGANIZATION

Chapter one provides an introduction to the research, including the main objectives developed to reach the aims of this study; as well as illustrating how this thesis is organised.

Chapter two contains a comprehensive literature review related to artificial shoulder joints, which establishes the relevant background for the following chapters. Chapter three describes the materials, methods, and instruments used in the experimental studies of shoulder joint replacements throughout the thesis. Chapter four gives the experimental results obtained from the *in vitro* and *ex vivo* studies.

In Chapter five the results are discussed, and limitations of these conducted tests are considered. Finally, the thesis is concluded in Chapter six with a summary of the major conclusions of this research and recommendations for potential areas for future work.

Chapter 2. LITERATURE REVIEW

2.1 TERMS OF ANATOMICAL REFERENCE

To describe the bones and joints and their motion relative to each other inside the human body it is necessary to introduce an anatomical reference system (axes and planes). There are three imaginary geometrical planes, which are defined from the orientation of the thorax (**Figure 2.1**); these are:

- *Sagittal plane:* is perpendicular to the coronal plane (Y–Z) and passes from the head to toes and front to back, dividing the body into left and right symmetrical halves.
- *Coronal plane:* also known as the frontal plane (Y–X), which is vertical to the thorax and passes from left to right and head to toes and bisects the body into anterior and posterior halves (front and back parts).
- *Transverse plane:* is perpendicular to both sagittal and coronal planes (X–Z) and it passes through the body and divides it into upper and lower halves (top and bottom parts).

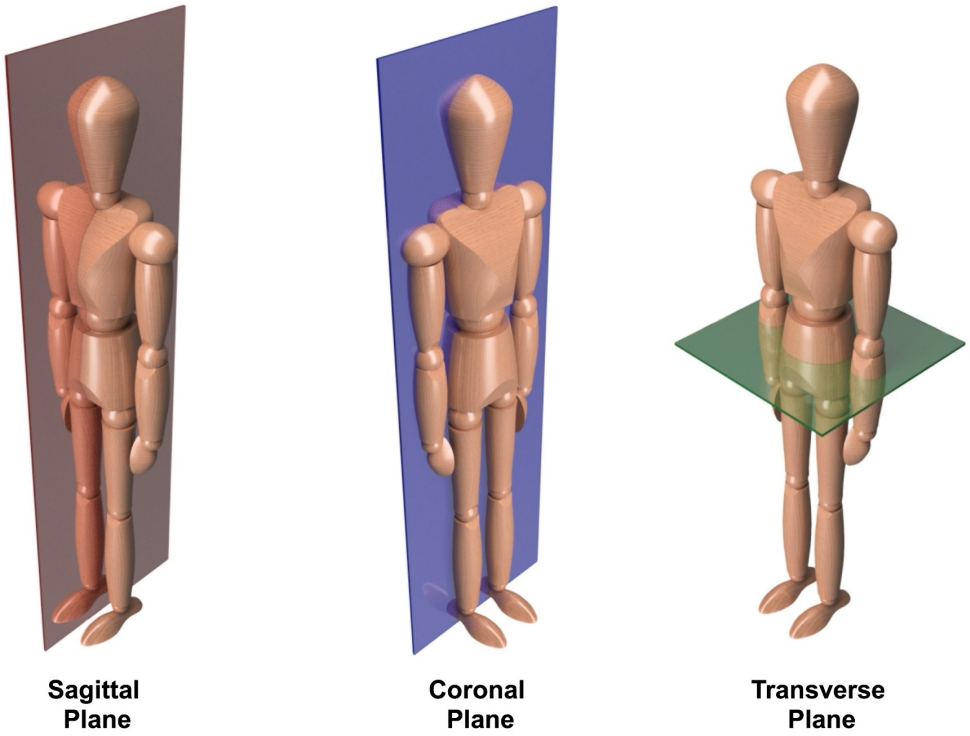

Figure 2.1 Three planes of motion of the human body

Similarly, there are three axes (perpendicular to the plane in which the motion occurs), which help to describe the position of each body segment during the motion (**Figure 2.2**):

- *Anterior/posterior:* this axis is the common line between the sagittal and transverse planes where anterior directed towards the front of the body and posterior towards the back.
- *Medial/lateral:* this axis is the common line between coronal and transverse planes where medial is defined as the direction towards the body and lateral way from it.
- *Superior/inferior:* this axis is the common line between coronal and sagittal planes where superior is directed upward and inferior in the opposite direction.

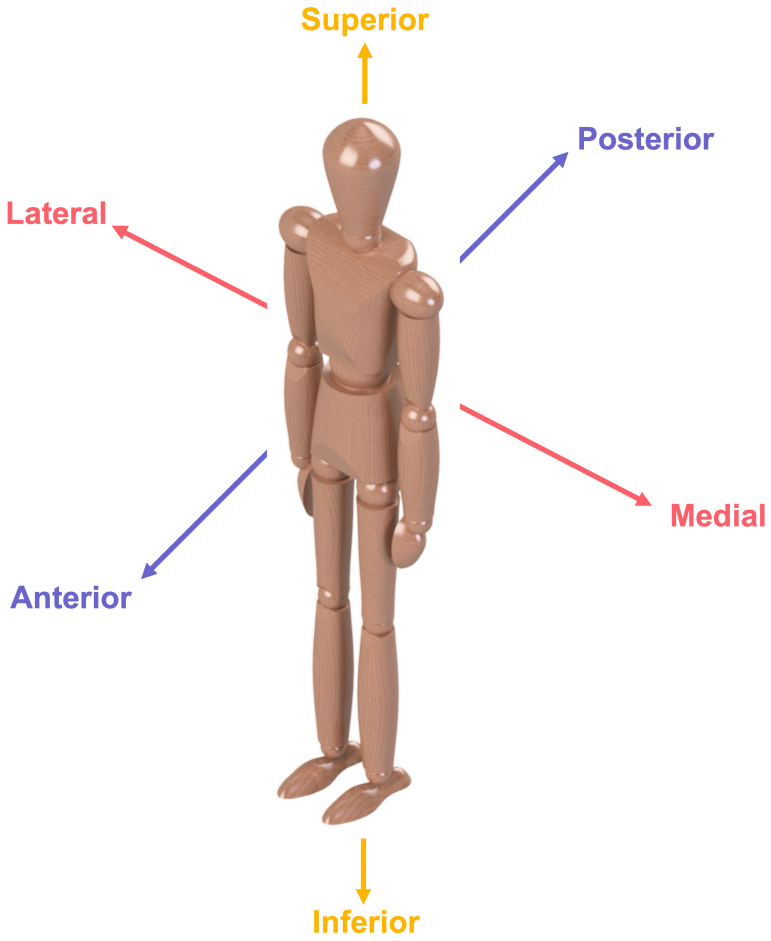

Figure 2.2 Anatomical directional terms

2.2 THE HUMAN SHOULDER JOINT COMPLEX

The human shoulder complex (Henry, 1918; Moore *et al.*, 2018; Drake *et al.*, 2019) comprises three main bones (the scapula, the clavicle, and the humerus) and four joints (the Glenohumeral (GH) joint, the Acromioclavicular (AC) joint, the Sternoclavicular (SC) joint, and the Scapulothoracic (ST) joint), which work collectively together to achieve shoulder movement and making possible a long list of activities of daily living.

2.2.1 Bony structures

The scapula (**Figure 2.3**) is a flat, large and triangular plate bone on the posterolateral aspect of the thoracic cage with three processes called the acromion, spine and coracoid process. It is commonly known as the shoulder blade and lies over the second to the seventh ribs. The scapula has two main surfaces: the costal (anterior, front facing) surface and the dorsal (posterior, rear facing) surface.

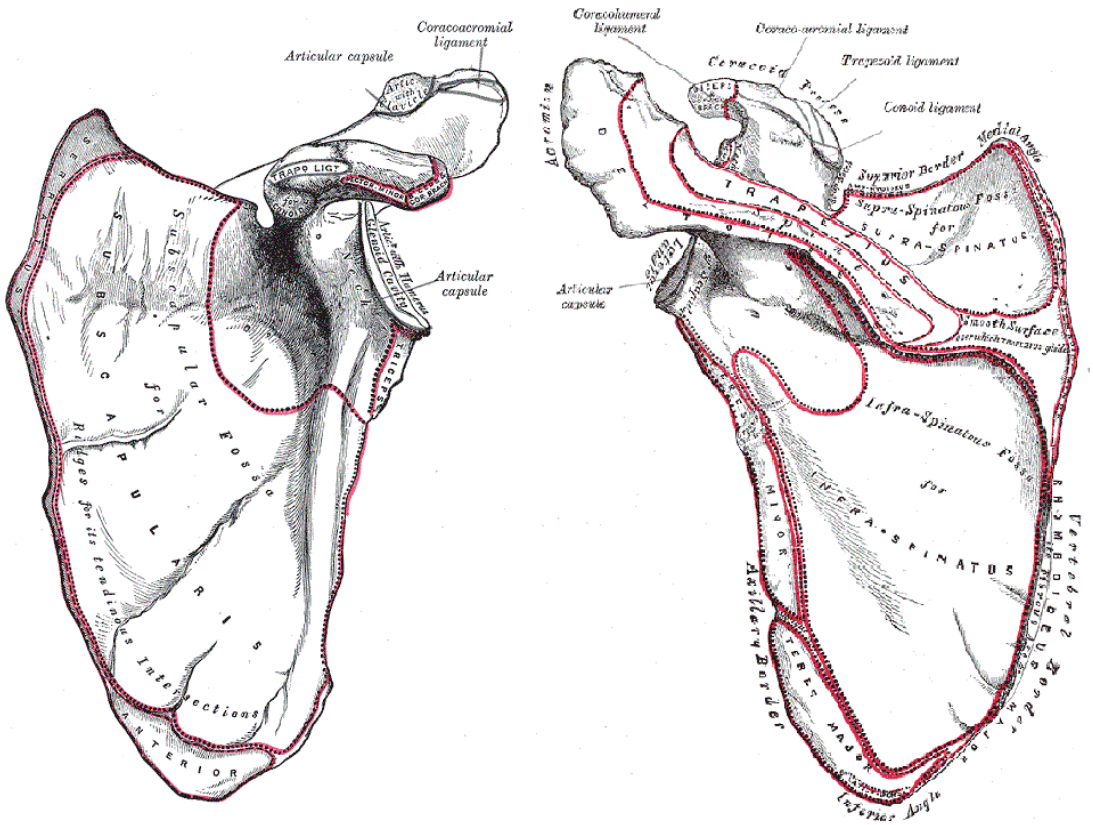

Figure 2.3 Left scapula. Costal surface (*left*) and dorsal surface (*right*). Reprinted from Henry (1918)

The glenoid *fossa* (**Figure 2.4**) is found on the lateral angle of the scapula as a shallow, pear-shaped depression (like an inverted comma) and receives approximately a third of the humeral head surface. The glenoid cavity radius of curvature may be flat or slightly concave articular surface, or it may have a socket-like appearance. The mean vertical dimension (height) of the glenoid is 35.5 mm (range, 30 to 43 mm), and the mean transverse dimension (width) is 27.8 mm (range, 24 to 33 mm) (Churchill *et al.*, 2001).

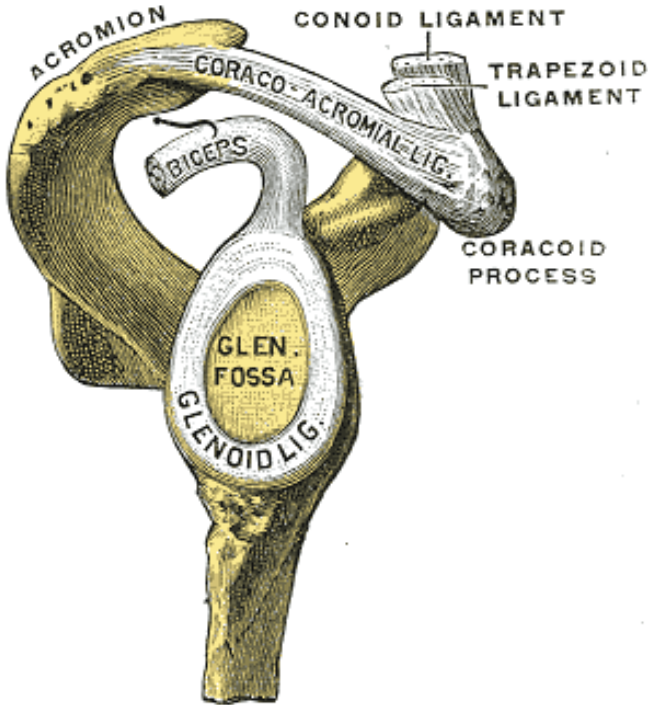

Figure 2.4 Glenoid *fossa* of right side. Reprinted from Henry (1918)

The clavicle is a large curved bone having an approximately "S" shape, and it is commonly known as the collarbone (**Figure 2.5**). It is the only bone that lies horizontally in the human body, and runs from the sternum to the acromion and supports the shoulder by transferring forces from the upper limb to the thorax. It is located at the anterosuperior part of the thorax and above the first rib. The clavicle is the most commonly fractured bone in the human body (Wange et al., 2015).

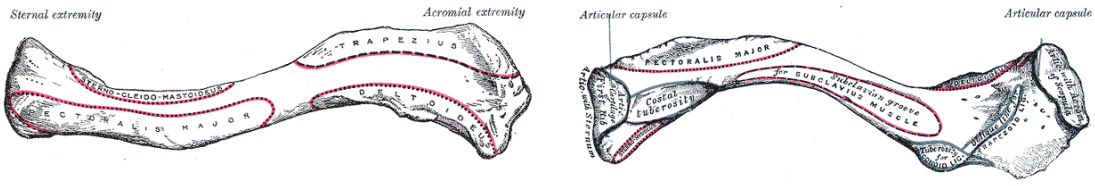

Figure 2.5 Clavicle (*left*) superior surface, (*right*) inferior surface. Reprinted from Henry (1918)

The humerus is the longest and largest bone in the upper limb. It begins proximally as a smooth rounded head and joins two processes (the greater and the lesser tubercle) through the neck of the humerus (**Figure 2.6**). The greater tuberosity and lesser tuberosity serve as the attachment location for the rotator cuff muscles. The almost hemispherical shape (partial ellipsoid) of the head of the humerus allows the humerus to move in a complete circle and rotate around its axis at the Glenohumeral joint. The mean vertical dimension (height) of the humeral head is 15.2 mm, with a mean diameter of 46.2 mm (Boileau and Walch, 1997).

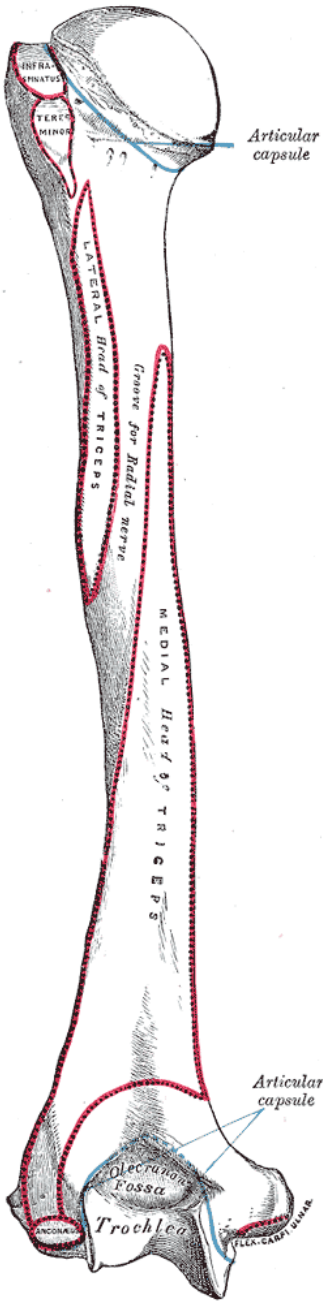

Figure 2.6 Left humerus. Posterior view. Reprinted from Henry (1918)

2.2.2 Articulations

The Glenohumeral joint is a non-confirming system with different radial mismatches (Zumstein *et al.*, 2014) formed by the articular surfaces of the glenoid cavity and the head of the humerus, allowing the arm to rotate inward and outward (internal/external rotation), move forward, backward (flexion/extension) and sideways (abduction/adduction). The significantly difference in size proportion between the articular surface of the glenoid *fossa* and that of the head of the humerus and the fact that almost no bony constraints restrict movement, make the GH joint the most mobile joint within the human body (Quillen *et al.*, 2004).

The Acromioclavicular joint is at the highest point of the shoulder blade, and is formed by the clavicle articulating with the acromion of the scapula and provides the ability to raise the arm above the head. The Sternoclavicular joint (**Figure 2.7**) is the only point of attachment between the upper limb and the axial skeleton. It is formed by the end of the clavicle and the face of the *manubrium* and allows free movement of the clavicle in three planes.

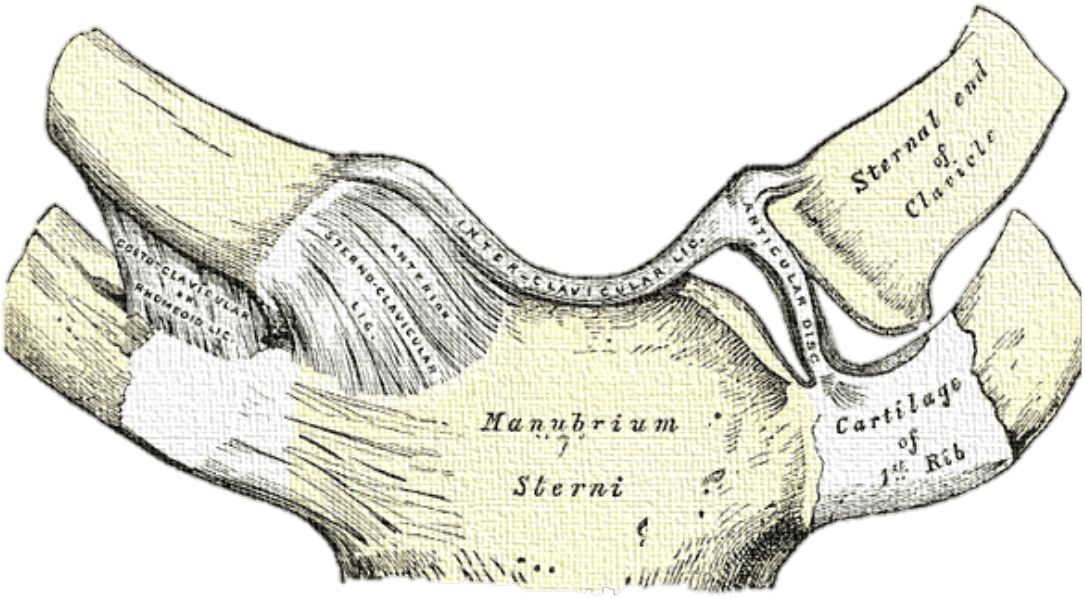

Figure 2.7 Sternoclavicular articulation. Reprinted from Henry (1918)

The Scapulothoracic joint is not a "true" anatomic joint and is commonly referred to as a "floating joint". It is an articulation formed by the surface of the back of the thoracic cage and the costal surface of the scapula, and its integrity depends on the AC and SC joints.

The natural shoulder joint commonly refers to the Glenohumeral joint, and is a type of synovial joint, also known as a ball-in-socket joint (spheroidal joint); the glenoid *fossa* constitutes the socket, while the upper head of the humerus is the ball. The shoulder complex is an assembly of muscles, tendons, ligaments, cartilages and bones; with a relationship of great mobility at the cost of stability (Matsen and Lippitt, 2003). Within the shoulder complex, the key joint is the glenohumeral joint (**Figure 2.8**).

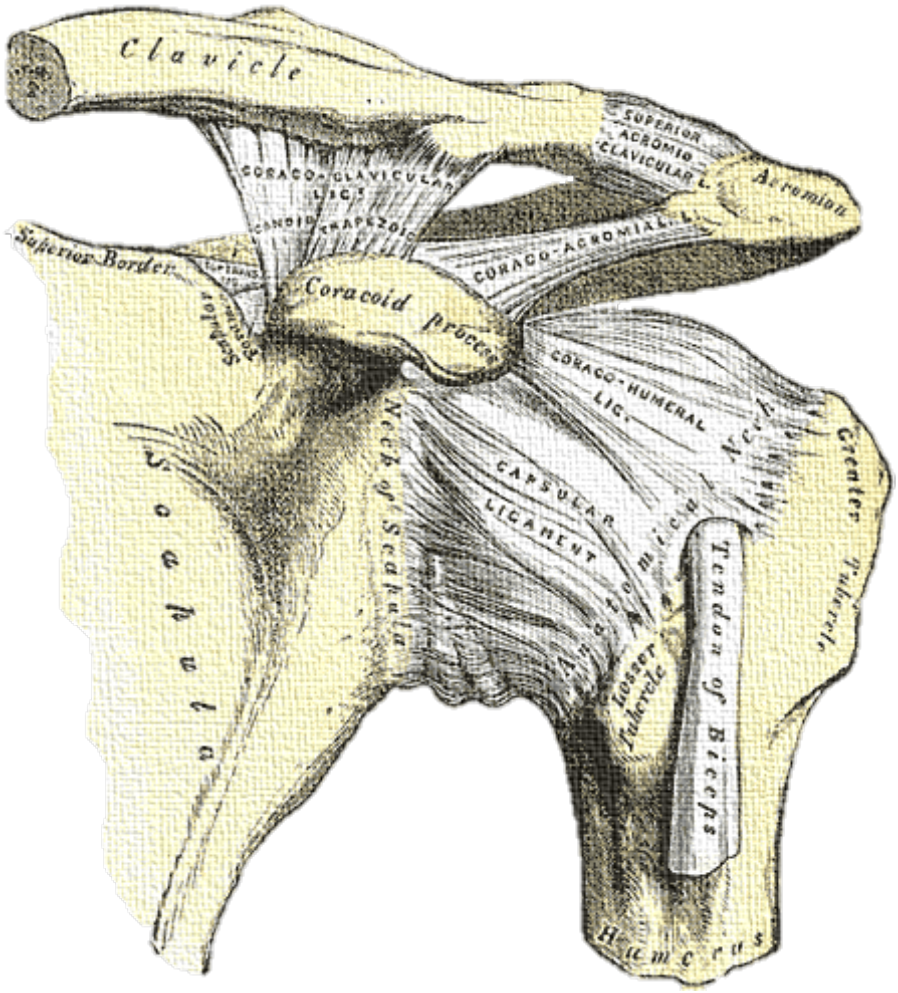

Figure 2.8 The glenohumeral joint is known a ball-on-socket joint: the glenoid *fossa* constitutes the socket, while the upper head of the humerus is the ball. Reprinted from Henry (1918)

2.2.3 Active musculature

The main muscles that produce the movement of the arm are the *deltoid*, *latissimus dorsi*, *pectoralis major* and *teres major* whilst the rotator cuff is the most crucial group of muscles for both the stabilisation and initiation of the shoulder movement. The *deltoid* (**Figure 2.9**) is the one of the primary drivers of humeral abduction, and has been shown to produce about one-half the moment required to produce glenohumeral abduction (Hess, 2000). In general, the *deltoid* muscle plays an important role in most of the upper arm movement and supports *supraspinatus* in resisting the downward drag of a loaded arm.

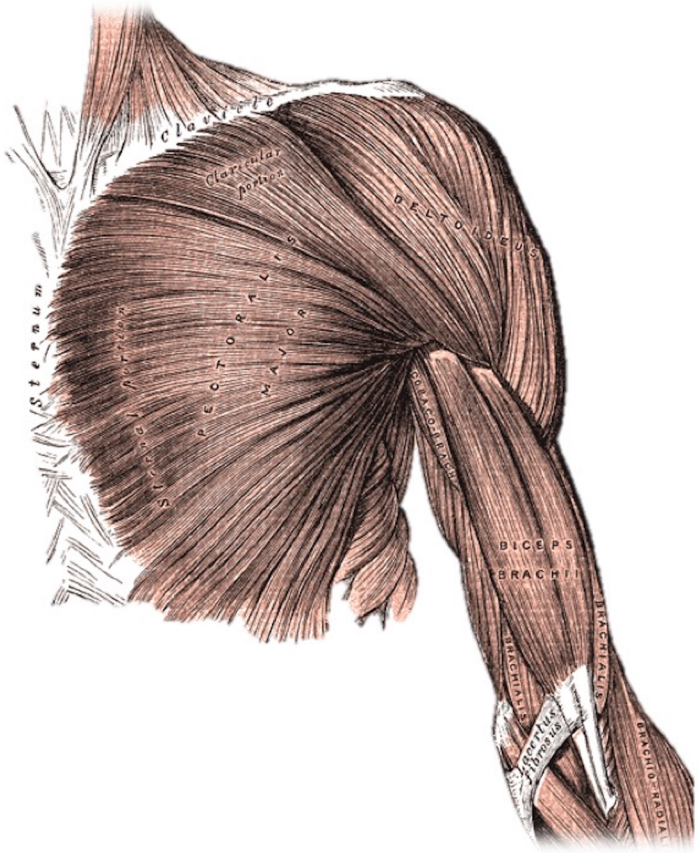

Figure 2.9 Superficial muscles of the chest and front of the arm showing the *deltoid* and *pectoralis major* muscles. Reprinted from Henry (1918)

The rotator cuff is composed of four scapulohumeral muscles: the *supraspinatus*, the *infraspinatus*, the *teres minor*, and the *subscapularis* (**Figure 2.10**). The rotator cuff surrounds the glenohumeral joint in all but the inferior aspect and provides stability to the joint during motion through the application of both adduction/abduction and internal/external rotation moments (Culham and Peat, 1993).

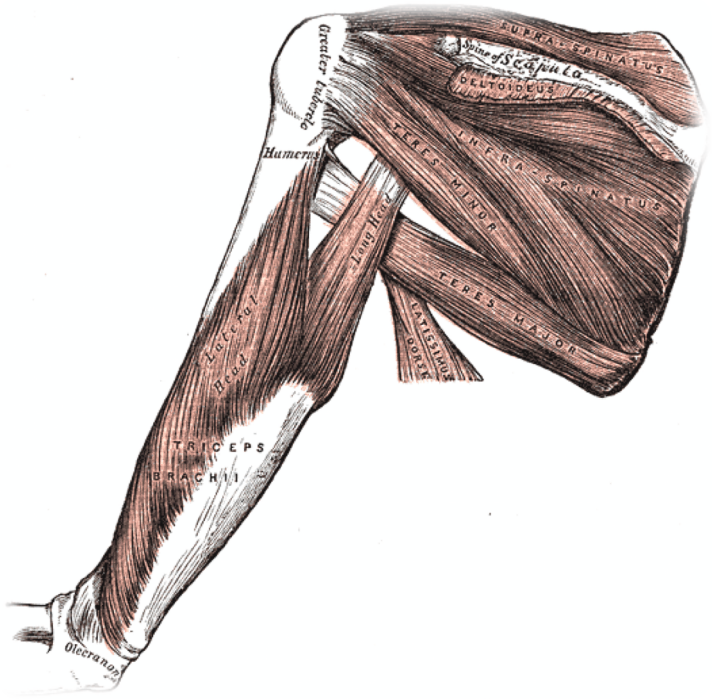

Figure 2.10 Muscles on the back of the scapula, showing the rotator cuff muscles. Reprinted from Henry (1918)

The *supraspinatus* compresses, abducts, and generates a small external rotation of the glenohumeral joint. The *infraspinatus* and *teres minor* muscles provide glenohumeral compression, external rotation, and abduction. These first three muscles act predominantly as external rotators of the shoulder and are fixed onto the greater tuberosity of the humerus. The *subscapularis* is fixed on the lesser tuberosity and acts to produce glenohumeral compression, internal rotation, and abduction (Bytyqi *et al.*, 2020).

2.2.4 Glenohumeral joint capsule

A "joint capsule" envelops and seals the shoulder from the glenoid *fossa* (or cavity) to the anatomical neck of the humerus (**Figure 2.11**). The surface area of the capsule is approximately twice that of the humeral head (OBrien *et al.*, 1998), and has a considerable amount of lax, thin tissue so that the shoulder is unrestricted as it moves through its large range of motion during daily activities (Warner *et al.*, 1992), but becomes adequately tensioned near the end limits of motion so as to passively restrict joint "hyper" mobility (Peat, 1986).

The joint capsule is mainly formed by three ligaments: the *superior*, the *middle*, and the *inferior* glenohumeral ligaments. In addition, and together with the muscles and ligaments the joint capsule helps to keep the shoulder joint stable and keep it from dislocation.

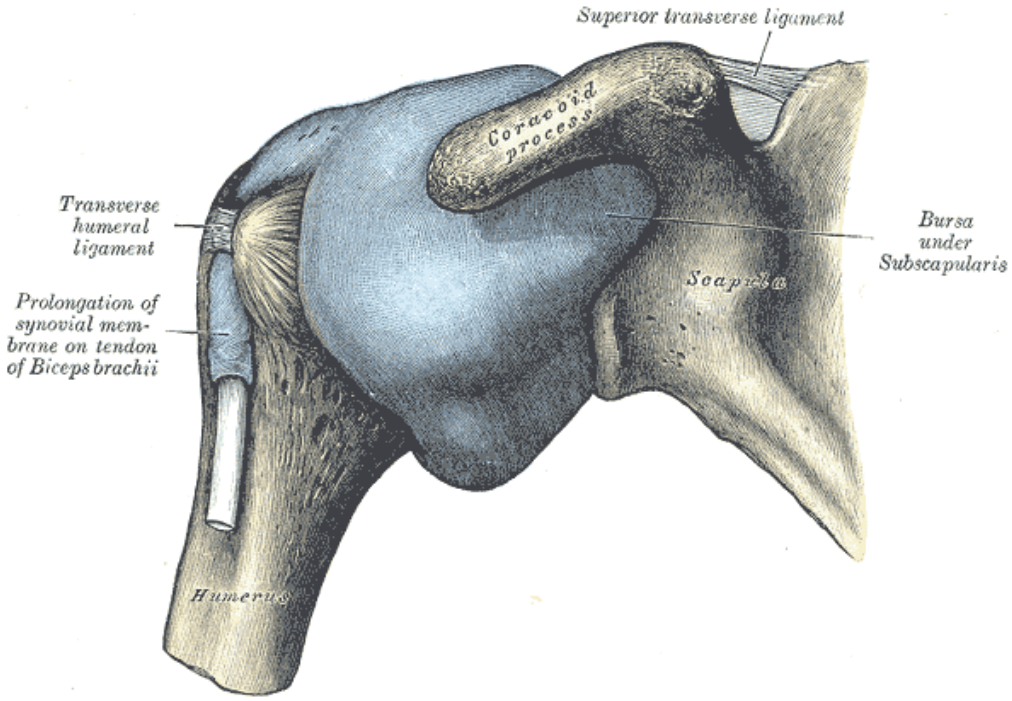

Figure 2.11 Capsule of shoulder joint (distended). Anterior aspect. Reprinted from Henry (1918)

2.2.5 Synovial fluid

A synovial membrane covers the inner surface of the articular capsule, which produces and secretes a viscous biological lubricant (synovial fluid). The principal role of human synovial fluid is reducing the friction, wear and tear between the articular surfaces of the shoulder joint during movement (Oates *et al.*, 2002; Tamer, 2013).

Synovial fluid contains a complex mixture of molecules, proteins, phospholipids, and cholesterol (Kitano *et al.*, 2001). Hyaluronic acid is the largest molecule in synovial fluid, and is thought to enhance viscosity but to have negligible boundary lubrication function (Cann, 2013). Healthy synovial fluid also contains soluble proteins, primarily albumin (56% of total protein content) and γ-globulin (Fang *et al.*, 2007).

As a non-Newtonian fluid, the viscosity of synovial fluid changes with shear rates. Viscosity for healthy synovial fluid at physiological shear rates ($>10^3$ s^{-1}) is typically in the range 0.01–0.10 Pa S. However, in diseased or periprosthetic joints, the effective viscosity (at physiological shear rates) can drop to less than 0.001 Pa S (Cooke *et al.*, 1978).

Human joints operate effectively under fluid-film and boundary lubrication regime conditions (Wright and Dowson, 1976). During daily life activities, such as walking, synovial joints may also function under mixed lubrication conditions, implying the coexistence of fluid and boundary lubrication conditions at the contact interface (Lewis and McCutchen, 1959; Schwarz and Hills, 1998; Neu *et al.*, 2008).

2.3 BIOMECHANICS OF THE SHOULDER JOINT

Activities of daily living (ADLs or ADL) is a term used to describe basic functions and typical routines that most people can perform on a day-to-day basis. The biomechanics of the shoulder joint relates to the forces and motion occurring in the shoulder joint as a result of these essential tasks.

2.3.1 Range of movement of the shoulder joint

The sophisticated architecture of a normal healthy shoulder joint allows three degrees-of-freedom (DoF) rotational motions in three planes of motion flexion/extension (FE) in the sagittal plane, abduction/adduction (AA) in the coronal plane, and internal/external (IE) rotation along the long axis of the arm (transverse plane) as can be seen in **Figure 2.12** and **Figure 2.13**.

The motion of moving the upper arm upwards to the front of the body is called flexion, the opposite of flexion is extension (moving the upper arm down to the rear). Abduction is the motion of moving the upper arm up to the side away from the body. Shoulder adduction is the opposite of shoulder abduction and consists of moving the upper arm down to the side towards the body. The movements that allow the shoulder to turn inward and outward are called internal and external rotations (touching the lower back with the back of the hand).

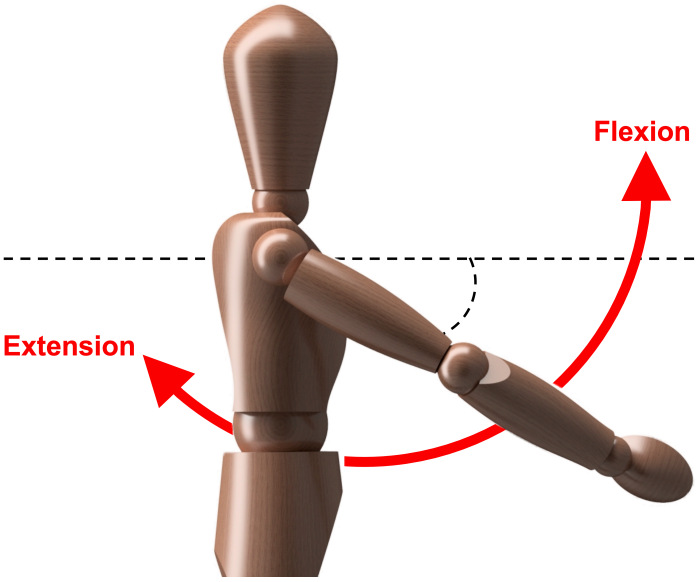

Figure 2.12 Shoulder flexion/extension (sagittal plane about the frontal axis)

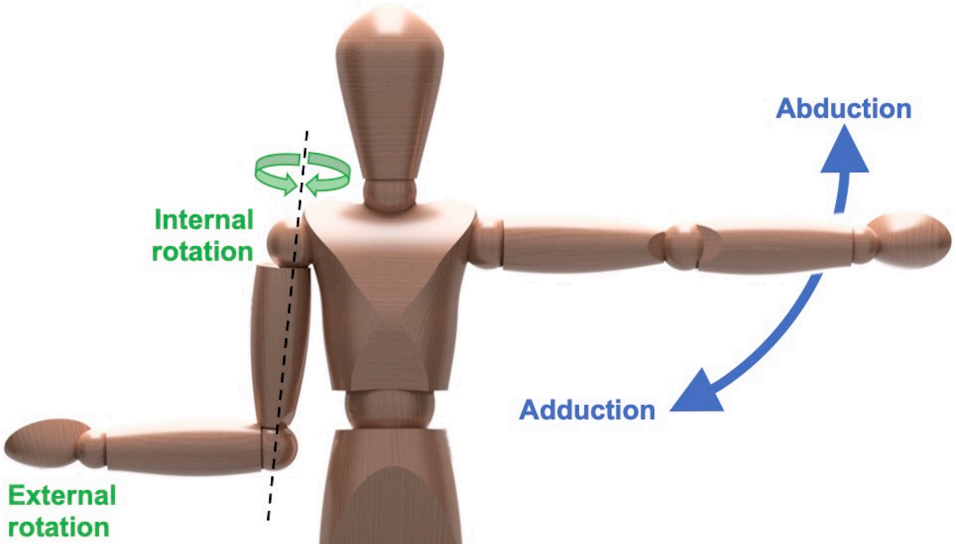

Figure 2.13 Shoulder abduction/adduction (sagittal plane about the frontal axis) and internal/external rotation (transverse plane about the vertical axis)

According to the American Academy of Orthopaedic Surgeons (AAOS), the average range of flexion in the shoulder joint is approximately 180 degrees of motion, while the range of shoulder extension is around 60 degrees. The average range of motion is approximately about 180 degrees of abduction and 75 degrees of adduction. Internal and external rotation are movements about a longitudinal axis through the humerus, with up to 70 degrees of internal rotation and approximately 90 degrees of external rotation (Subrata, 2014).

In addition to the previous mentioned DoF, another three DoF movements about the trunk occur as the scapula is connected to the trunk through the clavicle in a sliding joint: protraction/retraction (movement toward the spine), elevation/depression (movement upward and downward), and upward/downward rotation (**Figure 2.14**). These movements induce the translational movement of the GH joint, which in healthy shoulders is in the range of 1.5 to 2.0 mm (Graichen *et al.*, 2005; Matsuki *et al.*, 2012).

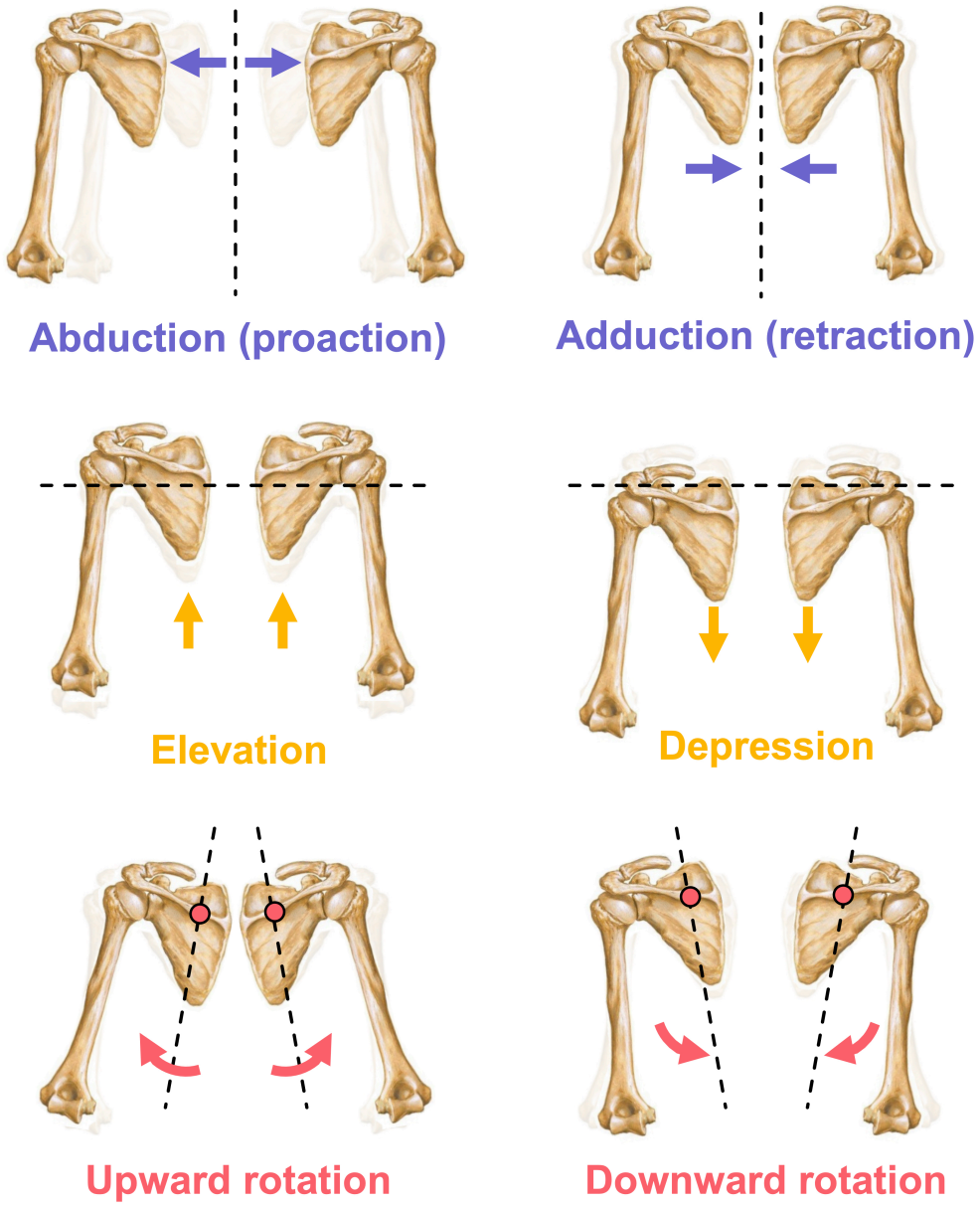

Figure 2.14 Shoulder scapula movements

2.3.2 Loading of the shoulder joint

In contrast with the lower limb (hip and knee), where the direction and magnitude of the load can generally be consistent, in the upper limb (arm, forearm, and hand) and specifically in the shoulder joint, the loads can vary widely; this is associated with a large number of degrees of freedom and the variety of tasks performed. The upper limb accounts for about 5.2% of the entire body weight, which is about 3.6 kg for a man with an average weight of 70 kg (McGeough, 2013a).

A series of indirect and direct measurement studies have been carried out to determine the forces that take place within the shoulder joint during certain tasks or activities of daily living. Using an elementary mechanical analysis to determine the force required to hold the arm in static equilibrium against its own weight (abduction) with only the *deltoid* and rotator cuff muscles taken into account, Inman *et al.* (1944) found that the reaction force was approximately 0.9 times body weight.

Based on this early work and using electromyographic and X-ray radiographic techniques and taking all the muscles active at each phase of the motion into account, Poppen and Walker (1978) determined the force that acts on the native shoulder joint as a result of abduction motion. They found that the resultant force generated across the shoulder joint system at 90 degrees of abduction (unloaded) reaches a maximum peak of 0.8 times body weight, which is consistent with the previous model calculation reported by Inman *et al.* (1944). With the introduction of three-dimensional shoulder computer models, van der Helm (1994) predicted a reaction force at the glenohumeral joint approximately 0.5 times body weight at 90 degrees of abduction.

Years later and combining previous mathematical models and motion capture systems, Anglin *et al.* (2000) determined the forces at the shoulder joint for five everyday functional tasks, including “standing up and sitting down into a chair using the arms”, “walking with a cane” and “lifting a prescribed weight” (5 kg box and 10 kg suitcase). The shoulder joint reaction forces generated were in the range of 1.3 to 2.4 times body weight (930 to 1,720 N) during “lifting a 10 kg suitcase” the activity of daily living with the highest force reported.

Until now, estimated loads acting in the glenohumeral joint were based on two or three-dimensional musculoskeletal models of everyday functional tasks. Measured data showed quite realistic predictions for isolated movements like abduction, however, even this simple motion leads to variations up to 30% (Inman *et al.*, 1944; Poppen and Walker, 1978). Factors contributing to such discrepancies can include: the large number of muscles involved and their unknown activation patterns, individual anatomical variations, and the change of muscle lever arms relative to the centre of the glenohumeral joint or muscles wrapping around bones (Westerhoff *et al.*, 2009).

Ten years later, Masjedi and Johnson (2010) modified a version of the three-dimensional Newcastle Shoulder Model developed by Charlton and Johnson (2006) and applied the recorded kinematic motion data from 12 'normal' subjects and 12 patients with reverse shoulder joint replacements during 12 activities associated with everyday tasks (feeding, personal hygiene and lifting everyday objects) to predict the resultant shoulder joint forces. The maximum and the least contact forces reported in this paper for normal subjects were 77% of body weight (572 N) for "lift shopping bag (2 kg)" and 29% body weight (215 N) for "reach to opposite axilla" respectively, with an average force of 296 N for all the tasks.

Nowadays, motion capture analysis is the most widely used non-invasive method to measure the glenohumeral contact forces and kinematics during primary joint function movement. The data is obtained using an optical motion camera system, which tracks the motion of external body markers mounted on the skin of healthy volunteers during a set of activities of daily life. The information collected is then used as an input for a musculoskeletal mathematical model system.

Using an optical motion tracking system and force plates, Klemt *et al.* (2018) analysed the glenohumeral contact forces during 26 functional activities of daily life in healthy volunteers with no history of shoulder pathology. They reported that the glenohumeral contact forces exceed 50% of body weight in 10 of 26 activities with a maximum contact force of 164% of body weight during the "sit to stand" task.

In summary, glenohumeral contact forces are achieved through compression of the humeral head into the glenoid concavity thought contraction of muscles surrounding the shoulder during activities of daily living. The forces acting on the glenohumeral

joint include: (1) weight of the arm, (2) abductor force by *deltoid* and *supraspinatus*, (3) downward pull of arm by *subscapularis*, *infraspinatus* and *teres minor*, and (4) the joint force (Lam *et al.*, 2007).

The joint force can be decomposed into 3 components: *compressive force, shear force, and resultant force*. As seen in **Figure 2.15**, the compressive force component is directed to the centre of the glenoid socket, while the shear forces components destabilise the joint by translating the humeral head toward the glenoid rim (Klemt *et al.*, 2018).

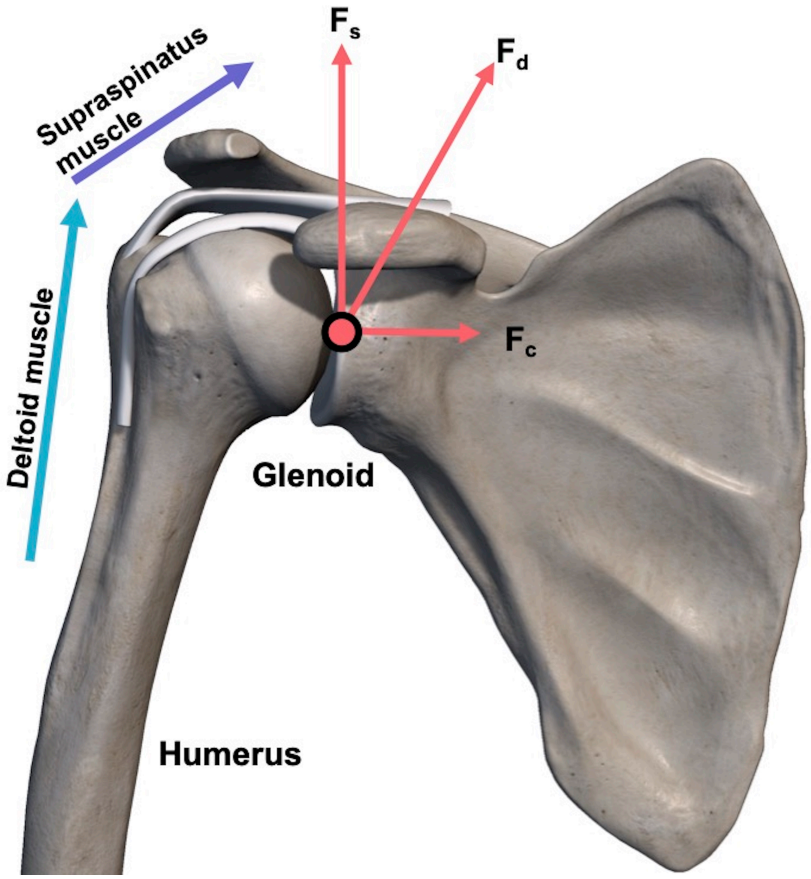

Figure 2.15 Components of glenohumeral joint contact forces. F_s: shear force or tangential force, F_d: resultant force, and F_c: compression force

The shoulder peak forces available in the literature range between 0.3 and 2.4 times body weight (**Table 2.1**). Nevertheless, the resultant forces and kinematics at the glenohumeral joint are just an insight into the real *in vivo* conditions.

Table 2.1 Loads at the shoulder joint predicted in a number of modelling studies

Study	Type of Measurement	Range of Force
Klemt *et al.* (2018)	Motion capture + Mathematical model	0.3 BW *Eat with hand* 1.64 BW *Sit to stand*
Masjedi and Johnson (2010)	Motion capture + Mathematical model	0.3 BW *Reach to opposite axilla* 0.8 BW *Lift shopping bag (2 kg)*
Charlton and Johnson (2006)	Motion capture + Mathematical model	0.4 BW *Reach to side and back of head* 0.8 BW *Lift block to shoulder height*
Anglin *et al.* (2000)	Motion capture + Mathematical model	1.3 BW *Sitting down into a chair* 2.4 BW *Lift 10 kg suitcase*
van der Helm (1994)	Mathematical model	0.5 BW *Abduction, no load*
Poppen and Walker (1978)	Electromyography + X-ray technique	0.8 BW *Abduction, no load* 1.4 BW *Abduction, 1 kg load*
Inman *et al.* (1944)	Electromyography technique	0.9 BW *Abduction, no load*

BW: body weight.

2.3.3 Joint forces after total shoulder arthroplasty

In vivo and cadaveric studies with instrumented shoulder implants have been carried out in order to estimate the resultant reaction forces generated after a shoulder joint replacement. Reliable knowledge about shoulder joint loads is essential to improve design and pre-clinical model predictions (*in vitro* and *in silico*) to determine whether the implant will survive the likely loading conditions in the human body (Favre *et al.*, 2009; Geraldes *et al.*, 2017; Klemt *et al.*, 2018).

In vivo joint forces have been measured mainly by the Bergmann group (Bergmann *et al.*, 2007; Westerhoff *et al.*, 2009; Bergmann *et al.*, 2011), where instrumented total shoulders were implanted in patients, and the loading was measured during activities of daily life. This modified anatomic shoulder implant (Bio-modular®, Biomet Inc., Germany) consisted of six semiconductor strain gauges and nine-channel telemetry,

which were arranged in the hollow short implant neck between the head and shaft in order to measure the forces and moments transferred inside the glenohumeral joint.

Bergmann *et al.* (2007) informed that the *in vivo* glenohumeral contact forces are lower than 100% body weight, while Westerhoff *et al.* (2009) showed that the glenohumeral joint can frequently be loaded with more than one's own body weight during most activities of daily living. Subsequently, Bergmann *et al.* (2011) determined the joint loads during forward flexion and abduction of the straight arm, reporting forces of up to 238% body weight and moments up to 1.74% body weight. Bergmann *et al.* (2007) concluded that the highest forces in the glenohumeral joint after a shoulder arthroplasty occur whenever high external loads act at long lever arms or when the active range of motion is reached.

The angles of contact forces (α_d) and the direction of maximum forces (α_p) remained quite constant during almost all the ADLs performed. Data were presented in the right-handed coordinate system for the right joint (+ X-axis points anteriorly, + Y-axis points cranially, + Z-axis points laterally in anatomical directions), as can be seen in **Figure 2.16**.

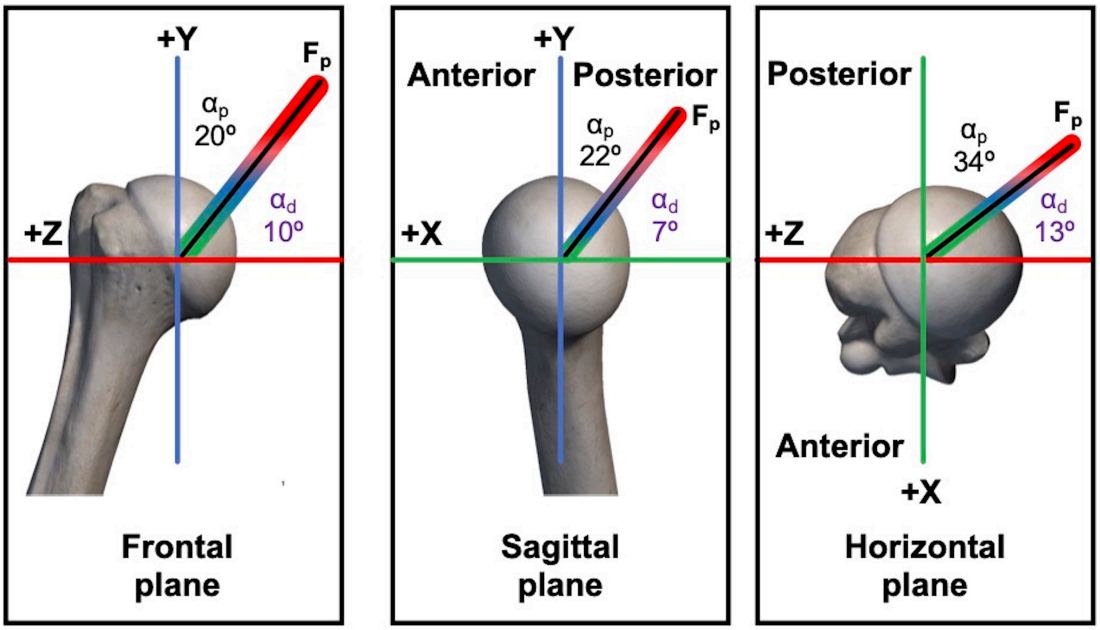

Figure 2.16 Force directions in three body planes (*right joint*). Black vector: peak force F_p. Colour ranges: magnitude-dependent ranges 20–40, <60, <80, <100% of F_p. α_p: direction of peak force F_p. α_d: angle variation of all forces >20% F_p. Adapted from Bergmann *et al.* (2007)

In the opposite scenario (reverse total shoulder replacements), Masjedi and Johnson (2010) used a motion capture system to record the position of ten markers attached on palpable bony landmarks to determine the *in vivo* glenohumeral forces in patients with Bayley-Walker implant. The internal glenohumeral forces reported during everyday activities were range between 67% up to 137% body weight.

The movements of the shoulder produce a resultant force vector, composed of both compressive and shear forces, that varies throughout the range of motion but that consistently passes through the joint's fixed centre of rotation, as can be seen in **Figure 2.17**.

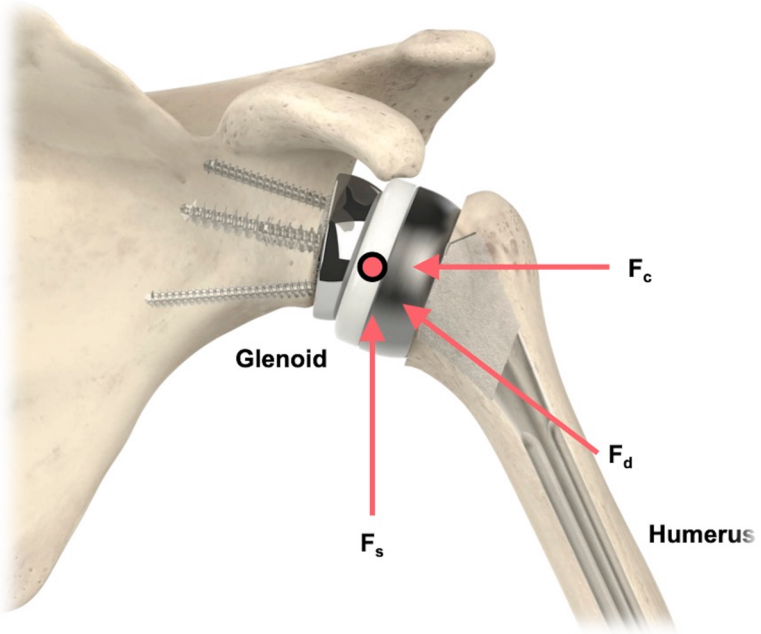

Figure 2.17 Components of glenohumeral joint contact forces. F_s: shear force or tangential force, F_d: resultant force, and F_c: compression force

Using a dynamic shoulder cadaver testing apparatus, which simulated 6 degrees-of-freedom in eight human cadavers before and after a Trabecular Metal reverse total shoulder implant (Zimmer Biomet, Warsaw, Indiana, U.S.) Ackland *et al.* (2011) determined that the joint's forces during abduction and flexion task decrease 41.5% BW and 42.4% BW respectively after a shoulder replacement was implanted. However, cadaveric studies may not accurately simulate *in vivo* conditions because muscle forces and joint forces are unknown (Bey *et al.*, 2010).

The inversion of the anatomic concavities and the inferior and medial shift of the joint centre of rotation in contemporary reverse shoulder designs, alters the relationship of each shoulder muscle to its normal physiologic function; which increases the moment lever arm resulting in a reduction of the shear forces and torques (Roche and Crosby, 2006; Ackland *et al.*, 2011). The shoulder forces reported in the literature range between 0.1 and 2.4 times body weight (**Table 2.2**).

Table 2.2 *In vivo* load data of shoulder joint using instrumented prostheses

Study	Type of implant	Range of Force
Bergmann *et al.* (2011)	Six patients with instrumented aTSR	0.7 BW *Forward flexion* 2.4 BW *Forward flexion (2 kg)*
Westerhoff *et al.* (2009)	Four patients with instrumented aTSR	0.1 BW *Holding weight (10 kg)* 1.3 BW *Board at head height (2 kg)*
Bergmann *et al.* (2007)	One patient with instrumented aTSR	1.0 BW *Most activities of daily living* 1.5 BW *Blocked steering wheel (both hands)*
Masjedi and Johnson (2010)	Twelve patients with instrumented rTSR	0.7 BW *Reach to opposite axilla* 1.4 BW *Lift a shopping bag (2 kg)*

BW: body weight.

2.3 HISTORY OF EARLY DESIGNS OF TOTAL SHOULDER REPLACEMENTS

Disease, trauma, or even overuse in the natural shoulder joint can result in severe pain and loss of function (decreased range of motion) for the patient, which can have a substantial impact on millions of people's lives. Shoulder replacement, also called shoulder arthroplasty, is a substantial surgical intervention that removes the damaged joint and replaces it with an artificial implant, typically compromised of metal and plastic components. The key aim of these prostheses is to replicate the movement function of a normal and healthy shoulder joint; allowing the patient to undertake once again normal daily activities, thus returning their quality of life.

2.3.1 Anatomic total shoulder arthroplasty (aTSA)

The history and development of shoulder replacement dates back to 1893, when the French surgeon Jules Émile Péan performed the first shoulder arthroplasty (**Figure 2.18**) in a 37-year old patient with tuberculous arthritis. Despite the satisfactory functional results (increase in strength and range of motion), the total implanted shoulder components which consisted of a platinum stem and rubber ball were removed after two years due to a new case of infection (Lugli, 1978).

Figure 2.18 Péan's first artificial shoulder joint, which consisted of a platinum stem, a rubber ball coated with paraffin, and two metal loops which attached the ball to the scapula and stem. Adapted from National Museum of Health and Medicine (NMHM)

In the early 1950s, the American orthopaedic surgeon Charles Sumner Neer II used a metallic prosthesis made of Vitallium alloy (65% cobalt- 30% chromium- 5% molybdenum) to treat 12 patients with complex fracture of the head of the humerus (Neer, 1955). This design concept of shoulder hemi-arthroplasty, called Neer I, reproduced the anatomy of the superior part of the humerus and consisted out of a single oversized humeral component and it was commonly known as "the monoblock shoulder implant".

Twenty-four years later in 1974, Charles S. Neer II introduced the first modern anatomic total shoulder replacement (aTSR) called Neer II, for the treatment of osteoarthritis (**Figure 2.19**), which consisted of a Vitallium humeral head component and a cemented polyethylene glenoid component (Neer, 1974).

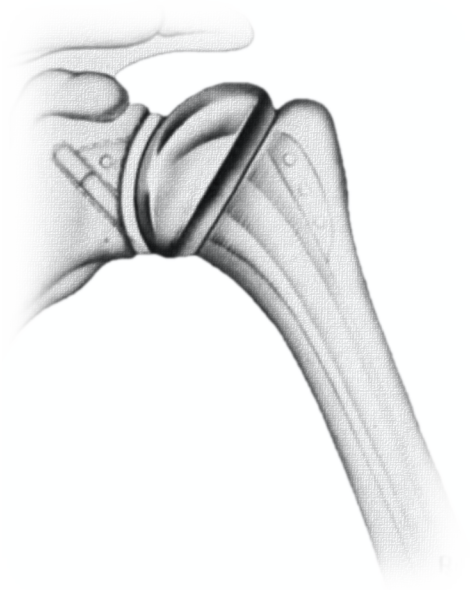

Figure 2.19 Anatomical total shoulder implant "Neer II". Adapted from Neer (1990)

Neer's aim for an anatomic total shoulder replacement was to retain as much of the normal shoulder anatomy as possible. The era of the "modular prostheses" or "interchangeable components" (in terms of variable head sizes to better match the damaged head) also started with the design concept of the Neer II, compared with the previous Neer I "monoblock" implant which had a stem and head as one unit.

Nowadays, modern anatomic total shoulder arthroplasty has emerged after these early designs of shoulder implant and has become an established treatment for advanced shoulder diseases such as severe primary osteoarthritis or secondary osteoarthritis caused by instability, osteonecrosis, inflammatory joint diseases and, in some cases complex proximal humeral fractures by relieving pain and improving functional deficit (Deshmukh *et al.*, 2005; Montoya *et al.*, 2013; Kiet *et al.*, 2015; Simovitch *et al.*, 2017), and thereby increasing the quality of life of thousands of patients.

In the latest annual report by the National Joint Registry (NJR) for England Wales Northern Ireland and the Isle of Man (2020) among 7,294 cases, 1,850 (25.4%) were

related to anatomic total shoulder arthroplasty. Osteoarthritis, which is the most common pathologic condition that leads to an anatomic total shoulder replacement, is a chronic condition that affects different joints. In the United States, osteoarthritis in the shoulder joint is estimated to affect up to 32.8% of the population above sixty years (Chillemi and Franceschini, 2013).

This occurs due to cartilage degeneration related to aging, hereditary components and heavy physical activity of the patient, which causes the bones to rub on each other and eventually become deformed. The shape changes of the humeral head and the glenoid cavity increase the friction coefficient resulting in a stiff joint and severe pain. This form of peripheral joint arthritis usually starts in people over the age of 45 years and is more common in women than in men; this may be due to the body changes that come with ageing (Versus Arthritis, 2018).

Anatomic total shoulder arthroplasty (aTSA) consists of removing the damaged joint surface of the humerus and replace it with an artificial humeral head (partial ellipsoid, ⅓ of sphere) typically made of cobalt-chromium alloy (CoCr) and attached to a metallic stem; which is fitted into the bone cavity of the humerus and can be cemented or non-cemented. On the counter side, the damaged surface of the glenoid *fossa* is also replaced with a glenoid insert component (ellipse or oval shape) typically made of ultra-high molecular weight polyethylene (UHMWPE) (**Figure 2.20**).

Figure 2.20 Total anatomic shoulder joint replacement. To the upper *right* is the UHMWPE glenoid insert with its titanium baseplate coated with hydroxyapatite. To the *left* is the humeral component, with the CoCr head atop a hydroxyapatite ceramic coated stem. Adapted from JRI VAIOS®

2.3.1.1 Glenohumeral mismatch in aTSA

In order to mimic the normal Glenohumeral joint biomechanics (rotations and translations), many aTSR implants designs incorporate a "radial mismatch", which is defined as the difference in curvature between the humeral head component and the glenoid (Walch *et al*., 2002).

Smaller radial mismatches limit the humeral head translation, make the joint more stable, but increase the stress to the glenoid component during shoulder motion. In contrast, larger radial mismatches allow greater humeral translation, but the point contact stress is higher, which can lead to earlier mechanical wear of the polymeric bearing material (Strauss *et al.*, 2009; Codsi, 2016; Hasler *et al.*, 2020). When the mismatch between the humeral head and the glenoid component becomes too high, there is a risk that the humeral head can translate to the edge of the implanted glenoid component producing an eccentric loading of the implant, a phenomenon described as the "rocking horse" by Franklin *et al.* (1988).

Radial mismatches similar to the normal anatomy of the glenohumeral joint, have been shown to perform better according to a retrieval study (Nho *et al*., 2008). Schoch *et al.* (2019), suggests an optimal radial mismatch range value between 4 mm to 8 mm for aTSR, in order to limit the contact stresses at the bone-cement interface and improve the implant longevity (Diop *et al.*, 2006; Sabesan *et al.*, 2015). Increased contact stresses may play a role in the development of glenoid lucencies (lesion of the bone), which have been shown to progress over time and may also promote glenoid loosening (Fox *et al.*, 2013; Gazielly *et al.*, 2015).

Current commercially available aTSR implant designs offer sizes ranging from 36 to 56 mm in diameter. The Global® (DePuy Synthes), Aequalis™ PerFORM™ (Tornier SAS–Wright Medical Inc.) and Comprehensive® (Zimmer Biomet) were the most commonly glenoid insert prostheses used in 2019 Australian Orthopaedic Association (AOA) (2020).

2.3.2 Reverse total shoulder arthroplasty (rTSA)

In 1985, a French orthopaedic surgeon Dr. Paul Grammont developed and implanted the first successful reverse total shoulder replacement (rTSR) in patients with arthritic shoulders and severe destruction of the rotator cuff (Grammont *et al.*, 1987). This revolutionary design, called Delta I (**Figure 2.21**), inverted the natural shoulder joint anatomy and consisted of: metallic convex glenoid component (glenosphere) initially ⅔ of sphere with a 42 mm diameter and a concave polyethylene humeral component (humeral insert).

Figure 2.21 Original Paul Grammont's reverse prosthesis design in 1985

In contrast with Neer's concept (anatomical design), the Delta I prosthesis moves the centre of rotation of the Glenohumeral joint closer to the body and downwards, which theoretically minimizes the shear forces across the components and provides a greater advantage for the muscles involved (Berliner *et al.*, 2015). Six years later, the second generation of Grammont's design (Delta III) medialized and stabilized the centre of rotation to the shoulder joint by changing the glenosphere from ⅔ of a sphere to ½ a sphere (Bytyqi *et al.*, 2020).

Since the first successful reverse shoulder joint replacement surgery was developed and implanted in 1985 and after being approved by the United States Food and Drug Administration (FDA) in 2004; the reverse total shoulder arthroplasty has become a standard treatment for complex shoulder conditions (Sirveaux *et al.*, 2004; Boileau *et al.*, 2006; Wall *et al.*, 2007; Drake *et al.*, 2010). Weakness, tear, tendonitis or laxity of

the rotator cuff muscles may negatively affect the ability of these muscles to stabilize the shoulder and must be treated. If the rotator cuff cannot be restored to a good level of function, such as in the cases of massive tissue tears or advanced age-related laxity, a rTSR may be considered (Labriola *et al.*, 2005; Guery *et al.*, 2006).

Among the 7,294 shoulder surgical interventions reported in the last annual report by the National Joint Registry (NJR) for England Wales Northern Ireland and the Isle of Man (2020) a total of 3,805 (52.2%) cases were related to reverse total shoulder arthroplasty. Cuff tear without arthroplasty was reported as one of the three most common leading reasons for reverse total shoulder arthroplasty at 82.5%, followed by cuff tear arthropathy (80.7%) and trauma sequelae (56.4%).

Reverse total shoulder arthroplasty (rTSA) typically consists of four main components (**Figure 2.22**): the shoulder baseplate, the glenosphere (rounded sphere), the humeral insert component (cup-shaped portion), and the humeral stem. The baseplate is generally fixed to the glenoid cavity with cortical screws, while the stem is inserted into the medullary channel of the humerus, either by cemented or non-cemented fixation.

Figure 2.22 Reverse total shoulder joint replacement. To the upper *right* is the CoCr glenosphere component with its titanium baseplate. To the *left* is the humeral component, with the UHMWPE humeral component atop a hydroxyapatite ceramic coated stem. Adapted from JRI VAIOS®

Nowadays, several other new designs have been developed with over 20 different options of rTSR available in the market (Middernacht *et al.*, 2016). The major differences between these and earlier versions are refined glenosphere components (in some cases with an inferior extension to prevent the risk of scapular impingement) and changes to the fixation method and humeral insert locations and size. Current commercially available rTSR implant designs offer sizes ranging from 36 to 44 mm in diameter.

In 2019, the most commonly used humeral insert prostheses were Delta Xtend™ (DePuy Synthes), SMR® (Lima Corporate) and Aequalis™ (Tornier SAS–Wright Medical Inc.) (Australian Orthopaedic Association (AOA), 2020). Although it was initially developed for rotator cuff arthropathy, the indications for rTSA have expanded to include proximal humerus fracture and revision of aTSA (Day *et al.*, 2015; Kiet *et al.*, 2015).

2.3.2.1 Biomechanical advantages of the reverse principle

Although modern designs may vary in detail, they are all based on the initial concept of Grammont's design (Grammont *et al.*, 1987):

i. The prosthesis should be stable, the weightbearing part must be convex, and the supported part must be concave.
ii. The centre of the sphere must be at or within the glenoid neck, and the centre of rotation should be fixed in a medial and inferior position.

The main biomechanical advantages of the reverse prosthesis according to Grammont's concept are as follows (Middernacht *et al.*, 2016; De Wilde, 2017):

i. The glenoid component which consists of a large hemisphere (glenosphere) offers a greater potential arc of motion without compromising stability compared to a previous small head.
ii. The small lateral offset (absence of neck) places the centre of rotation directly in contact with the glenoid surface and reduces the torque and shear force generated at the glenosphere-bone interface.

iii. Medializing the centre of rotation recruits more of the *deltoid* for elevation or abduction.

iv. Lowering the humerus increases tension on the *deltoid*.

The glenosphere offers a greater potential arc of movement of the humerus before impingement of the humeral component occurs. By medializing the centre of rotation and translating the humerus inferiorly, Grammont's rTSA tensions the *deltoid* and lengthens its functional lever arm. This gives the *deltoid* a significant biomechanical advantage to perform overhead activities in the absence of a functional rotator cuff. Hence, the reverse total shoulder replacement will rely on the *deltoid* muscle, instead of the deficient rotator cuff, to power and position the arm (Boileau *et al.*, 2005; Kiet *et al.*, 2015).

2.4 Incidence of shoulder arthroplasties in the United Kingdom

Since the first anatomic and reverse total shoulder replacements were performed, favourable outcomes have resulted in an increased use. According to the 17th Annual report by the National Joint Registry (NJR) for England Wales Northern Ireland and the Isle of Man (2020) shoulder joint arthroplasty is now the third most prevalent joint replacement with 45,784 procedures after knee replacements (1,300,897 procedures) and hip replacements (1,191,253 procedures) in the United Kingdom.

Between April 2012 and 31st of December 2019, a dramatic increase of almost 189% shoulder arthroplasties (from 2,527 to 7,294 procedures) has been taken place in the countries covered by the NJR. Registry data reveals that in 2019, shoulder joint arthroplasties were more commonly performed in females (females 76.8%; men 23.2%), with a median age of 74 years at primary operation.

Reverse total shoulder arthroplasty has been reported as the most frequently performed procedure carried out in 52.2% (3,805 procedures); followed by anatomical total shoulder arthroplasty with 25.4% (1,850 procedures). These clinical procedures were largely due the treatment of osteoarthritis (46.9%) and cuff tear arthropathy

(80.7%). As can be seen from **Figure 2.23**, the number of anatomical total shoulder replacements in the National Join Registry (NJR) has demonstrated a small decrease by 1% in the last year passing from 1,870 procedures to 1,850 procedures, while the number of reverse total shoulder replacements has continued steadily increasing since 2012.

Originally rTSR was only indicated for patients with rotator cuff arthropathy, however, more recently indications for rTSR have expanded to include severe glenohumeral osteoarthritis, revision arthroplasty, irreparable rotator cuff tears, rheumatoid arthritis, tumours, proximal humerus fractures, and fracture sequelae (Rittmeister and Kerschbaumer, 2001; Wall *et al.*, 2007; Gerber *et al.*, 2009; Nam *et al.*, 2010a; Brorson *et al.*, 2013), which has helped to promote its growing popularity and its increased used in the last years.

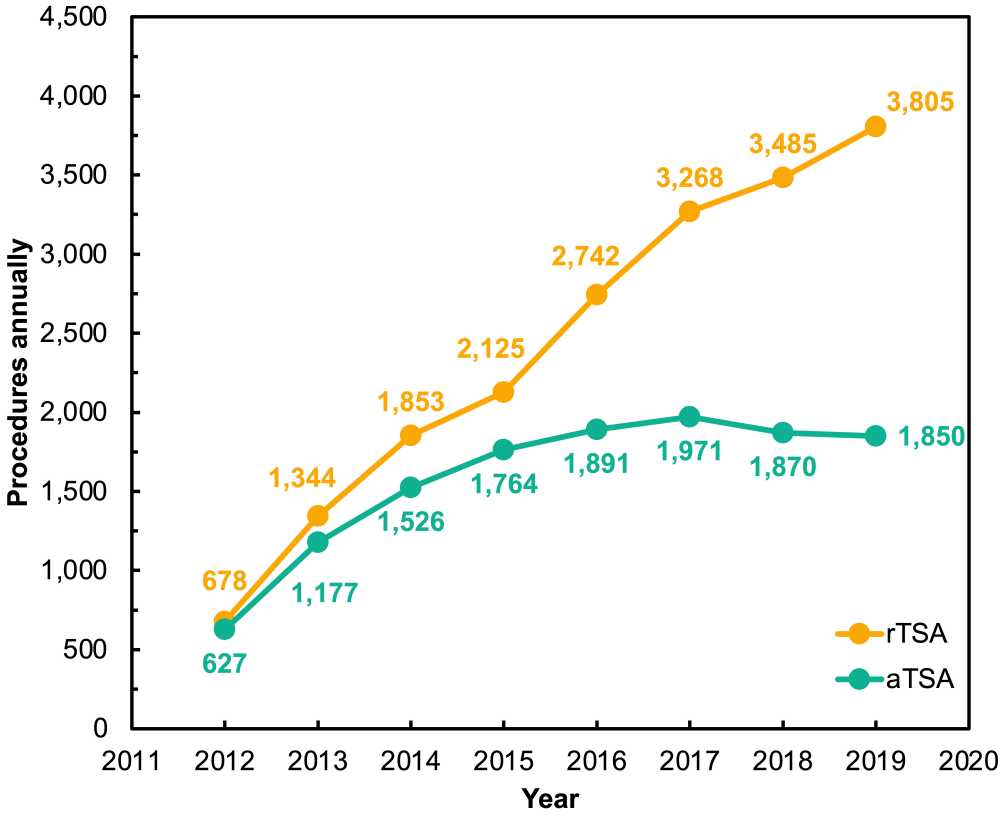

Figure 2.23 Current trend in total shoulder arthroplasties. Reverse total shoulder arthroplasty (rTSA) and anatomic total shoulder arthroplasty (aTSA). Retrieved from NJR annual reports (2013–2020)

2.4.1 Other National joint registries

As can be seen in **Figure 2.24** and **Figure 2.25**, over the last decade, the number of shoulder replacements implanted has also increased worldwide. European national registries data reported that in Norway the frequency of shoulder arthroplasties increased by about 68% between 2012 (500 procedures) and 2019 (842 procedures) (The Norwegian Arthroplasty Register (NAR), 2020), while in Sweden almost doubled in the period from 2012 (1,322 procedures) to 2019 (2,233 procedures) (The Swedish Shoulder Arthroplasty Registry (SSAR), 2020). According to the Australian Orthopaedic Association (AOA) (2020), the annual rate of shoulder arthroplasties has increased by almost 229% between 2012 (18,164 procedures) and 2019 (59,787 procedures), while in New Zealand shoulder replacement usage increased by 114% between 2012 (4,782 procedures) and 2018 (10,234 procedures) (New Zealand Orthopaedic Association (NZOA), 2019).

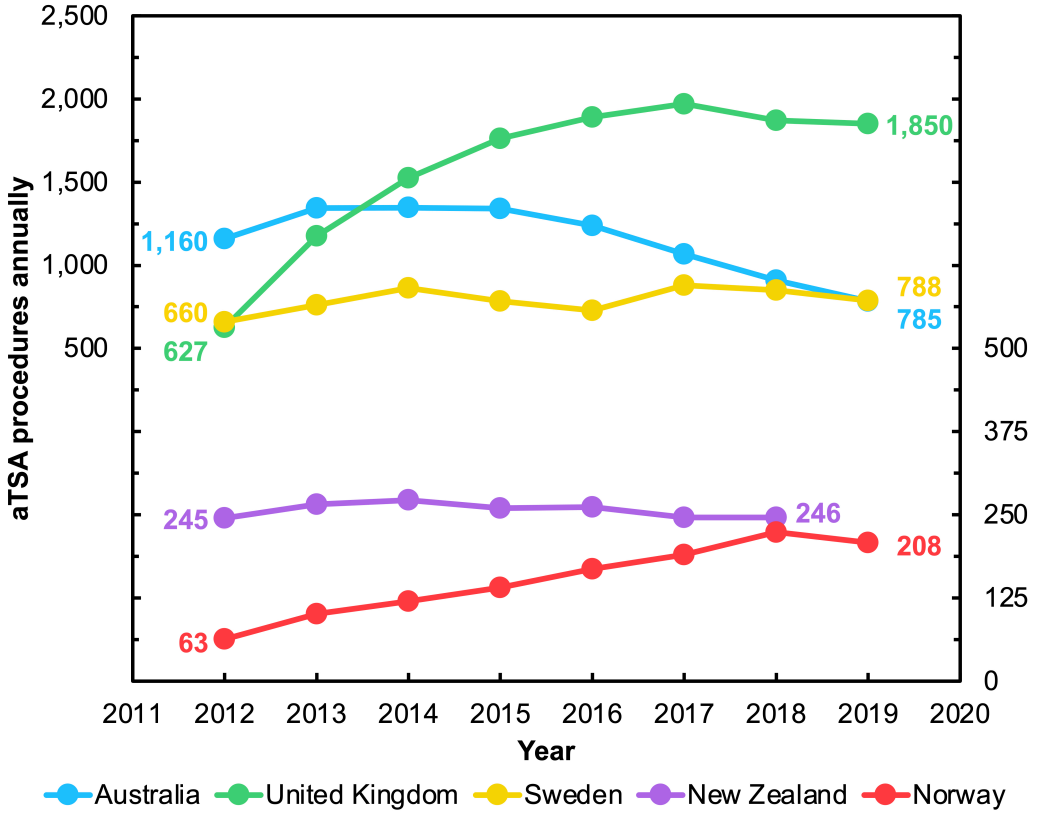

Figure 2.24 Annual incidence of anatomic total shoulder arthroplasties. Retrieved from AOA, NAR, NJR, NZOA, SSAR annual reports (2013–2020)

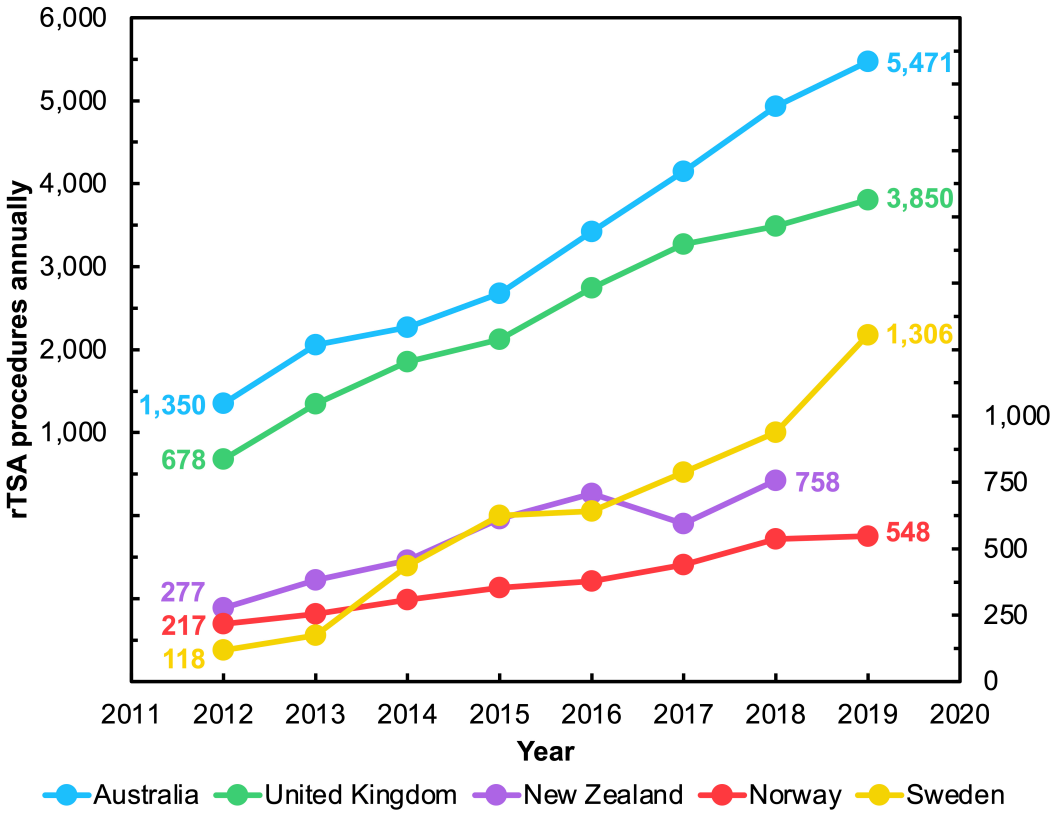

Figure 2.25 Annual incidence of reverse total shoulder arthroplasties. Retrieved from AOA, NAR, NJR, NZOA, SSAR annual reports (2013–2020)

In the United States, shoulder arthroplasty is being performed with increasing frequency, a recent analysis by Sivasundaram *et al.* (2016) suggested that more than 100,000 shoulder arthroplasties are performed yearly. This worldwide trend is expected to continue in the next years due to the life expectancy, the aging population, the increasing prevalence of osteoarthritis, and the popularity of sports with high injury risks.

According to the United Nations Department of Economic and Social Affairs, in the mid-2019 world's population reached 7.7 billion and is expected to reach 9.7 billion in 2050, this represents a 26% increase in only 30 years term (United Nations, 2019b). It is also projected that in 2050, 1 of 6 people in the global population will be over the age of 65 (United Nations, 2019a).

2.4.2 The financial cost for total shoulder replacements

The global market for joint replacement implants (hips, knees, shoulders, elbows, ankles, and small joints) was valued at nearly $19.1 billion in 2018. This market is projected to continue increasing at a compound annual growth rate of 7.2%, reaching a market size of nearly $26.9 billion by the end of 2026 (Fortune Businnes Insights, 2019). In the same tendency, the global shoulder arthroplasty implants market was valued at $1.0 billion in 2016 and is expected to reach $1.8 billion by 2024 (Marqual IT Solutions Pvt. Ltd (KBV Research), 2019).

During a comparative analysis of the outcomes and costs of anatomic or reverse total shoulder replacements in a cohort of 51,052 adult patients during January 2011 and December 2011, Ponce *et al.* (2015) found that aTSR patients had a lower mean hospital cost ($52,006 ± 25,964; n = 29,359 patients) in comparison with rTSR patients ($64,383 ± 32,767; n = 21,693 patients). Furthermore, patients undergoing aTSR also reported a shorter length of hospitalization (2.1 ± 1.3 days vs 2.6 ± 2.1 days). Patients undergoing rTSR experienced inpatient complications at a greater rate that those who received aTSR. Individually, the complication rates were 13.1% for aTSR and 24.3% for rTSR ($\rho < 0.001$).

In 2015, Triplet *et al.* (2015) and Kiet *et al.* (2015) reported that patients treated with aTSR reported significantly greater satisfaction with the surgery and outperformed those who had rTSR in American Shoulder and Elbow Society (ASES) total function score. Therefore, it can be argued that, based on these figures, aTSR is superior to rTSR.

The higher financial difference between aTSR and rTSR can be attributed to numerous factors, such as: age of the patient, the indication of surgery, type of the shoulder implant, use of bone graft, and the price of the shoulder implant (Chalmers *et al.*, 2019). According to market data in 2013, the price of the rTSR implant was approximately $3,000 more expensive than the aTSR implant, which could be explained by the difference in the number of components of each total shoulder replacements (screws, baseplate, etc.).

2.5 REVISION SHOULDER ARTHROPLASTY

However, despite the success and increased usage over recent years, shoulder arthroplasties are not without complications. Over time, shoulder implants will wear and need to be revised, often due to loss of function or pain. Revision rates after a total shoulder replacement is one of the most common outcome measures of joint replacement surgery (Labek *et al.*, 2011). A review published in 2006 documented failures rates of over 14% in shoulder arthroplasty studies reporting clinical results at more than two years (Bohsali *et al.*, 2006).

Revision replacement surgery is a new clinical intervention performed on a previously replaced shoulder joint to remove, replace, add or manipulate one or more of these components. According to the National Joint Registry (NJR) for England Wales Northern Ireland and the Isle of Man (2020) from a total of 37,916 primary shoulder surgery a total of 1,158 patients underwent a shoulder revision surgery, and 105 of these have also a further re-vision.

As can be seen in **Table 2.3**, datasets by the New Zealand Orthopaedic Association (NZOA) (2019) for the period of January 2008 to December 2018, suggested that the mean revision rate after shoulder replacement is higher to those of hip and knee replacement, with 0.95 revisions per 100 observed component years.

Table 2.3 Revision rate after total joint replacement

Implant	Number of primary	Number of revised	Mean follow-up period (years)	Observed component*	Rate/100 component**
Shoulder	10,324	523	5.31	54,863	0.95
Hip	135,461	6,965	7.18	972,138	0.72
Knee	110,076	3,652	6.85	753,723	0.48

* This is the number of registered primary procedures multiplied by the number of years each component has been in place.

** This is equivalent to the yearly revision rate expressed as a percent and is derived by dividing the number of prostheses revised by the observed component years multiplied by 100. It therefore allows for the number of years of post-operative follow up in calculating the revision rate.

2.5.1 What can go wrong with total shoulder replacements?

Ex vivo studies have shown that a common complication in the long-term clinical performance of shoulder arthroplasties systems is the failure of the polyethylene component and the potential problems associated with the generation of wear debris and its adverse reaction (Wirth *et al.*, 1999; Mabrey *et al.*, 2002; Matsen *et al.*, 2008; Goodman *et al.*, 2009).

During activities of daily living in patients with shoulder implants, the articulating components are subjected to large dynamic loads and wide range of motion producing volumes of polyethylene wear debris (Williams and Abboud, 2005), which can cause an biological inflammatory response in the surrounding bone leading to an osteolytic process (Amstutz *et al.*, 1992) and implant loosening (Klimkiewicz *et al.*, 1998). This complication due to the bioreactivity of polyethylene particles (dependent on particle size, shape, composition, and concentration) has also been described and frequently reported as a limitation in the long-term survival of hip and knee replacements. It is reported that a key factor in triggering biological reactions due to UHMWPE particles is the size of the wear particles, having a 'critical' size range of 0.2 to 0.8 μm (Illgen *et al.*, 2009). Studies into the biological response of the UHMWPE particulate size concluded that the most reactive particle size is 0.24 μm (Green *et al.*, 2000; Ingham and Fisher, 2000). In total shoulder replacements, the size of the UHMWPE particles has been determined in studies on failed implants, with an average equivalent diameter of 1.04 ± 0.03 μm (Wirth *et al.*, 1999) and 1.183 ± 0.07 μm (Mabrey *et al.*, 2002).

As defined by (Marshall *et al.*, 2008) osteolysis is a ‘silent disease’ that can progress without showing symptoms in the patient, up to the inevitable catastrophic failure or mechanical loosening of the implant components. Osteolysis occurs as a chronic cytokine-driven inflammatory response produced by the body’s macrophages to implant derived wear debris, resulting in increased local bone resorption (Green, 1998; Purdue *et al.*, 2007; Hallab *et al.*, 2012). The clinical presentation of implant loosening (aseptic loosening) can be explained as an attack on the bone tissue by the immune system as a result of the polyethylene wear debris present in the local area (Harris, 2001; Di Puccio and Mattei, 2015). Therefore, one of the factors that compromises the longevity of total shoulder replacements is the “durability” of the polyethylene bearing

components; the glenoid insert in the case of anatomic total shoulder replacement and the humeral component for reverse total shoulder replacement. In the latest annual report by the Australian Orthopaedic Association (AOA) (2020), the Registry has recorded 1,182 (8.3%) revisions of anatomical total shoulder replacement (aTSR), and 1,111 (3.7%) revisions of reverse total shoulder replacement (rTSR). Aseptic loosening caused by osteolysis is one of the three most common leadings reasons for revision in both cases (**Table 2.4**).

Table 2.4 Reasons for revision in total shoulder replacements

Type of shoulder replacement	Reason for revision	Number	Percent%
Anatomic total shoulder replacement (aTSR)	Rotator cuff insufficiency	301	25.5
	Instability/dislocation	265	22.4
	Aseptic loosening	208	17.6
Reverse total shoulder replacement (rTSR)	Instability/dislocation	379	34.1
	Infection	246	22.1
	Aseptic loosening	193	17.4

2.6 MATERIALS FOR TOTAL SHOULDER IMPLANTS

Metal–on–polyethylene (MoP) has been considered the standard bearing materials combination in shoulder arthroplasties for the last 50 years (Section 2.3 History of early designs of total shoulder replacements), where a highly polished metallic component typically made of cobalt-based alloy is coupled against a polymeric counter component usually made of *conventional* ultra-high molecular weight polyethylene (UHMWPE) or *highly cross-linked* UHMWPE (HXLPE).

2.6.1 Metals

Stainless steel (AISI 316L), cobalt-based alloy ($CoCr_{28}Mo_6$), and titanium alloy (Ti-6Al-4V) are the most common metallic materials used in the manufacturing of shoulder replacements. Due to their high modulus of elasticity and yield strength, these materials are capable of bearing significant loads in orthopaedic applications without

suffering large plastic deformations or permanent deformation. **Table 2.5** summarizes the mechanical and physical properties of these metals.

Table 2.5 Overview of mechanical and physical properties of metal materials used in shoulder replacements (Hasirci and Hasirci, 2018b)

Metal properties	Stainless steel	CoCr alloys	Ti-6Al-4V
Density, g/cm^3	8.0	8.5	4.4
Young's modulus, GPa	200	210–250	90–115
Yield strength, MPa	190–620	450–1,600	6580–950
Tensile strength, MPa	480–950	650–1,800	600–1,100
Fatigue limit, MPa	240–820	200–950	810

2.6.1.1 Stainless steel (iron-based alloy)

Stainless steel was promoted as a metallic alloy for the manufacturing of implant applications in 1943. Nowadays, the most common version of stainless steel used for implants is the American Iron and Steel Institute (AISI) austenitic low carbon (L) AISI 316LV.

However, its use in hip and knee replacements has been reduced due to the susceptibility to corrosion and pitting of its surface (Antunes and de Oliveira, 2012) and the introduction of cobalt- and titanium-based alloys. As can be seen in **Table 2.6**, this iron-based alloy is characterized by the high percentages of chromium (Cr) and nickel (Ni) in its chemical composition. The reaction to metal ions of these elements during the corrosion process can produce allergy and toxicity sensitization in some patients (Davis, 2003).

Table 2.6 Chemical composition (wt.%) of AISI 316L (ASTM F138)

Cr	Ni	Mo	Mn	C	Si	Fe
16.0–18.0	12.0–15.0	2.0–3.0	2.0 max	0.03 max	1.0 max	Balance

In addition, stainless steel tends to produce higher amounts of wear debris in comparison, with cobalt- and titanium-based alloys when it is used in metal–on–polyethylene total joint replacements (Konttinen *et al.*, 2014). Up to date, just Aston

Medial company continues using this iron-based alloy for the manufacture of a glenosphere shoulder component (Duocentric® Reverse Shoulder prosthesis).

2.6.1.2 Cobalt-based alloys

In the case of MoP shoulder prostheses, the articular metallic bearing component is typically made of high carbon grade cobalt-chromium-molybdenum (Co-Cr-Mo) alloy commercially known as 'Vitallium®' (Howmedica Inc.) based on the American Society for Testing and Materials (ASTM) standard for surgical implant application. This alloy usually exhibits considerable corrosion resistance, wear resistance, superior mechanical properties, satisfactory biocompatibility (Mani, 2016), and depending on the manufacturing method or process the $CoCr_{28}Mo_6$ alloy can be classified as cast version (ASTM F75) or wrought version (ASTM F799). The chemical composition of these alloys is provided in **Table 2.7** and **Table 2.8**.

Table 2.7 Chemical composition (wt.%) of ASTM F75

Co	Cr	Mo	W	Ni	Mn	Si	Fe	C	N	P	Al	S
58.9–69.5	27.0–30.0	5.0–7.0	0.2	2.5	1.0	1.0	0.75	0.35	0.25	0.02	0.30	0.01

Table 2.8 Chemical composition (wt.%) of ASTM F99

Co	Cr	Mo	Ni	Mn	Si	Fe	C	N
58.0–59.0	26.0–30.0	5.0–7.0	1.0	1.0	1.0	1.5	0.35	0.20

Cobalt (Co) element in the alloys provides a continuous phase for basic properties. Chromium (Cr) is responsible for the improvement of corrosion resistance properties and chemical inertness as it forms a passivating oxide film on the implant surface. Molybdenum (Mo) increases strength, ensures resistance to corrosion, durability, and reliability of the implants. This alloy can also contain traces of other elements, such as manganese (Mn), iron (Fe), tungsten (W), and silicon (S). The size and distribution of the carbide phase contributes to the hardness and mechanical behaviour of the alloy. In comparison with surgical stainless steel (iron-based alloy) used in other orthopaedic implant applications (mostly fracture treatments), cobalt-based alloys exhibit a superior

fatigue life, better wear resistance, and greater moduli of elasticity (210 to 250 GPa) than stainless steel (~200 GPa) (Hanawa, 2010), which has promoted its popularity and use in total shoulder arthroplasties.

2.6.1.3 Titanium and titanium alloys

Titanium (Ti) and its alloys (e.g., Titanium-6Aluminum-4Vanadium) show exceptional biocompatibility and superior corrosion resistance when compared to stainless steel and cobalt-based alloys. However, their mechanical strength, ductility and wear resistance are inferior compared to cobalt-based alloys. The spontaneous oxide layer (TiO_2, 'Titania', 2 to 6 nm of thickness) created on its surface when it is exposed to environmental conditions (passivation process) provides a natural shield against corrosive agents inside the human body. However, this stable and protective oxide film layer can be easily broken by wear damage, triggering a rapidly replace process called re-passivation. This process produces so much oxide that the surrounding implant tissue becomes dark black (Ti metallosis). Its biological effects are usually harmless, but in some cases, they can induce necrosis in the tissue around the implant (Konttinen *et al.*, 2014).

Fatigue strength in Ti alloys is directly related to their microstructure (α type, α + β type, or β type), which is a result of the alloy composition and thermo-mechanical processing (Niinomi, 2007; Hosseini, 2012). Alpha phase alloys exhibit good corrosion resistance, however, their utility in biomedical applications is principally limited by their low ambient temperature strength. Beta phase alloys offer high strength, good formability, and high hardenability. Dual phase α + β Ti alloys contain a mixture of both phases and are generally used in applications requiring higher strength, good toughness, good fatigue behaviour, and excellent corrosion resistance (Niinomi, 2008; Zhang and Chen, 2019). Ti-6Al-4V (ASTM F136 alloy and ASTM F1108 alloy) is the most common metal used for total joint replacements including knees, hips, and spinal discs. The fatigue strength of this titanium α + β type alloy can reach up to 810 MPa (Luo *et al.*, 2013). The chemical composition of Ti-6Al-4V alloy is provided in **Table 2.9**.

Table 2.9 Chemical composition (wt.%) of ASTM F136

Al	V	Fe	O	N	C	H	Ti
5.5–6.5	3.5-4.5	0.25	0.13	0.05	0.08	0.012	Balance

One further possible risk of this F136 alloy is the high content of Aluminium (Al) on its chemical composition, which is known as cause osteomalacia (softening of the bones) and has also been tentatively associated with dementia (Konttinen *et al.*, 2014). In the last years, Lima Corporate company has introduced the use of Ti-6Al-4V alloy in its manufacturing process of humeral heads and glenosphere components for anatomic and reverse total shoulder replacements (SMR® Shoulder System).

2.6.2 Polymers

2.6.2.1 Polytetrafluoroethylene (PTFE)

Polytetrafluoroethylene (PTFE), commonly known as Teflon®, has a low coefficient of friction between 0.04 and 0.20 depending on the materials and testing conditions (Dowson and Wright, 1981). PTFE was used by Charnley in his first total hip arthroplasty, however, within the first three years of implantation, acetabular cups showed excessive wear. The wear debris from PTFE led to adverse soft tissue reactions and pain in more than 300 patients (Stauffer, 1982). Despite its good biocompatibility properties (highly inert material), the poor wear characteristic of PTFE made it unsuitable for most medical bearing applications (Downson, 2014). **Table 2.10** summarizes the physical and mechanical properties of PTFE (Teoh *et al.*, 2016).

Table 2.10 Typical average physical properties of polytetrafluoroethylene (PTFE)

Materials properties	PTFE
Density, g/cm^3	2.10–2.20
Tensile modulus of elasticity, GPa	0.3–0.7
Tensile ultimate strength, MPa	15–40
Poisson's ratio	0.44–0.47

2.6.2.2 Ultra-high molecular weight polyethylene (UHMWPE)

Since Sir John Charnley used with successfully used an ultra-high molecular weight polyethylene (UHMWPE) acetabular cup paired against stainless steel femoral head in total hip replacements in 1962, UHMWPE has become the articular bearing surface of choice against harder counterfaces such as metals or ceramics in orthopaedic joint replacements. The early implementation of the UHMWPE acetabular cup component in total hip arthroplasty achieved a significant reduction in the wear compared with previous PTFE cups (Charnley, 1979).

A polymer is defined as a big molecule composed of many ('poly-') small molecules joined together via chemical covalent bonds. The small molecules are known as monomers and work as building blocks for these large molecules. The medical-grade ultra-high molecular weight polyethylene used in joint implants is generally classified as a linear 'homopolymer', which is made up of extremely long monomer chains of ethylene. The term "ultra-high" in its name refers to an average molecular weight, which is larger than 1.5 million g/mol (McGeough, 2013b; Kurtz, 2016; Hasirci and Hasirci, 2018c). From the clinical perspective, UHMWPE presents unique properties like toughness, low coefficient of friction, wear resistance, non-stick surface, and great biocompatibility (Wang and Ge, 2007; Affatato, 2014). **Table 2.11** summarizes the physical and mechanical properties of UHMWPE (Kurtz, 2016).

Table 2.11 Typical average physical properties of ultra-high molecular weight polyethylene (UHMWPE)

Material properties	**UHMWPE**
Density, g/cm^3	0.925–0.945
Molecular weight, 10^6 g/mol	3.5–7.5
Tensile modulus of elasticity, GPa	0.5–0.8
Tensile yield strength, MPa	21–28
Tensile ultimate strength, MPa	39–48

However, the lifetime of UHMWPE implants in metal–on–polyethylene bearings is still limited due to wear damage. In addition, further clinical complications are triggered by the reaction of micron and submicron polyethylene wear debris. To date,

conventional UHMWPE is one of the 'best' polymers available for artificial joints, such as knees, ankles, shoulder and elbows.

2.6.2.3 Highly cross-linked (HXLPE) for joint replacements

In an effort to improve the wear resistance of the traditional UHMWPE components in the total joint replacements, new types of polyethylene have been developed with encouraging long-term clinical results in hip and knee replacements.

In 1998, *highly cross-linked* UHMWPE (HXLPE) was clinically introduced in order to reduce wear and the incidence of revision resulting from osteolysis in total joint arthroplasty (Kurtz *et al.*, 2011; Mall *et al.*, 2011). When *conventional* UHMWPE material is exposed to high doses of gamma (γ) or electron beam (e-beam) radiation in the range of 65 kGy to 95 kGy, its chemical bonds begin to break creating free radicals, which start a recombination reaction in its structure forming a *highly cross-linked* UHMWPE (HXLPE). Crosslinking of *conventional* UHMWPE reduces the length and mobility of the polyethylene chain, which is necessary for large-scale plastic deformation, thus improving wear resistance (Grobbelaar *et al.*, 1978). However, an increase in the dose of gamma radiation during the crosslinking process can also significantly reduce the resistance against fractures.

Despite all of these improvements, *conventional* UHMWPE is the most common widely used polymer material for the manufacture of shoulder components. According to the Australian Orthopaedic Association (AOA) (2020) among the total of 9,649 polyethylene glenoid components implanted to date, 3,742 cases were made from *highly cross-linked* UHMWPE, and although its use has increased from 10.7% in 2008 to 30.6% in 2019, its use is still lower than *conventional* UHMWPE (5,907 cases).

2.6.3 Alternate bearing surfaces

Metal–on–polyethylene is a 'safe' and cost-effective bearing combination used in orthopaedic implants; however, polyethylene wear is still one of the most limiting

factors since its wear debris can trigger an inflammatory response ('osteolysis'), leading to implant failure. Recently, to try to enhance the performance and lifespan of shoulder implants, a range of new features have been proposed including new bearing materials and the inversion of *conventional* bearing materials.

2.6.3.1 Inverted bearing materials

The reverse total shoulder replacement moves the joint centre of rotation medially by up to 20.9 mm relative to the anatomic shoulder (Ackland *et al.*, 2010), this change improves the biomechanical function of the shoulder, but can also lead to scapular impingement or "notching" of the implant, which was initially reported by Sirveaux *et al.* (2004). Scapular notching is one of the major concerns related to rTSR, and it describes a phenomenon whereby there is impingement of the UHMWPE humeral component against the scapular neck upon adduction of the arm, which causes a gradual erosion of the polyethylene component implant.

In order to reduce the accelerated wear caused by this phenomenon, an inversion of the *conventional* bearing materials used in rTSR has been promoted in the last few years (Kohut *et al.*, 2012; Irlenbusch *et al.*, 2015; Merolla *et al.*, 2017). Therefore, a polyethylene glenosphere articulating against a metal humeral insert counterpart is used as shown in **Figure 2.26**.

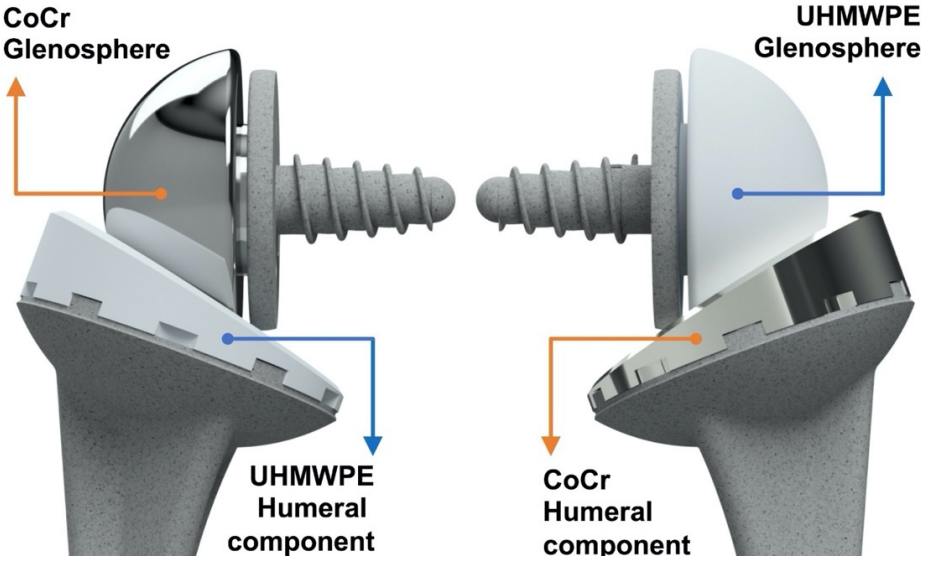

Figure 2.26 Reverse total shoulder replacement (*left*) with inverted bearing materials (*right*)

While not eliminating notching, this inversion of bearing materials has the advantage that it creates less polyethylene debris when scapular notching occurs, and theoretically, this will induce less active osteolysis in rTSR (Kohut *et al.*, 2012; Vaupel *et al.*, 2012; Ackland *et al.*, 2015; Irlenbusch *et al.*, 2015). It should be mentioned, that the inversion of the bearing materials in rTSR has not resulted in a significant difference in wear between both material configurations (Kohut *et al.*, 2012).

2.6.3.2 Ceramics in total joint replacements

For more than 30 years, ceramics materials have been used as an alternate bearing surface in total hip arthroplasty (femoral heads) and in total knee arthroplasty (femoral components) (Kluess *et al.*, 2014). The introduction of ceramics in total joint replacements has resulted in a significant reduction in their wear rates in comparison with the high wear rates obtained from the traditional metal–on–metal (MoM) and metal–on–polyethylene (MoP) bearings used in total hip arthroplasty (McGeough, 2013b). In addition, the use of ceramic articulations eliminates the clinical issues associated with metal allergies in MoM and polyethylene wear debris ('osteolysis') reactions in MoP.

However, these advantages are to some extent reduced by the danger of a rare but devastating fracture of the ceramic liner or head (Traina *et al.*, 2013) and the occurrence of squeaking (Keurentjes *et al.*, 2008). Another possible drawback of ceramics compared with MoP is their cost. Ceramic–on–ceramic (CoC) hips are more expensive than ceramic–on–polyethylene (CoP) hips, which in turn are more expensive than MoP hips (Carnes *et al.*, 2016; Sahoo *et al.*, 2019).

Aluminium oxide (Al_2O_3, 'alumina') was the first ceramic material used in the manufacture of orthopaedic devices since 1970s. Despite the excellent mechanical properties (corrosion resistance, low friction, hardness, and strength) to *in vivo* environments, the brittle nature of this material has been widely questioned after catastrophic failures (breakdown or fracture, with the release of 'hard' debris) in ceramic head components in total hip joint replacement (Pokorny and Knahr, 2012; Binazzi, 2014).

In 1985, zirconium dioxide (ZrO_2, 'zirconia') was introduced as a solution to address the fracture toughness (this is a property, which describes the ability of a material containing a crack to resist fracture) of the alumina in orthopaedic applications (Dorozhkin, 2018). The advantage of this second-generation ceramic material is lower hardness, stiffness and its higher density and almost twice the flexural strength compared to alumina. However, zirconia components are not exempt of complications, since an undesirable ageing process (low-temperature degradation) affects their performance.

Mechanical properties in ceramic materials are governed by the grain size, porosity, and composition. A combination of a small grain size and low porosity results in superior strength properties. Such a microstructure is capable of inhibiting static fatigue and slow crack growth while the ceramic is under load (Choi *et al.*, 2018). The physical and mechanical properties of ceramics used in joint replacement bearings are tabulated in **Table 2.12**.

Table 2.12 Physical and mechanical properties of ceramics used in joint replacements (Hasirci and Hasirci, 2018a)

Material properties	Alumina	Zirconia	Zirconia–toughened alumina
Chemical composition	Al_2O_3	ZrO_2	$Al_2O_3 + ZrO_2 + Y_2O_3$
Grain size, μm	1–5	0.1–1.0	1–2
Density, g/cm^3	3.98	5.74–6.08	4.40
Young's modulus, GPa	420	210	300–350
Hardness, HV	1,975	1,250	1,600–1,800
Fracture toughness, MPa m$^{1/2}$	4–5	6–12	6–10
Poisson's ratio	0.22	0.30	0.22

Recent advances in material processing have led to the development of a third generation of composite ceramic components for total joint replacements; alumina-toughened zirconia (ATZ) and zirconia-toughened alumina (ZTA). These new ceramics exhibit superior strength and toughness and have been found to be more wear-resistant than *conventional* alumina and zirconia (Hastings *et al.*, 2016), which has promoted it used also for shoulder prosthesis systems (**Figure 2.27** and **Figure 2.28**).

Figure 2.27 Zirconia-toughened alumina ceramic (CeramTec, Biolox® *delta*) humeral heads for shoulder arthroplasty

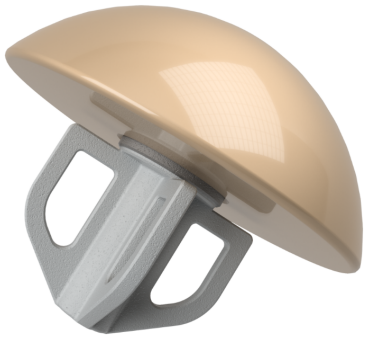

Figure 2.28 Alumina-toughened zirconia humeral head for short stemmed total shoulder prosthesis

In terms of wear, humeral heads made of ceramic material (Biolox® *delta*) provide a significant reduction of the UHMWPE wear rate by 27% in comparison with the CoCr metallic humeral heads in aTSR (Mueller *et al.*, 2017). When humeral components made of ATZ ceramic material (Ceramys®) were paired against UHMWPE glenospheres in rTSR, this combination showed a significant 37% lower wear rate compared to the standard coupling of CoCr with UHMWPE (Lerf *et al.*, 2016). However, long-term clinical follow-up will confirm if these *in vitro* wear-reductions lead to longer *in vivo* survival of total shoulder arthroplasties.

2.6.3.3 Pyrolytic carbon (PyroCarbon)

The development of a ceramic-like shoulder component (**Figure 2.29**), such as a humeral head graphite core coated with up to 1 mm thickness of pyrolytic carbon (PyroCarbon, PyC) by chemical vapor deposition (CVD) at high temperatures provides one such alternative bearing material.

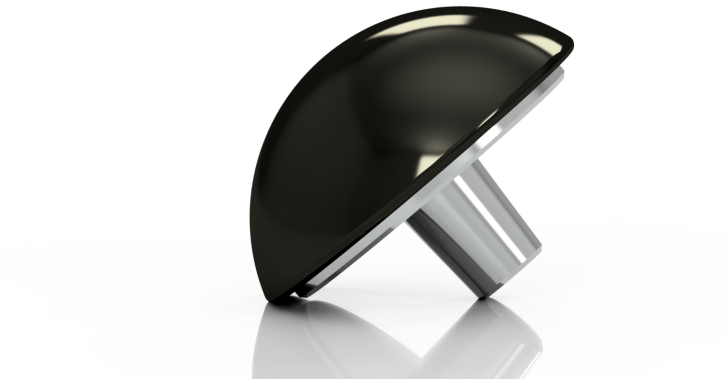

Figure 2.29 PyroCarbon humeral head for partial shoulder replacement

Since PyroCarbon was introduced in the late 1970s in artificial heart valves (Bokros, 1977; Bokros, 1983) and then in upper limb joint replacements (hand and wrist arthroplasty) in the 1990s (Beckenbaugh *et al.*, 2006; Daecke *et al.*, 2006), it has proven to be a high wear resistance biomaterial with excellent biocompatibility and wettability, low friction, and a modulus of elasticity similar to that of cortical bone (18 GPa) (Sweets and Stern, 2011; Ross *et al.*, 2014). **Table 2.13** summarizes the physical and mechanical properties of pyrolytic carbon (Carpenter *et al.*, 2016).

Table 2.13 Pyrolytic carbon (PyroCarbon, PyC) properties

Material properties	**PyC**
Density, g/cm^3	1.93
Young's modulus, GPa	29.4
Hardness, HV	236
Poisson's ratio	0.28
Fracture toughness, MPa m$^{1/2}$	1.68
Coefficient of friction	0.15

Clinical success in small joint replacements including the proximal interphalangeal (PIP) joint and the metacarpophalangeal (MCP) joint has been reported from *in vivo* (Dickson *et al.*, 2015), *in vitro* (Naylor *et al.*, 2015), and *ex vivo* studies (Bone *et al.*, 2014). However, it is also known that the manufacturing process of PyroCarbon joint replacements requires complex technologies and numerous steps to create a finished implant (Bellemere, 2018), which increases the price of these components.

According to the Pharmaceutical Management Agency (PHARMAC) for New Zealand (2017), a humeral head for shoulder-hemiarthroplasties of 43-mm diameter made of CoCr alloy has a list price of $2,340, while the same component but manufactured in PyroCarbon costs $3,800 New Zealand dollars.

2.7 TRIBOLOGY IN SHOULDER REPLACEMENTS

Tribology is a very old science; the first recorded cases dated from the year 2,400 BC, when the Egyptians were able to pull heavy stone blocks along the ramps and massive statues on sleds during the pyramid construction, pouring water or oil as a lubricant under the sledge and reducing the friction.

However, the term tribology was not coined until 1966 in the Jost Report (Lubrication (tribology) Education and Research, Department of Education and Science, HMSO, 1966), a study commissioned by the British government to investigate damage due to wear and friction.

Tribology was then defined as "*The science and technology of interacting surfaces in relative motion and the practices related thereto*"; and is derived from the Greek word "*tribos*" which means rubbing and friction. It includes three key aspects: wear, friction, and lubrication.

2.7.1 Wear

Wear can be defined as the progressive loss of material (mass), due to relative motion between two adjacent articulating surfaces. For a given material, bearing design and

surface finish wear depends on three main factors: the load compressing the two surfaces and determining their contact stress, the relative motion (kinematics) that continuously modifies the location and extent of the contact area, and the lubricant interrupting the direct contact of the two surfaces.

There are four main types of mechanisms that may lead to wear of the surface in an artificial joint ASTM G40 (2017) "Standard Terminology relating to Wear and Erosion" and can be briefly summarized as follows:

1. *Abrasive wear* is the displacement of a certain volume of soft surface materials such as polymer caused by hard particles or abrasive particles trapped between the moving surfaces, which often results in grooves, scratches or indentations on the surface.
2. *Adhesive wear* is the transfer of material from one surface to another at localized sites during relative motion. Transferred materials can usually be seen on surfaces.
3. *Fatigue wear* is the loss of material as a result of cyclical stress variation, which can lead to additional failure when cracks in the surface joint together.
4. *Corrosive wear* occurs due to the chemical or electrochemical interaction of one or both surfaces with the environment conditions.

In the case of MoP total shoulder replacements, *in vitro* (Section 2.11 *In vitro* wear of shoulder replacements) and *ex vivo* (Section 2.12 *Ex vivo* wear of shoulder replacements) studies have shown that the most common type of wear mechanism that affect the UHMWPE performance is abrasive wear; typically leading to aseptic loosening in long-term use, and it occurs when the asperities of a rough surface (metallic components) slides across a softer counterpart (polyethylene components). Abrasive wear may occur with two bodies (metal against polyethylene components) typically resulting in a series of grooves or scratches in the wear direction, or with three bodies (external material trapped between the bearing surfaces) which causes additional wear.

2.7.1.1 Wear factor

The wear factor (k, mm^3/Nm) is the coefficient used to characterise the wear of the materials and it was suggested by Lancaster (1973), where the total volume of material removed (V/mm^3) is divided by the product of the applied load (P, N) and the sliding distance (x, m), as shown in **Equation 2.1**:

$$k = \frac{V}{Px}$$

Equation 2.1 Lancaster wear equation

Also, different terms are often used to describe the wear damage in the surface of total shoulder joint replacements. These include scratching, pitting, burnishing and delamination on polyethylene bearings (Harman *et al.*, 2011).

- Scratches – visualized as thin lines in irregular or ordered directions.
- Pitting – visualized as depressions with rough surfaces
- Burnishing – visualized as smooth, highly polished regions that are highly reflective of incident light.
- Delamination – visualized as thin layers of polyethylene material separated from the surface.

Furthermore, the wear of the UHMWPE shoulder components not only depends on the wear phenomenon and mechanisms but also depends on multiple factors including:

- Surgeon factors – variation in positioning during the shoulder arthroplasty (Walch *et al.*, 2012). In a failure analysis on revised implants, Hasan *et al.* (2002) estimated that the rate of technical errors was around 23%.
- Patient factors – age, gender, loading, motion, and physical pattering during the activities of daily living (Anakwenze *et al.*, 2017).
- Mechanical design – implant size, clearance between the surfaces, the thickness of the component, etc.

2.7.2 Friction

The friction force (F) is defined as the resistance that opposes the relative motion between two bearing surfaces in contact and was studied for the first time by Leonardo DaVinci (Hutchings, 2016). The force friction is described using the Amontons's first law: "the friction force is directly proportional to the load applied to the surface and friction coefficient", and it is explained in **Equation 2.2**:

$$F = \mu N$$

Equation 2.2 Friction force equation

where F is the frictional force, N is the normal load, and μ is the coefficient of the friction (dimensionless scalar value). An important aspect that determines the frictional force in joint replacements is the type of bearing material used and the contact between the two articulating surfaces (Brockett *et al.*, 2012). **Table 2.14** shows the coefficient of friction for materials used in artificial joints.

Table 2.14 Typical coefficient of friction values for various bearings for artificial hip joints in the presence of diluted bovine *serum* (Jin *et al.*, 2006)

Bearing	Coefficient of friction (μ)
Metal–on–polyethylene (MoP)	0.06–0.08
Ceramic–on–polyethylene (CoP)	0.06–0.08
Metal–on–metal (MoM)	0.022–0.27
Ceramic–on–metal (CoM)	0.002–0.07
Ceramic–on–ceramic (CoC)	0.002–0.07

2.7.3 Lubricant and lubrication

A lubricant is a substance introduced to reduce their friction, minimize the wear between two sliding surfaces, transport the wear debris away from the interface, and at the same time provide cooling (Wimmer and Laurent, 2012). Human synovial fluid would be the "best" and "ideal" type of lubricant option (same lubricant condition as *in vivo*) when an *in vitro* wear test of shoulder implant bearing components is performed. However, due to practical and ethical complexities bovine *serum* (well

known as calf *serum*) is often used as a substitute for this medium in wear test (Mazzucco *et al.*, 2002).

The protein content of commercial bovine *serum* is much greater (range, 63 to 83 g/L) than a human synovial fluid with a range of 20 to 35 g/L, therefore for wear simulation it is generally diluted with deionized water in order to obtain a ratio of fluid protein concentration inside that range. For this research, a value of 26 g/L of protein concentration was chosen as it is reported (Wang *et al.*, 2004) to match the level seen in synovial fluid in human joints with diseases such as osteoarthritis and rheumatoid arthritis. Protein concentration has shown to have a marked effect upon the friction factors for the different bearings (Brockett *et al.*, 2007). In fact, as the protein concentration decreases, the friction factor also decreases (Williams *et al.*, 2007).

2.7.3.1 Lubricant regimes

Metal–on–polyethylene bearing surfaces used in orthopaedic applications usually operate under boundary-to-mixed lubricating regimen conditions (Brockett *et al.*, 2007).

- In a *boundary lubricant condition* ($1 < \lambda$), the thickness of the fluid film becomes insignificant and there is significant contact between the surface protuberances at all times.
- In the case of *mixed lubrication condition* ($1 < \lambda < 3$) the thickness of the fluid film increases, and few protuberances are in contact.
- *Fluid-film lubricant condition* ($\lambda > 3$), the articulating surfaces are completely separated by a relatively thick film of lubricant, resulting in minimum wear and low friction.

The lubrication regime that the shoulder replacements operated under can be determined by the lambda ratio (λ), as shown in **Equation 2.3**:

$$\lambda = \frac{h_{min}}{R_a} = \frac{h_{min}}{[\,(R_{a1})^2 + (R_{a2})^2\,]^{\frac{1}{2}}}$$

Equation 2.3 Lubrication regime equation

where the lambda ratio refers to the ratio of minimum fluid film thickness (h_{min}) in relation of the surface roughness (R_a) of the two bearing components ("ball-on-socket"). Where R_{a1} refers to the surface roughness of the ball and R_{a2} to the socket.

2.7.3.2 Lubricating film thickness

For metal–on–polyethylene bearing surfaces, the minimum effective film thickness (h_{min}) can be calculated using the Hamrock and Dowson (1978) **Equation 2.4**:

$$\frac{h_{min}}{R_x} = 2.80 \left(\frac{\eta u}{E^* R_x}\right)^{0.65} \left(\frac{L}{E^* R_x^2}\right)^{-0.21}$$

Equation 2.4 Hamrock and Dowson equation

where R_x is the equivalent radius (m), η is the viscosity of the lubricant (Pa s), u is the entraining velocity (m/s), E^* is the equivalent elastic modulus (Pa), and L is the load (N). The equivalent radius (R_x) can be calculated from the **Equation 2.5**:

$$\frac{1}{R_X} = \frac{1}{R_1} - \frac{1}{R_2}$$

Equation 2.5 Equivalent radius equation

where R_x is in function of to the radii of curvature of the ball (R_1) and socket (R_2) component. The equivalent modulus of elasticity (E^*) can be determined from the **Equation 2.6**:

$$\frac{1}{E^*} = 0.5 \left(\frac{1 - v_1^2}{E_1} + \frac{1 - v_2^2}{E_2}\right)$$

Equation 2.6 Equivalent modulus of elasticity equation

where E refers to the Young's modulus, and v to the Poisson's ratio of the components and subscript 1 (E_1; v_1) refers to the ball and subscript 2 (E_2; v_2) to the socket of the total shoulder replacement.

2.8 WEAR TESTING

Wear testing carried out on simulators is a critical preclinical method to assess the wear characteristics and performance of different materials used for bearing combinations in metal–on–polyethylene orthopaedic applications.

Pin-on-disk (POD) wear-testers are often used as a relatively inexpensive test method for the evaluation of materials in relatively similar clinical conditions (Saikko and Ahlroos, 1999; Saikko, 2006; Saikko and Kostamo, 2011; Saikko, 2017). Here, cylindrical pins and circular disks are manufactured to mimic the articulating surfaces of different total joint replacements. These components are then mounted perpendicular to the plane of motion (vertically) in the POD wear tester and immerse in a lubricant.

The effect of the CoCr counterface surface finish on the wear of *conventional* and *highly cross-linked* UHMWPEs has been studied by Saikko *et al.* (2001) using a circularly translating pin-on-disk (CTPOD) test principle (Saikko, 1998), who showed that the wear rate increased with counterface roughness in the disks with an average surface between R_a= 14 nm and 240 nm as observed in explanted femoral heads. The wear factors of *cross-linked* polyethylene (XLPE) against a rough counterface were still smaller than that of *conventional* UHMWPE against a smooth counterface. The great success of this type of 'classic' wear test is based on four key points:

1. Adjustable contact stress between the components (range of 1.1 to 3.5 MPa).
2. Bovine *serum* as a based-lubricate during the test.
3. Large scale wear test (up to 100 specimens in one test) (Saikko, 2005).

In summary, POD wear tests can provide an insight into the weight loss, the effect and change of the surface roughness, and wear rate of the materials. The next stage in wear testing is the full artificial joint (e.g., hip and knee) simulator testers, where an 'advanced' wear simulator is specifically developed in order to test full-scale implants under realistic physiological movement patterns and loads.

2.9 HISTORICAL DEVELOPMENT OF SHOULDER WEAR SIMULATORS

Over the past years, lower limb joint simulators (knee and hip) have been widely used in preclinical tests in order to obtain and describe the wear mechanisms and function of these artificial joint replacements. Wear testing became a fundamental laboratory's request when new material or design is introduced in the market and has not been used in patients before (Affatato *et al.*, 2006).

In the case of the shoulder joint replacements, the use of a wear test simulator is a relatively new development and only came into use in the last years. The correct replication of an *in vivo* range of motion and loading can only be achieved using a complex artificial joint simulator. This machine needs to be capable of mimicking with high reliability the motion between the artificial bearing surfaces inside the human body; in order to re-create and re-produce the effects of the multi-directional motion profile and loading patterns of the joint.

The work carried out by Pijl *et al.* (2004) was the first attempt to test a shoulder prosthesis *in vitro*. The use of axial mechanical system to replicate the abduction/adduction shoulder motion in a single-station machine could be considered the first stage towards the development of the actual shoulder replacement wear simulators systems. Their simulator input for the load profile was between 150 N to 650 N and the test was performed for 2 million cycles.

A step further in the history of shoulder simulator was marked by Geary *et al.* (2010), who incorporated two degrees of motion, and two axes of variable loading (arm abduction (50° to 120°) and internal/external rotation (25° to 60°)) in a single-station simulator potentially giving a better replication of the shoulder's range of motion.

The use of lower limb joint simulator with multiple-stations to test shoulder prostheses started with Wirth *et al.* (2009), who used a six-station knee simulator to carry out a wear test on *conventional* UHMWPE and *cross-linked* UHMWPE components for anatomic total shoulder prostheses. A constant load of 756 N (1 to 2 times body weight) based on the previous work by Poppen and Walker (1978) and Anglin *et al.* (2000) was employed.

Three years later, Vaupel *et al.* (2012) converted a 12-station hip wear simulator with two axes of motion and the variable loading into a reverse shoulder wear simulator, which replicated the shoulder movements of adduction/adduction and flexion/extension. The sinusoidal loading profiles were based on *in vivo* contact forces obtained by Bergmann *et al.* (2007) during a trial in seven patients with hemiarthroplasty replacements, 20 to 618 N (0.9 times body weight) and 20 to 297 N (1.35 times body weight).

Separately, Kohut *et al.* (2012) used a multi-station hip simulator with three axes of motion (flexion/extension, abduction/adduction and internal/external rotation) to test two types of reverse shoulder replacements, which allowed replication of a maximum range of motion; which was said to result in a more complete wear test in comparison with the previous one and two axis simulator studies.

Dieckmann *et al.* (2013) performed a pilot wear study using a single-station machine with two axes of motion (abduction/adduction and flexion/extension) and the incorporation of an additional third axis (longitudinal motion). Haider *et al.* (2013) used an adapted hip simulator, which applied abduction/adduction motion and internal/external rotation with a sinusoidal load rising and falling in the range of 50 to 1,700 N to undertake a wear study in reverse shoulder implants. No further wear protocol details were provided.

2.10 THE NEWCASTLE SHOULDER WEAR SIMULATOR

The Newcastle Shoulder Wear Simulator (Smith *et al.*, 2015; Smith *et al.*, 2016) is an advanced multi-station rig dedicated to testing artificial shoulder joints, with fully programmable loading and motion input profiles. The inclusion for the first time of three axes of motion (flexion/extension (FE), abduction/adduction (AA) and internal/external rotation (IE)), and dynamic loading (L) make it possible to reproduce common shoulder related activities of daily living (ADLs). This contrasts with the early single-station machines designed; and the adaptation of available knee and hip simulators with no more than two axes of motion. Also, these previous simulator studies have only applied simplified patterns of sinusoidal motion and loading. In addition, as will be seen, the Newcastle Shoulder Wear Simulator was modified so that, as well as the three axes of motion, a translational motion was added too, to mimic that motion seen in natural glenohumeral joints (Smith *et al.*, 2018).

The Newcastle Shoulder Wear Simulator consists of five test stations with an additional control station (**Figure 2.30**), which is used to monitor the mass changes due to fluid absorption of the polyethylene components of the shoulder implant during the wear test. The complexity of this unique machine allows it to carry out comprehensive wear tests of any type of shoulder prosthesis with the appropriate physiological patterns of motion and loading, which can replicate a range of different ADLs.

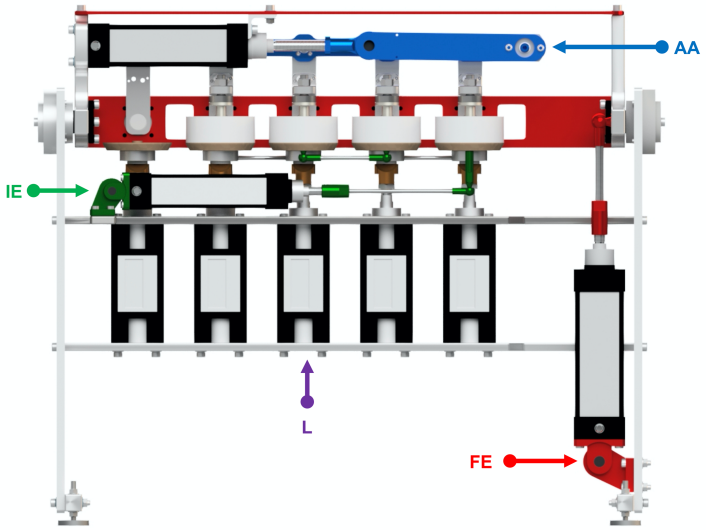

Figure 2.30 The Newcastle Shoulder Wear Simulator. Five test stations can be seen, four of which to the right-hand side have test chambers added. The three pneumatic cylinders which drive the three axes of motion (flexion/extension (FE), abduction/adduction (AA), and internal/external (IE) rotation) can be seen

The simulator can apply up to 110° of motion (range, –55° to 55°) in the abduction/adduction (AA) and flexion/extension (FE) axes and up to 90° (range, –45° to 45°) in the internal/external (IE) rotation axis; and up to 1,500 N of dynamic load in each station. The load is applied to the test samples through pneumatic pistons positioned beneath each station.

The National Instrument LabView program feeds the user's desired outputs to an external control box, which controls each pneumatic actuator in the wear simulator. The desired ADL's profiles are programmed by entering the voltages corresponding to the displacement of each individual actuator; these values are proportional to the angles of motion.

2.10.1 Working conditions

Flexion/extension (FE) and abduction/adduction (AA) rotations are applied to the "upper components", whose axis mechanisms are visible in **Figure 2.31**, coloured in red (*y*: medial-lateral direction) and blue (*x*: posterior-anterior direction), respectively. In addition, internal/external (IE) rotation, is applied to the loaded component ("lower components"). In particular, the load (L) is applied along the axis of the IE rotation, i.e. in vertical direction (*z*: inferior-superior direction).

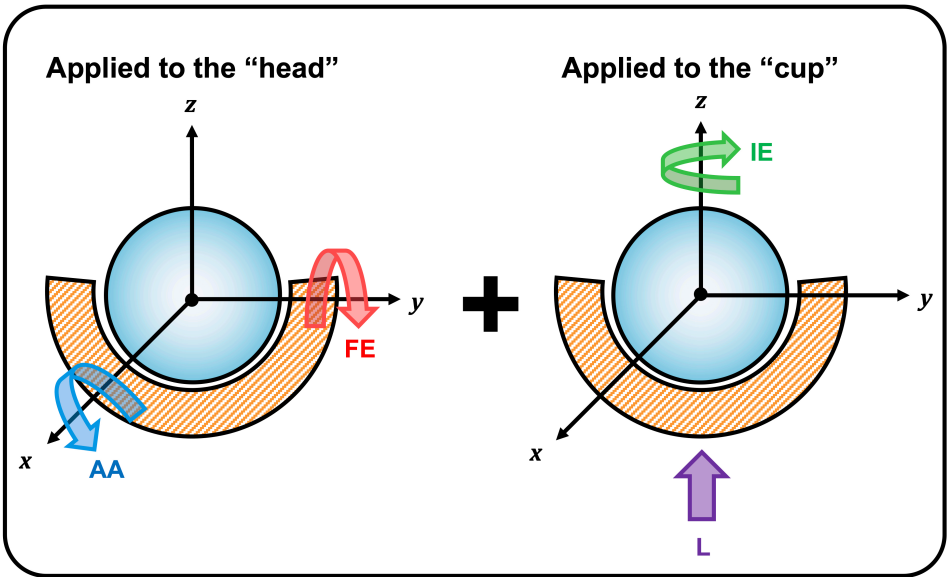

Figure 2.31 Working conditions of the Newcastle Shoulder Wear Simulator. Application of rotations and load to the "head" and "cup". FE: flexion/extension; AA: abduction/adduction; IE: internal/external rotation, L: load

2.10.1.1 Translational sliding motion

A translational movement along the *y*-axis can be added to the Newcastle Shoulder Wear Simulator to replicate rolling, sliding, and cross-shear mechanisms present in the glenohumeral joint in the specific case of patients with anatomical total shoulder arthroplasties (Smith *et al.*, 2018). A mechanism with a rotational centre eccentric to the *z*-axis, and driven by the internal/external motion placed between the loading cylinder and lubricant bath chamber make this possible. The bespoke mechanism consists of a modified shaft, a shaft step, and an alignment bar. The step component is necessary to drive the rotation of the lubricant bath chamber causing the glenoid insert to be offset from the centre of rotation, while the alignment bar maintains the offset direction in the correct phase and alignment.

2.10.2 Cycle frequency

The simulator operates at a frequency of 1 Hz (60 cycles/min), as is commonly used in hip implant wear testing ISO 14242 (2014) "Implant for surgery-Wear of total hip-joint prostheses" and knee implant wear testing ISO 14243 (2009) "Implant for surgery-Wear of total knee.joint prostheses". At 1 Hz frequency 500,000 cycle wear test takes just short of six days, or over eight weeks to complete five million cycles, continuous testing. Total test duration however will be longer due to periodic stopping to clean and measure the specimens.

If the shoulder simulator run at higher cycling rate than the 1 Hz, then substantially highly bearing surface temperatures and greater amounts of protein precipitation may be expected. This could, in turn affect the boundary lubricating property of the *serum*, the physical properties of the bearing materials, and thereby, the relative wear resistance of the components being tested (Saikko, 2005).

2.10.3 Calibration

To ensure that the Newcastle Shoulder Wear Simulator performs correctly the input profiles, a static and dynamic calibration is undertaken before each wear test. The static

calibration consists of manually shifting the moving components on the simulator through various angular positions to the extremes, whilst noting the corresponding voltage at each location. The ranges of motion are calibrated for the three axes of motion: flexion/extension (FE), abduction/adduction (AA), and internal/external rotation (IE).

While the dynamic calibration consists of performing the activity of daily life and determine whether the simulator accurately replicates the physiological motion of the shoulder, ensuring the wear tests will provide valid results that will accurately reflect the clinical shoulder replacement's life cycles.

2.11 IN VITRO WEAR OF SHOULDER REPLACEMENTS

Despite the popularity of shoulder joint replacements and acknowledgment that wear is a limitation to long-term survival, to date, few *in vitro* wear studies have been conducted to assess the wear performance (wear rate; mm^3/million cycles) and topographical changes of the articulating components in shoulder joint replacements.

Various national and international standards have been established in an attempt to allow comparison of one wear test to another by defining the test conditions. Unfortunately, such standards do not currently exist for the wear testing of shoulder joint replacements.

The results available in the **Table 2.15** for anatomic total shoulder replacements and **Table 2.16** for reverse total shoulder replacements show a wide range of wear rates of polyethylene components, which may be due to the different loading and motion conditions applied, the lubricant protein concentration and the use of single-station machines or adapted hip and knee simulators. These multiple variations in the methods for shoulder implant wear testing make it difficult to compare results obtained from different research centres.

Table 2.15 Summary of previous aTSR wear studies' methods and results

Author	Type of simulation	Load range (N)	Motion range	Lubrican (protein content)	aTSR prostheses	Wear rate (duration and results)
Alexander *et al.* (2019)	" Shoulder III" joint simulator	–250 to 1,000	FE: 20º, AA: 35º, SI: ± 1.5 mm	Bovine *serum* (not specified)	3 × 51 mm Affinis®	500,000 cycles, 16.6 ± 2.2 mm^3/million cycles
Smith *et al.* (2018)	Newcastle Shoulder Wear Simulator	180 to 250	FE: 28º, AA: 13º, IE: 25º, SI: 4 mm	Newborn calf *serum* + deionized water (26 g/L)	5 × 42 mm JRI VAIOS®	5 million cycles; 21.5 ± 5.4 mm^3/million cycles
Mueller *et al.* (2017)	AMTI hip simulator	200 to 1,100	FE: 20º, AA: 90º, SI: 3.5 mm	Calf *serum* + deionized water (20 g/L)	3 × 54 mm Biolox® *delta*	3 million cycles; 49.0 ± 1.4 mm^3/million cycles
Dieckmann *et al.* (2013)	Dresden shoulder simulator	100 to 500	FE: 20º, AA: 70º, SI: ± 7 mm	Bovine *serum* + bi-distilled water (30 g/L)	1 × 54 mm CAPICA®	5 million cycles; 9.9 mm^3/million cycles
Wirth *et al.* (2009)	AMTI knee simulator	Constant value of 756	AA: ± 8º, SI: ± 2 mm	Bovine *serum* (62 g/L)	3 × 48 mm CAPICA®	5 million cycles; 49.4 mm^3/million cycles

FE: flexion/extension; AA: abduction/adduction; IE: internal/external rotation; SI: superior-inferior translation.

Table 2.16 Summary of previous rTSR wear studies' methods and results

Author	Type of simulation	Load range (N)	Motion range	Lubrican (protein content)	rTSR prostheses	Wear rate (duration and results)
Langohr *et al.* (2016)	MATCO hip simulator	813 to 914	FE: 45º, AA: 45º, IE: – –	Alpha calf *serum* + PBS solution (30 g/L)	1 × 42 mm Reverse Delta Xtend®	1 million cycles; 42.0 mm^3/million cycles (XLPE), 38.8 mm^3/million cycles (HXLPE)
Smith *et al.* (2016)	Newcastle Shoulder Wear Simulator	180 to 250	FE: 28º, AA: 13º, IE: 25º	Newborn calf *serum* + deionized water (26 g/L)	5 × 42 mm JRI Reverse VAIOS®	4.5 million cycles; 14.3 ± 1.6 mm^3/million cycles
Haider *et al.* (2013)	AMTI hip simulator	50 to 1,700	FE: – –, AA: 41º, IE: 57º	Not specified	12 × 36 mm (not specified)	2.5 million cycles; 19.1 ± 0.9 mm^3/million cycles (XLPE), 3.6 ± 0.2 mm^3/million cycles (HXLPE)
Kohut *et al.* (2012)	Hip-E simulator	250 to 1,100	FE: 46º, AA: 46º, IE: – –	Bovine *serum* (30 g/L)	12 × 36 mm (not specified)	500,000 cycles; 14.1 mm^3/million cycles
Vaupel *et al.* (2012)	MTS Hip simulator	20 to 618, 20 to 927	FE: 46º, AA: 46º, IE: – –	Calf *serum* + deionized water (21 g/L)	16 × 36 mm (not specified)	5 million cycles; 125.7 ± 28.2 mm^3/million cycles

FE: flexion/extension; AA: abduction/adduction; IE: internal/external rotation.
PBS: phosphate-buffered saline; XLPE: *cross-linked* polyethylene; HXLPE: *highly cross-linked* polyethylene.

2.12 EX VIVO WEAR OF SHOULDER REPLACEMENTS

Analysis of shoulder implants retrieved at revision surgery can play a key role in the study of the *in vivo* performance of the prosthesis, developing a better understanding of the complex wear mechanisms that occur during time *in vivo*. The assessment of clinical and implant failure variables provides detailed information related to the factors that lead to the failure and can directly affect implant longevity.

The most common 3D inspection techniques used to determine the volumetric wear (mm^3), wear rate (mm^3/year) and penetration depth that occurs during *in vivo* time on retrieved polymeric shoulder components are geometrical measurements carried out by coordinate measuring machine (CMM) and micro-computed tomography (micro-CT). Both techniques need an unworn component in order to compare and determine the wear damage produced during *in vivo* time.

In contrast with the *in vitro* studies, where the mass change of a pristine shoulder component is assessed to account for the volume loss through the test (gravimetric measurements), the absence of an unworn geometry represents a difficulty at the moment of determining the accurate volume loss in retrieval studies.

To date, there is limited retrieval data on shoulder components, however, scratching, burnishing, and abrasion have been reported as the most common and similar types of polyethylene wear damage on retrieved reverse and anatomic total shoulder components. **Table 2.17** and **Table 2.18** summarize the studies available in the literature with their key outcomes.

Where surface "irregularities" or change of the articular geometry were found to be more predominant and severe in the inferior quadrant of both polymeric components, suggesting a propensity for an impingement mechanism. In the case of the reverse components, wear in the inferior quadrant is a result of direct contact between the polyethylene humeral component and the lateral edge of the scapular bone (scapular nothing), or with the inferior locking screws (rim damage) (Nam et al., 2010b; Day et al., 2012; Wiater et al., 2015).

In contrast, anatomical components showed signs of impingement related to the contact of the glenoid insert with the humerus. As the humerus impinges on the glenoid, a shear force results in a direction closely aligned with major fixation interfaces, causing increased stress at the bone-implant interface (Scarlat and Matsen, 2001; Gunther et al., 2002; Nho et al., 2009). Additionally, the humeral head translates inferiorly and superiorly during daily motion producing eccentric forces on the glenoid rim, which ultimately causes an edge deformation or rim loading. This phenomenon has been shown to be correlated to patients with postoperative rotator cuff tear (Braman et al., 2006; Moore et al., 2017).

Table 2.17 Summary of previous rTSR ex vivo studies' methods and results

Author	Cohort of *ex vivo* shoulder devices	Average time *in vivo* (months)	Type of analysis	Results
Kurdziel *et al.* (2018)	32	25 ± 16 (range, 3.6 to 56.8)	Micro-computed tomography technique	Volumetric wear: 181 ± 208 mm^3 Wear rate: 115 ± 160 mm^3/year
Lewicki *et al.* (2017)	10	27 ± 35 (range, 1.5 to 107.6)	Coordinate measurement machine protocol	Volumetric wear: 27 ± 37 mm^3 Wear rate: 470 mm^3/year (maximum)
Wiater *et al.* (2015)	50	20 (range, 0 to 81.5)	Wear damage mode analysis	Scratching (86%), pitting (72%), and burnishing (52%)
Day *et al.* (2012)	7	25 ± 8 (range, 15.6 to 39.6)	Micro-computed tomography + optical microscopy	Rim wear damage with a penetration depth of 0.1 to 4.7 mm.
Nam *et al.* (2010b)	14	6 ± 6 (range, 0.7 to 23.0)	Wear damage mode analysis	Scratching (100%), abrasion (93%), and pitting (43%)

Table 2.18 Summary of previous aTSR ex vivo studies' methods and results

Author	Cohort of *ex vivo* shoulder devices	Average time *in vivo* (months)	Type of analysis	Results
Moore *et al.* (2017)	50	68 (range, 2 to 267)	Wear damage mode analysis	Scratching, dishing, and/or pitting (70%), edge deformation (58%), and delamination (14%)
Nho *et al.* (2009)	78	48 ± 53 (range, 1.2 to 230.4)	Wear damage mode analysis	Scratching (100%), pitting (94%), burnishing (69%), and abrasion (68%)
Braman *et al.* (2006)	20	NA	Laser surface scanning	Three different patterns of wear: " radial mismatch" , " diffuse" , and " rim"
Gunther *et al.* (2002)	10	53 (range, 7 to 198)	Wear damage mode analysis	Scratching (90%), abrasion (68%), pitting (60%), and delamination (58%)
Scarlat and Matsen (2001)	39	30 ± 20 (range, 1.8 to 79.3)	Observation of the surface contours	Rim erosion (68%), surface irregularities (68%), fracture (29%), and central wear (22%)

NA: data not available.

2.13 IN SILICO WEAR OF SHOULDER REPLACEMENTS

Terrier *et al.* (2009) developed a finite element mathematical model to estimate the UHMWPE wear performance (*non-crosslinked*) on anatomical and reverse total shoulder replacements (Aequalis™; Tornier Inc., Edina Minnesota). This model simulated the metal–on–polyethylene volumetric wear over a period of one year (one million cycles, under with a maximum loading of 750 N), based on the kinematic data collected (arm position; abduction) during the daily activities from 31 healthy individuals (Coley *et al.*, 2008).

This mathematical musculoskeletal model included the scapula, the proximal part of the humerus, and six scapulohumeral muscles, where the bones were rigid, and the muscles were deformable and could contract. For the reversed prosthesis, the muscles of the rotator cuff were deactivated, since this configuration is used when these muscles are partly or completely deficient. The metallic components were assumed to be rigid, while the polymeric components were elastic (E (elastic modulus) = 500 MPa, v (Poisson's ratio) = 0.4). Their wear model in combination with Archard wear model estimated that aTSR (48 mm diameter with a radial mismatch of 6 mm) would show a wear rate of 8.4 mm^3 per year compared to rTSR (36 mm diameter perfectly congruent); which generate as much as five times more wear 44.6 mm^3 in 1 year. The notable disparity between the volumetric wear values among both shoulder prostheses can be associated with the magnitude of the glenohumeral contact pressure on the polyethylene, as it has been estimated to be approximately 20 times lower for the reversed (1.2 MPa) than for the anatomical prosthesis (19 MPa). The design of the polyethylene humeral component in rTSR provides a more conforming articulating surface with lower contact pressure in contrast with the glenoid insert in aTSR.

Additionally, the differences in the design of the rTSR articular components provide a more conforming surface with lower contact pressure in contrast with aTSR. However, the difference in volumetric wear suggested in this computational modelling has not been yet supported by clinical studies. To date, no volumetric wear rates have been assessed during aTSRs retrieval analysis, as is the case with rTSRs, where wear rates (range,115 to 470 mm^3 per year) have been reported to be greater than the value obtained by Terrier *et al.* (2009).

Chapter 3. Materials and Methods

3.1 Materials

This section will provide a general overview of the pristine anatomic and reverse total shoulder components tested as part of the *in vitro* shoulder wear simulator studies and the worn retrieved reverse total shoulder implants used for the *ex vivo* assessment study (**Figure 3.1**).

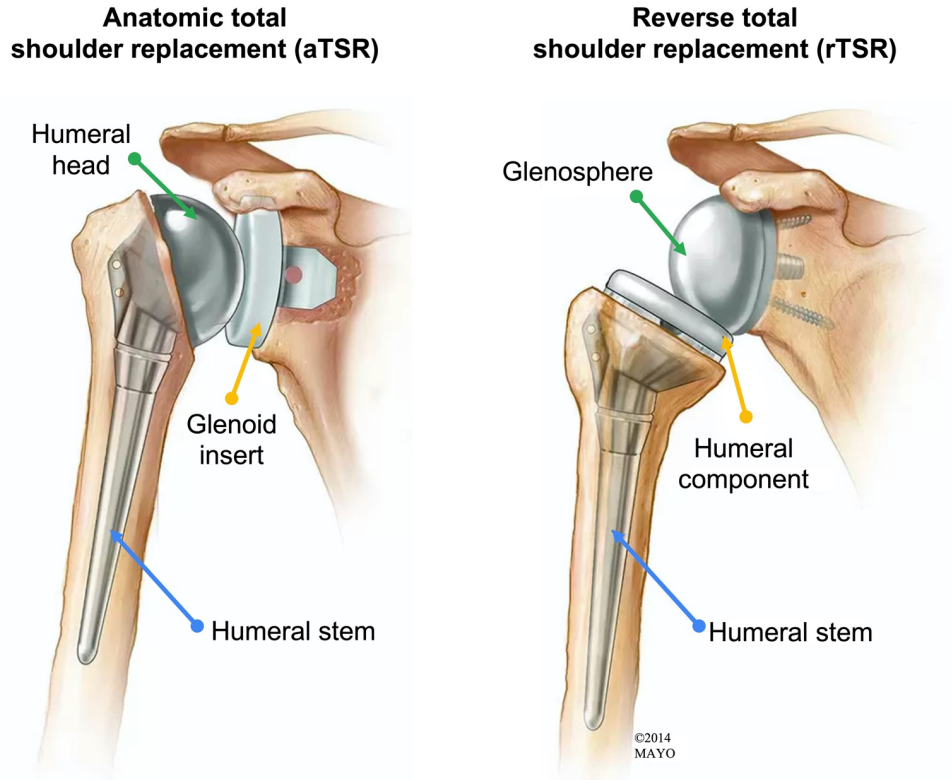

Figure 3.1 On the *left* is a standard (anatomic) total shoulder replacement. The components of the humeral head (ball) and glenoid insert (cup) are reversed on the *right*: a reverse total shoulder replacement. Adapted from Torborg (2014)

3.1.1 In vitro simulator components

As the wear of UHMWPE in replacement shoulder joints has been recognized as a critical concern, shoulder wear simulator tests under adverse conditions were carried out to determine the wear performance in two different bearing combinations and designs. First, a reverse total shoulder replacement using metal–on–polyethylene (MoP). Second, an anatomic total shoulder replacement using PyroCarbon–on–polyethylene bearings (PyCoP).

3.1.1.1 Reverse total shoulder replacement

Four new 42 mm diameter CoCr glenospheres and *conventional non-crosslinked* UHMWPE humeral components (VAIOS® Reverse Shoulder System; JRI Orthopaedics, Sheffield, UK) were wear tested. The glenospheres had a nominal radius of 21.0 mm, while that of the humeral inserts was 21.1 mm. The CoCr glenospheres had a 6.5 mm diameter hole through the pole, this allows for the option of using a locking screw *in vivo*.

As shown in **Figure 3.2**, humeral components were mounted parallel to the horizontal plane in the test chambers, with the glenosphere component above to form a reverse total shoulder replacement. Each glenosphere component was held in a titanium taper, specially designed and manufactured to reproduce the clinically relevant support provided by the titanium baseplate during *in vivo* time.

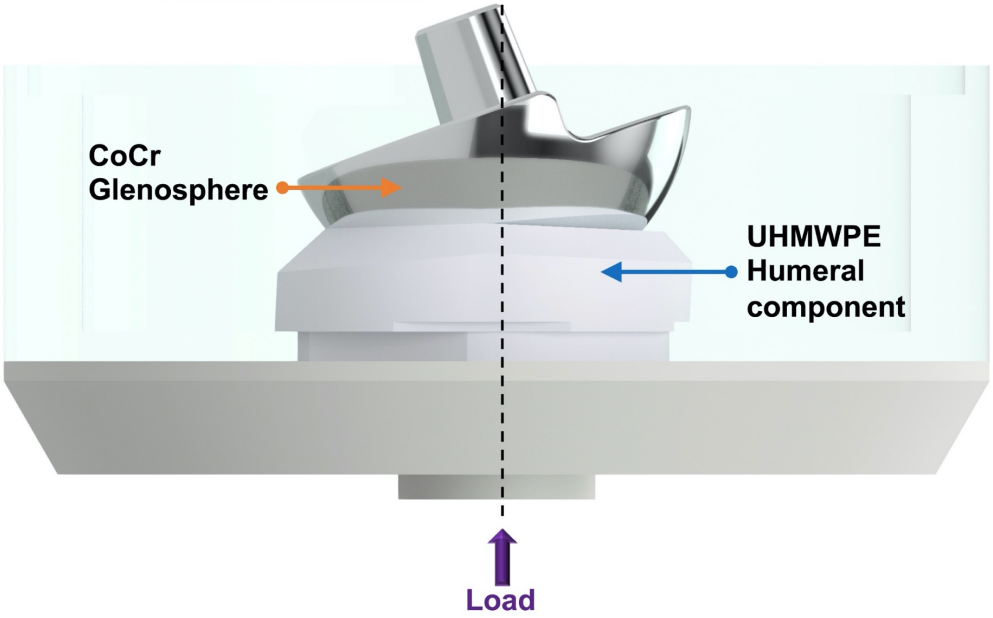

Figure 3.2 Schematic diagram of MoP reverse total shoulder implant used in the wear test

3.1.1.2 Anatomic total shoulder replacement

The shoulder implants tested consisted of four new Aequalis™ PerFORM UHMWPE (*non-crosslinked*) glenoid inserts and Aequalis™ PyroCarbon hemiarthroplasty humeral heads components (Tornier SAS; Montbonnot–Saint–Martin, France).

The PyroCarbon humeral head implant was assembled on a cobalt-chromium metallic male trunnion, and for this test was mounted on top of the UHMWPE components to form an anatomic total shoulder replacement with a radial mismatch of 4 mm. A superior/anterior translation of 1.5 mm was applied, to replicate the sliding motion in the GH joint (Graichen *et al.*, 2005; Matsuki *et al.*, 2012). Each PyroCarbon humeral head component was held in a titanium taper, specially designed and manufactured to reproduce the clinically relevant support provided by the titanium baseplate during *in vivo* time as shown in **Figure 3.3**.

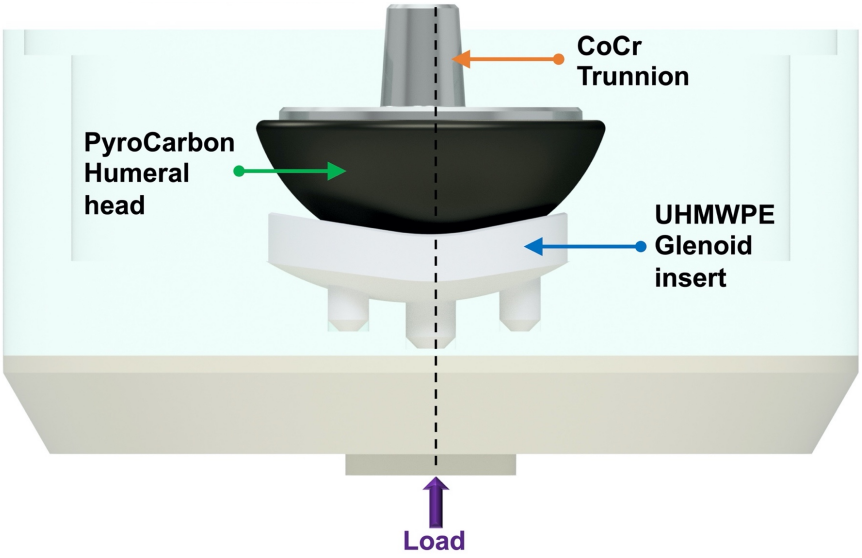

Figure 3.3 Schematic diagram of PyCoP anatomic total shoulder implant as mounted for the wear test

Glenoid insert components had a pear-shaped contour that reproduced the anatomical shape of the glenoid whit a nominal articulating radius of curvature of 17.5 mm, while the humeral head components had a nominal radius of curvature of 21.5 mm and spherical-shaped. The value of radial mismatch in this system was selected according to Schoch *et al.* (2017), who after evaluating multiple studies, suggested a range between 4 mm and 8 mm radial mismatch for anatomic total shoulder arthroplasty.

3.1.1.3 Fixturing components

The glenospheres and the humeral heads (upper components) were press-fitted into Ti-6Al-4V tapers, which were bolted onto CoCr holders and then screwed into the upper position of the simulator stations (**Figure 3.4)**. A reference marked line was used on the shoulder components as an alignment guide to ensure repeatable positioning of the components through the test after cleaning procedure.

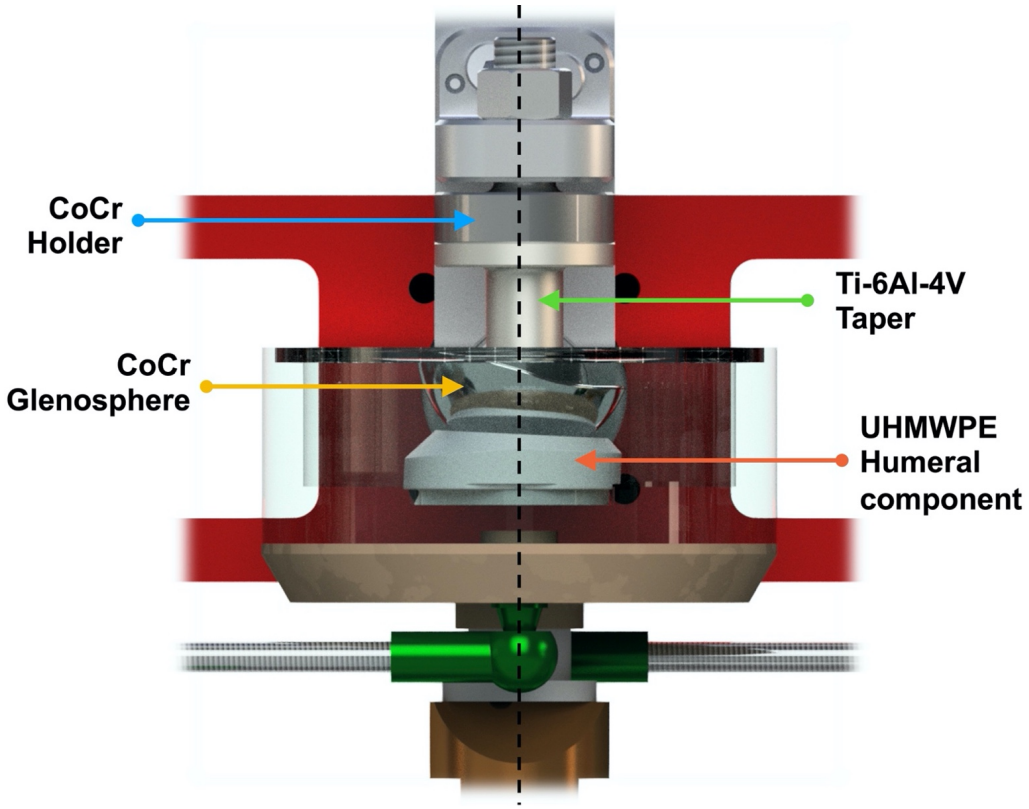

Figure 3.4 Schematic diagram fixturing components

The humeral components and the glenoid inserts (lower components) were mounted below the upper components in a lubricant bath chamber to ensure more consistent wetting of the bearing surfaces (Brown and Clarke, 2006). Each chamber was covered by a two-piece lid, which reduced the risk and amount of lubricant contamination and evaporation, while still allowing large ranges of motion.

3.1.2 Ex vivo shoulder components

Thirteen (13) reverse total shoulder prostheses were obtained from revision surgeries at the Rizzoli Orthopaedic Institute (Bologna, Italy). Clinical data including shoulder number, manufacturer, age at revision surgery, gender, primary diagnosis, revision diagnosis and time *in vivo* are presented in **Table 3.1**.

As also presented in **Figure 3.5**, the 13 reverse total shoulder explants were of different designs and from different manufacturers, including SMR® Reverse Shoulder System and SMR® Reverse HP Shoulder System (Lima Corporate, Villanova di San Daniele del Friuli, Udine Italy; $n = 6$), Trabecular Metal™ (Zimmer Biomet, Warsaw, Indiana, U.S.; $n = 2$), Delta Extend™ (DePuy Synthes, Warsaw, Indiana, U.S.; $n = 1$), Affinis® Inverse (Mathys Ltd., Bettlach, Switzerland; $n = 1$), Duocentric® Expert (Aston Medical, Saint–Étienne, France; $n = 1$), Aequalis™ Reversed II (Tornier SAS–Wright Medical Inc., Bloomington, Minnesota, U.S.; $n = 1$), and Humelock™ Reversed (FX Solutions, Viriat, France; $n = 1$).

In 9 out of the 13 cases, the glenosphere was metallic (*conventional* bearing materials); seven were made of cobalt-chromium alloy (CoCr), one of stainless steel and one of titanium alloy (Ti-6Al-4V). The diameter of the metallic glenosphere was 36-mm for seven cases (78%), 38-mm in one case (11%), and 40-mm for the remaining case (11%). In the other four explants (*inverted* bearing materials), the glenosphere component was made of polyethylene material with a diameter of 39-mm in one case (25%), 40-mm in two cases (50%), and 44-mm in the final case (25%). Among the retrieved glenosphere components, 10 of the 13 cases (77%) had a central hole to allow use of a fixation screw *in vivo*.

A glenoid baseplate with location for locking screws was used in 12 cases, between one and four screws were used for baseplate fixation. Among the humeral stems, six were uncemented (46%) and the other four were cemented (31%). Three retrieved cases (23%) did not include a stem component.

Table 3.1 Clinical information for the thirteen rTSR prostheses

	Shoulder No.	Manufacturer	Age at revision	Gender	Right *or* left	Primary diagnosis	Revision diagnosis	Time *in vivo* (months)
Conventional bearing material	1	Aston Medical	50	M	L	Revision	Loosening humeral component	25
	2	DePuy Synthes	82	F	L	Fracture	Septic loosening	24
	3	FX Solutions	72	F	L	Revision	Recurrent dislocation	24
	4	Lima Corporate	70	M	L	Fracture	Recurrent dislocation	6
	5	Lima Corporate	70	F	R	Arthrosis	Septic loosening	15
	6	Lima Corporate	74	F	R	Fracture	Septic loosening	22
	7	Tornier	71	M	L	NA	Septic mobilization	3
	8	Zimmer Biomet	77	F	L	Revision	Recurrent dislocation	8
	9	Zimmer Biomet	78	M	R	NA	Septic loosening	5
Inverted bearing material	10	Lima Corporate	70	F	R	Dislocation	Recurrent dislocation	1
	11	Lima Corporate	75	F	R	Fracture	Septic loosening	17
	12	Lima Corporate	81	F	R	NA	Septic loosening	22
	13	Mathys	72	M	R	Arthrosis	Septic loosening	36

NA: data not available.

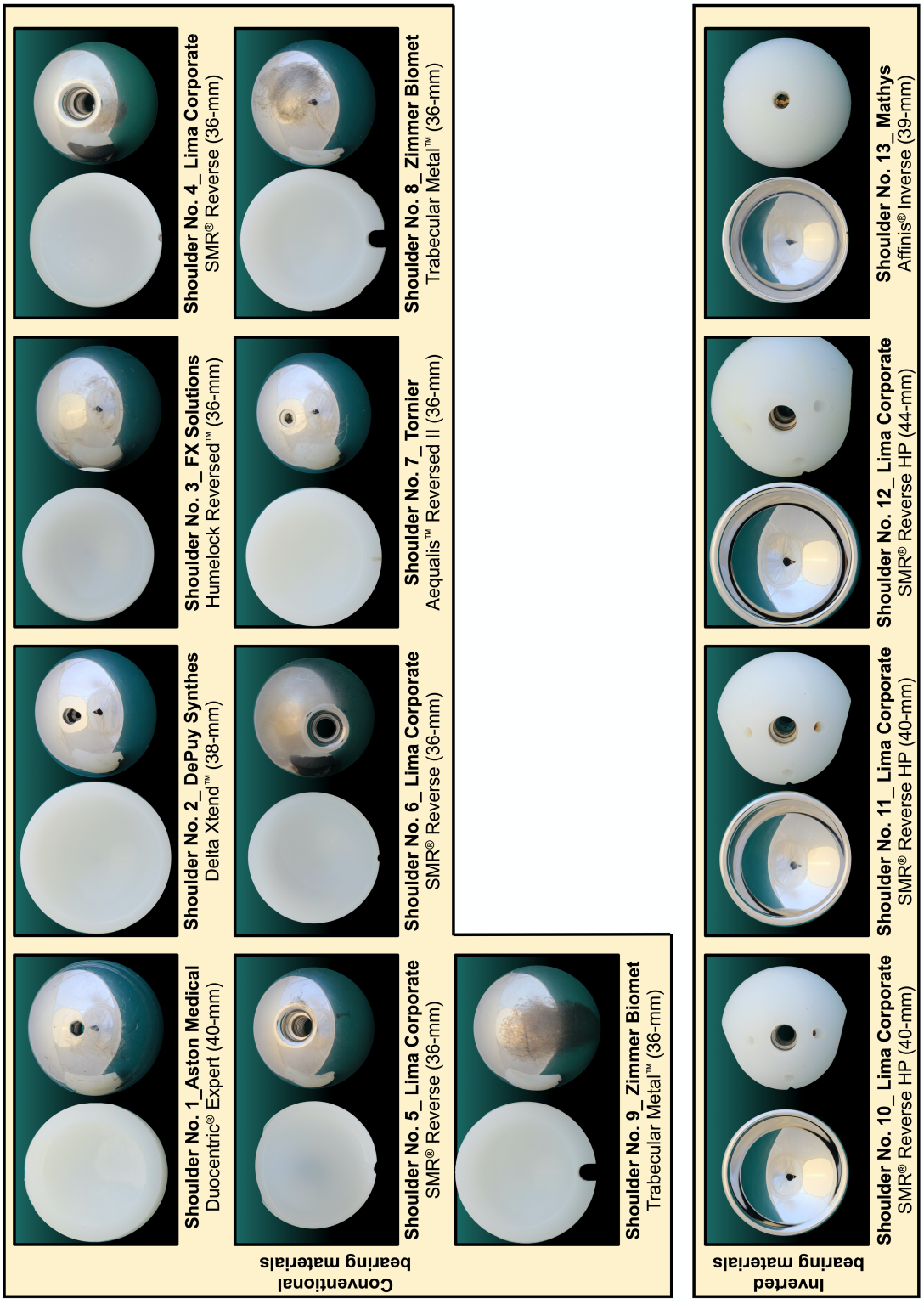

Figure 3.5 Overview of the rTSR studied components

3.2 GENERAL METHODS

3.2.1 Cleaning protocol

The wear simulator components were cleaned every 500,000 cycles, when the simulator was stopped (equating to approximately 5 days) and the *serum* was collected in individual bottles and frozen at -18°C. Tested components were carefully removed from the test stations to be cleaned, air dried and weighed (**Table 3.2**) based on the International Organization for Standardization (ISO) specification given in ISO 14242 (2016) "Implants for surgery - Wear of total hip-joint prostheses", as there is no similar ISO protocol for shoulder prostheses. Components were visually examined for any damage due to the wear test.

Table 3.2 Cleaning protocol procedure

1. Wear powder free blue nitrile gloves:
➢ Vibrate for 10 minutes ultrasonic bath with deionized water; ➢ Rinse in deionized water; ➢ Vibrate for 10 minutes in 50 mL of ultrasonic cleaner and 250 mL of deionized water; ➢ Rinse in deionized water; ➢ Vibrate for 10 minutes in deionized water; ➢ Rinse in deionized water; ➢ Vibrate for 3 minutes in deionized water; ➢ Rinse in deionized water.
2. Wear powder free indigo nitrile gloves:
➢ Dry the components carefully using lint-free cloths; ➢ Dry the component with a jet of inert gas; ➢ Soak the components in isopropanol for 5 minutes ± 15 seconds; ➢ Dry the components carefully using lint-free cloths; ➢ Dry the component with a jet of inert gas; ➢ Air dry the components for at least 12 hours.

In the case of the *ex vivo* components and prior to analysis, all components were washed in an ultrasonic bath with a cleaning solution (50 mL of ultrasonic cleaner in 250 mL of deionized water) for 5 minutes, rinsed in distilled water, wiped carefully with isopropanol using a lint free cloth, dried with a jet of inert gas and then allowed to air dry for 12 hours. The shoulder explants were then photographed using an 18-megapixel digital camera (EOS 600D; Canon Inc., Tokyo, Japan) in a combination with a 100 mm macro lens.

3.2.2 Gravimetric wear measurements

Gravimetric measurements were carried out to determine the mass loss of the pristine shoulder components tested in the wear simulator. Mass change was not determined for the retrieved components, as no pre-implantation mass data was available for comparison.

Each *in vitro* tested component was weighed three times to ensure repeatability at regular interval every 500,000 cycles, which corresponded to the lubricant change intervals when the specimens were removed from the wear testing machine (Section 3.2.1 Cleaning protocol), using an analytical balance (TB-215 D; Denver Instruments, Germany) with a readability of 0.1 mg and the arithmetic mean and standard deviation were calculated. If the three measurements were found to deviate by more than 10 µg, the measurement was repeated.

The difference between the mass before and after undergoing a certain number of wear cycles; and after being compensated by the weight change due to the lubricant uptake (soak control) corresponds to the amount of material lost due to wear.

3.2.3 Soak control

The uptake in the UHMWPE shoulder components may affect the accuracy of the wear measurements, and therefore, can have a crucial impact on the estimation of wear rates. Therefore, during both *in vitro* studies, a fifth shoulder prosthesis of the same size and design was used as a "soak control" and subjected only to the same loading profiles without motion in a dedicated control test station (**Figure 3.6**), thereby causing the same amount of fluid uptake without the loss of material or wear.

Any uptake of lubricant (mass gain) by the test components was accounted for by using data from the control station at each measurement interval, allowing the true material loss to be determined. These control components were subjected to the same cleaning and weighing protocol as the test components.

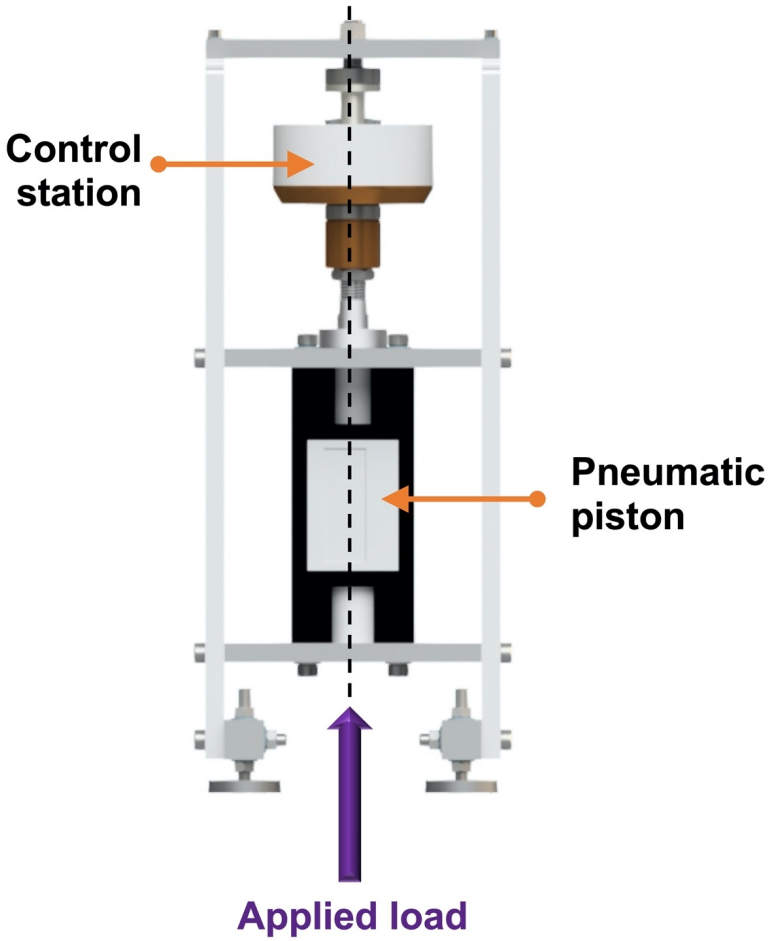

Figure 3.6 The six non-articulating but loaded station to provide a loaded soak control for gravimetric measurements

3.2.4 Volumetric wear measurements

Mass loss was subsequently converted into volume loss (mm^3) using a density values of 0.938 mg/mm^3 for UHMWPE (Kurtz, 2016), 8.330 mg/mm^3 for CoCr (Hasirci and Hasirci, 2018b) and 1.930 mg/mm^3 for PyroCarbon (Carpenter *et al.*, 2016) components respectively.

The wear rates of the tested components were then calculated using the slopes of the linear regression lines (volume loss as a function of the number of cycles; mm^3/million cycles).

3.2.5 Surface roughness assessment

The surface roughness of each articulating surface was evaluated using a NewView 5000™ non-contacting white light profilometer (**Figure 3.7**) equipped with advance texture analysis MetroPro® software (Zygo; Zygo Corporation, Middlefield, CT, U.S.). The profilometer had an out-of-plane (vertical) resolution of 0.001 μm in a field of view of 0.3 by 0.4 mm (Joyce *et al.*, 2009; Joyce *et al.*, 2011b).

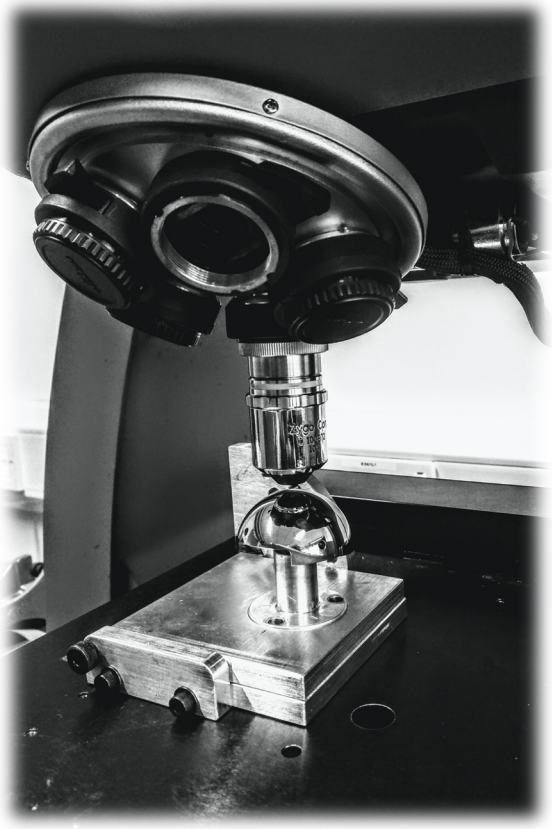

Figure 3.7 Three-dimensional (3D) surface roughness measurements using Zygo NewView™ 5000 on CoCr glenospehre component

The assessment of the intricate surface roughness of each component can provide an insight into the changes in the surface topography during *in vitro* or *in vivo* time and how these changes may have affected the performance of the prosthesis. Surface roughness parameters can typically be categorised into three groups depending on its functionality: amplitude parameters, used to measure vertical characteristics of the surface deviations; spacing parameters, used to measure horizontal characteristics of the surface deviations; and hybrid parameters, a combination of both amplitude and spacing.

Roughness parameters could be calculated in either two-dimensional (2D) or three-dimensional (3D) forms. 2D roughness parameters are calculated measuring a single line across the surface area analysed, while 3D roughness parameters are calculated for the entire surface area. If parameters are evaluated on the 3D surface, parameters are denoted with the capital letter "S".

For the purpose of this study, amplitude parameters were used (arithmetic average height (S_a), root mean square roughness (S_q), and skewness (S_{sk})), as these parameters may describe the effect of the surface contact during the shoulder wear simulations and the change of the surface topographies of the retrieved components. The surface roughness result parameters will be presented in different profile indicators based on ISO 25178 (2012) "Geometric product specification (GPS) –Surface texture", which are described in **Table 3.3**.

Due to the variations in size (range, 36 mm to 44 mm in diameter) and geometrical shape (glenosphere, humeral component, humeral head, and glenoid insert) across the shoulder implants, no single set of points could be defined for taking the measurements on all samples. Therefore, measurements were made depending on the type of shoulder replacement in the case of the *in vitro* tested components, and at the discretion of the operator in the case of the *ex vivo* components; attempting to represent the entirety of each valid region with a minimum number of 76,000 valid data points acquired during the measurements. The ZYGO sphere remove filter was used on the convex and concave components so that surface roughness values could be obtained.

An adjustable baseplate with 90 degrees from horizontal to a vertical platform position as well as 360 degrees rotation about the vertical axis, was designed and manufactured for setting up the analysed components. The tapered fixture with the shoulder component was then mounted in the baseplate platform and positioned at one of eighteen discrete angles using a locking screw.

Table 3.3 Description of 3D surface roughness parameters selected

Parameter	Definition	Selection Criteria
Arithmetic average height of the surface, S_a	$S_a = \frac{1}{A}\iint_A \lvert z(x,y)\rvert dxdy$	S_a is the most common roughness parameter to describe and quantify surface texture on orthopaedic components. It provides a good overall description of height variations on the surface.
Root mean square height of the surface, S_q	$S_q = \sqrt{\frac{1}{A}\iint_A z^2(x,y)dxdy}$	Because height values are squared in the calculation, S_q roughness statics are more sensitive to deviation from main line (highs and lows), making it a valuable complement to S_a. S_q parameter is also useful to define the surface separation between bearing surfaces.
Skewness of height distribution, S_{sk}	$S_{sk} = \frac{1}{S_q^3}\left[\frac{1}{A}\iint_A z^3(x,y)dxdy\right]$	A positive S_{sk} value means a predominance of peaks on the sampling area and a negative S_{sk} value suggests more pronounced valleys along the surface profile. The skewness of a surface could provide insight on whether material has been removed (abrasive wear) or added (adhesive wear) during the time.

*Note:
The surface roughness values of pristine implant components depend on its manufacturing methods.
Hence, S_a (absolute magnitude of the surface heights) should be used cautionary, as different processes (e.g., ground vs. polished) can lead to the same surface roughness value, but with grossly different surface characteristics.

3.2.5.1 In vitro metal–on– polyethylene; rTSR

Every 500,000 cycles, two-dimensional surface roughness (R_a) and three-dimensional surface roughness (S_a) readings were taken at the pole, at four points 10°, and at 20° from the pole in a defined pattern on the humeral components and at the glenospheres as can be seen in **Figure 3.8**. The 10× objective lens was used and combined with a 2× manual zoom, resulting in a field of view of 75,446 µm^2 (317 × 238 µm). A total of nine and eight measurements were taken for the UHMWPE humeral component and the CoCr glenosphere respectively, and the mean roughness parameters and standard deviations were then calculated for the evaluation of the articulating surfaces.

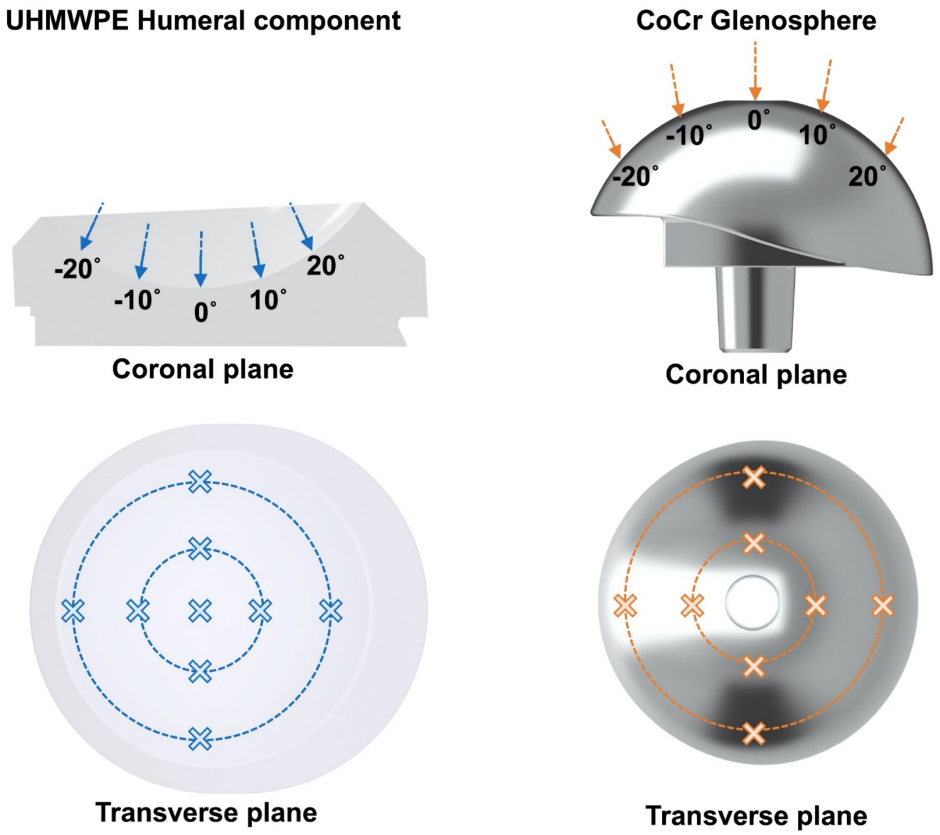

Figure 3.8 Surface roughness measurement points pattern for UHMWPE humeral component (*left*) and CoCr glenosphere (*right*)

3.2.5.2 In vitro PyroCarbon–on–polyethylene; aTSR

Every 500,000 cycles, three-dimensional surface roughness (S_a) readings were taken in a defined pattern on the glenoid inserts and at the humeral heads; starting at the polar then at four points 10°, and at 25° from the pole as shown in **Figure 3.9**. The 10× lens was used and combined with a 2× manual zoom, giving a field of view of 75,446 μm^2 (317 × 238 µm). A total of ten measurements were taken for each component (UHMWPE glenoid inserts and PyroCarbon humeral heads), and the mean roughness parameters and standard deviations were then calculated for the evaluation of the articulating surfaces.

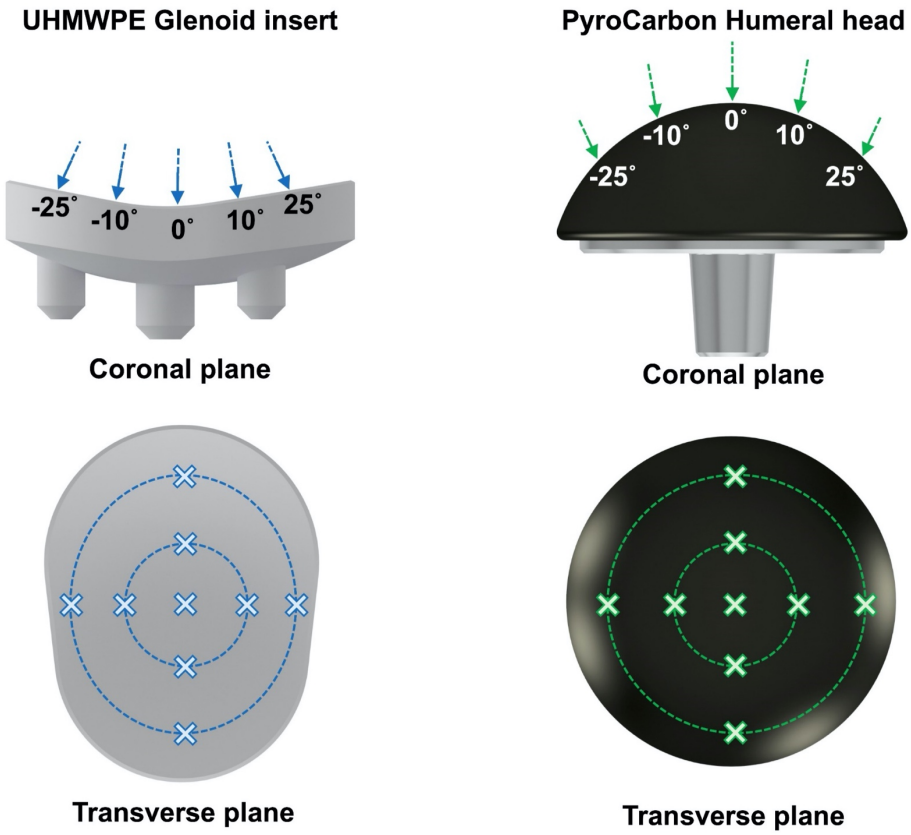

Figure 3.9 Surface roughness measurement points pattern for UHMWPE glenoid insert component (*left*) and PyroCarbon humeral head (*right*)

3.2.5.3 Explanted components, metal–on–polyethylene

For the polymeric components, three-dimensional measurements (S_a, S_q, S_{sk}) were taken using a 10× objective lens and combined with a 1× manual zoom, the field view was sampled in 634 × 475 μm. The measuring points were taken in a defined pattern on the glenosphere (*inverted* bearing component) and humeral insert (*conventional* bearing component) with a total of twenty to twenty-one readings points sampled from the articulating surface of each component, corresponding to a total of 248 independent observations.

In the case of the metallic components, two different regions were considered, the unworn surface finish area and areas with dense light scratching (worn). The 10× lens was used with a 2× manual zoom, giving a field of view of 317 × 238 μm. A total of fifteen region points was taken corresponding to a total of 195 independent observations.

A larger area of view was used for the polymeric components compared to the metallic components as these polymeric components, as might be expected, tended to have higher roughness values and showed greater damage area. The surface roughness of the polymeric component of the shoulder sample number 6 (Lima Corporate, SMR® Reverse) was not possible to examine, due to disassembly complications, therefore it was excluded from the roughness analysis.

For a visual comparison of the retrieved surfaces, the pole region at the centre of the humeral insert component was chosen, while in the glenosphere components a region at 25 degrees tilt from the pole region was selected. The difference between the regions selected was due to the fact that some glenosphere explants have a central hole in the pole region, which restricted a comparative analysis of the surface topography. The ZYGO “remove sphere” filter was used on the concave and convex geometries of the articulated components, so that surface roughness values could be obtained.

3.2.6 Data and statistical methods

Data collected were statistically analysed using Minitab® 17.1.0 Statistical Software (State College, PA: Minitab, Inc.). Throughout the present study, the mean values were calculated for all the parameters along with standard deviation (SD).

In the *in vitro* shoulder simulator, pre and post-test dependent surface roughness measurements of the articulated bearing components were evaluated using a paired t-test to determine whether there was a significant difference. A scatter plot was used to observe and show the relationship between the mean volumetric wear and the number of cycles, while bar graphs were used to show how the surface roughness changed over the test. For all analysis, a ρ-value of less than 0.05 was considered to show significant difference within 95% confidence.

A two-sample student's t-test was used to determine whether there is a significant difference between two independent data set during the assessment of the retrieved components. To explore the potential effect of clinical data (age at surgery, gender, and duration of implantation *in vivo*) and surface roughness measurements in the retrieval study, linear regression and Pearson's correlation analysis were performed. Data were presented as median and quartiles (25%, 75%), as appropriate using box plots. The black line shows the median value, and the "×" the mean values of the groups. For all analysis, a ρ-value of less than 0.05 was considered to show significant difference.

3.3 DEVELOPMENT OF SHOULDER WEAR SIMULATOR PROTOCOL

At present, there is no agreed international standard on wear testing of artificial shoulder joints. Although a standard for testing shoulder prostheses does exist, ASTM F2028 (2017), "Standard test methods for dynamic evaluation of glenoid loosening or disassociation", it is not a wear test, rather a mechanical stability test based on the concept of "rocking horse effect" (Franklin *et al.*, 1988) and the work by Anglin *et al.* (2000). This test protocol does not require any type of lubrication, it applies unidirectional motion and load on a glenoid component, and the overall duration is relatively low at 100,00 cycles.

In contrast, international standards have been developed and implemented for the wear testing of hip ISO 14242 (2014) "Implant for surgery- Wear of total hip-joint prostheses" and knee implants ISO 14243 (2009) "Implant for surgery- Wear of total knee-joint prostheses", where a repeated motion under dynamic loading is generally applied for typically five million cycles in a dedicated simulator with a varying degree of complexity. These simulators apply and reproduce the loading and motion patterns experienced by the lower limb joints during gait conditions of human beings while the test implants are immersed in a lubricant that mimics the synovial fluid. Unidirectional motion and reciprocating motion have been used in previous studies to pre-evaluate the wear performance of different clinical bearing materials (Section 2.8 Wear Testing). Here, pin-on-disk wear tester machines drive simplified and controlled motion under a constant load.

In the case of shoulder implants, the addition of a static load, regularly interspersed with a repeated motion under dynamic loading, might cause increased damage to the implants. While the addition of a static load is uncommon in the tribological testing of artificial joints, such loading is probably more clinically relevant than a joint undergoing, say, 1 million cycles, without stopping. Also, there is the potential that, at each 'start-up' of the bearing, there will be contact between the two surfaces and so the hard component (CoCr) could remove material from the softer counterpart (UHMWPE). In other words, the regular inclusion of a static load with no motion could lead to increased wear.

3.3.1 Commissioning work

Prior to the author's work on the Newcastle Shoulder Wear Simulator, the simulator had accumulated over 11 million cycles in service over a 3-years period (Smith *et al.*, 2015; Smith *et al.*, 2016; Smith *et al.*, 2018). During these studies, an evident hysteresis was noticed between the request motion (physiological) and the final motion performed by the simulator during the commissioning trials. These values were reported by Smith *et al.* (2016) as a root square mean error over a cycle, being 3.3° in flexion/extension, 1.4° in abduction/adduction, and 2.0° in internal/external rotation (**Figure 3.10**).

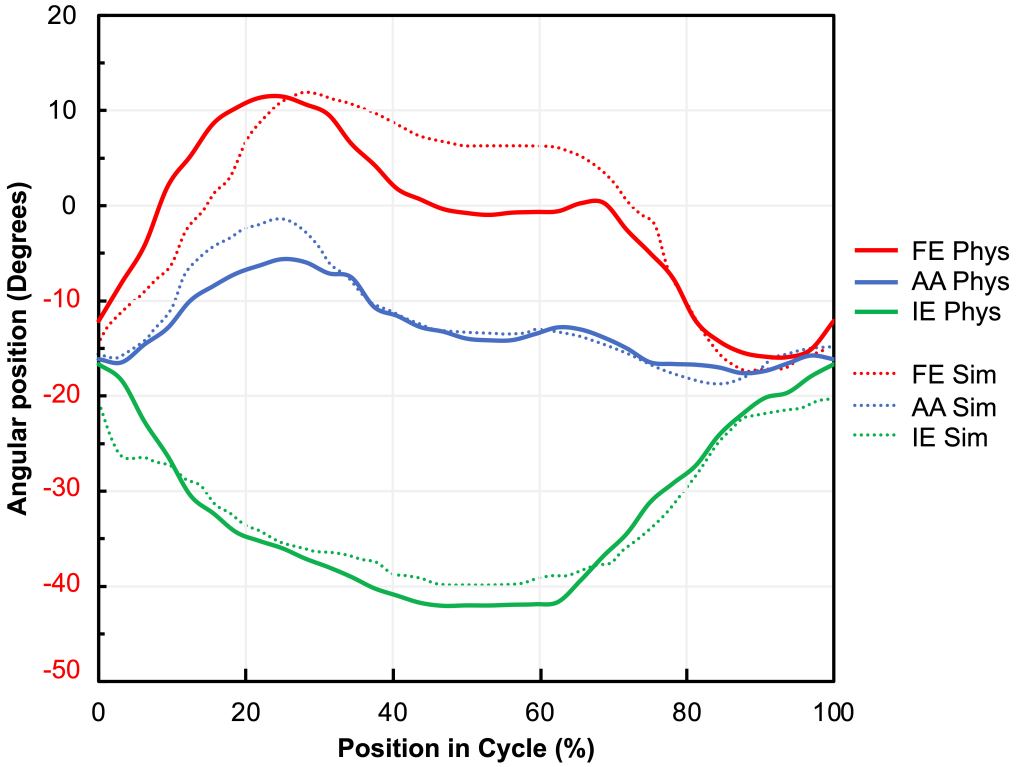

Figure 3.10 The physiological (solid lines) and simulator (dotted lines) motion cycles in each of the three axes (flexion/extension (FE), abduction/adduction (AA) and internal/external (IE) rotation) for "mug to mouth" ADL

In general, the lifetime of pneumatic cylinders and ball bearings are fairly well-controlled due to the availability of new materials and improved production processes; however, these components have a finite life. Based on the large number of cycles performed during the previous tests, the finite life of the components, and the hysteresis reported, the three pneumatic pistons responsible for applying the movement were dismounted from the simulator, disassembled, and the major parts were cleaned. The solenoids of the proportional valves were cleaned out using a piece of lint-free material

to remove any moisture from the fitting or housing. All the angular contact ball bearings from the simulator were also replaced with brand-new components. In addition, the script code in LabView was rewritten, changing some of the true/false conditions, and a series of low-pass sign filters were incorporated in order to eliminate the slight lag between the signals.

Together, mechanical and computational modifications achieved an optimized final performance of the Newcastle Shoulder Wear Simulator, which compensated in its totality the lag between the request (physiological) and response (simulator) signal (**Figure 3.11**). Additional to these modifications, a new user's interface was created, which allowed visualization and recording of each motion and loading profile during the test course.

3.3.2 Repeated–motion–load protocol (RML)

A novel protocol (repeated–motion–load, RML) was developed based on the combination of two challenging activities of daily living in patients with shoulder joint replacements. These realistic activities have been previously shown to be two of the twelve most challenging ADLs (**Table 3.4**) during a trial in 12 patients with implanted reverse total shoulder replacements (Masjedi and Johnson, 2010). Specially, "mug to mouth" or when a person lifting a cup to their mouth offered the widest range of motion and "lift to shoulder height (0.5 kg)" one of the highest glenohumeral forces.

Table 3.4 Activities of daily living

Task protocol	
1. *Mug to mouth (drinking)*	7. *Pouring from kettle standing (5 N)*
2. *Reach to the opposite axilla*	8. *Lift shopping bag (2 kg)*
3. Wash lower back	9. *Lift tray (0.5 kg) use both hands*
4. *Brush opposite side of head*	10. *Sitting position lift to shoulder height (0.5 kg)*
5. *Answer telephone*	11. *Reach to as far as you can*
6. *Pouring from kettle sitting (5 N)*	12. *Sitting position lift to head height (0.5 kg)*

Resting periods (e.g., 2 to 5 seconds interval) during the frequency and duration of daily activities in patients after a total shoulder arthroplasty compromise a substantial

part of day-to-day life. Thus, the continuous motion used in previous shoulder simulator studies may not represent *in vivo* conditions.

Therefore, the RML protocol consists of 100 cycles of real patient activity pattern of "mug to mouth" followed by 5 seconds of "lift block to shoulder height". The latter comprised a high peak load of 450 N with no motion. This "high" load value represents a severe and realistic condition during the RML protocol, as in a finite element study a maximal joint force was calculated for a reverse shoulder prosthesis resulting in a value of 313 N (Terrier *et al.*, 2008).

"Mug to mouth" was employed in an earlier wear test of 42 mm VAIOS® (without central hole for fixation) reverse shoulders (Smith *et al.*, 2015), therefore a direct comparison of the effect of adding in a repeated static load was achieved. **Figure 3.11** shows the "mug to mouth" physiological motion and load cycle, which had a range of motion of: –16º to +11º in flexion/extension (FE), –18º to –6º in abduction/adduction (AA) and –42º to –17º in internal/external rotation (IE), while the dynamic load ranged from 180 N to 250 N. One cycle of "mug to mouth" takes 1 second to complete.

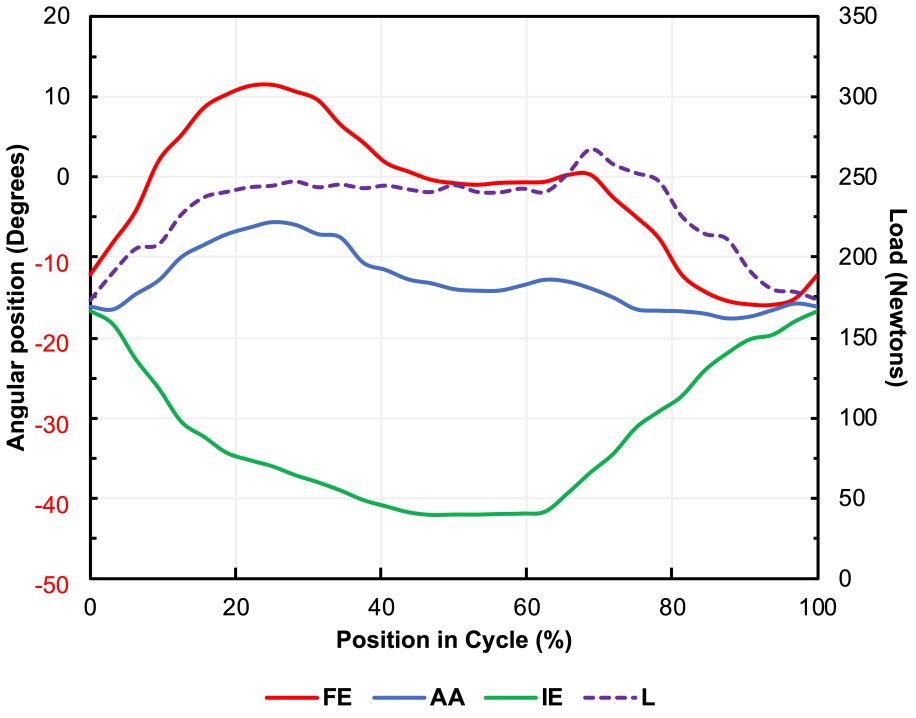

Figure 3.11 Physiological motion (flexion/extension (FE), abduction/adduction (AA) and internal/external (IE) rotation) and load cycle applied during "mug to mouth". L=load

3.3.3 Testing setup

To undertake the five million cycles wear simulations, the Newcastle Shoulder Wear Simulator was used (Smith *et al.*, 2015; Smith *et al.*, 2016; Smith *et al.*, 2018), as there was not a commercially available equipment at the commencement of this work (**Figure 3.12**).

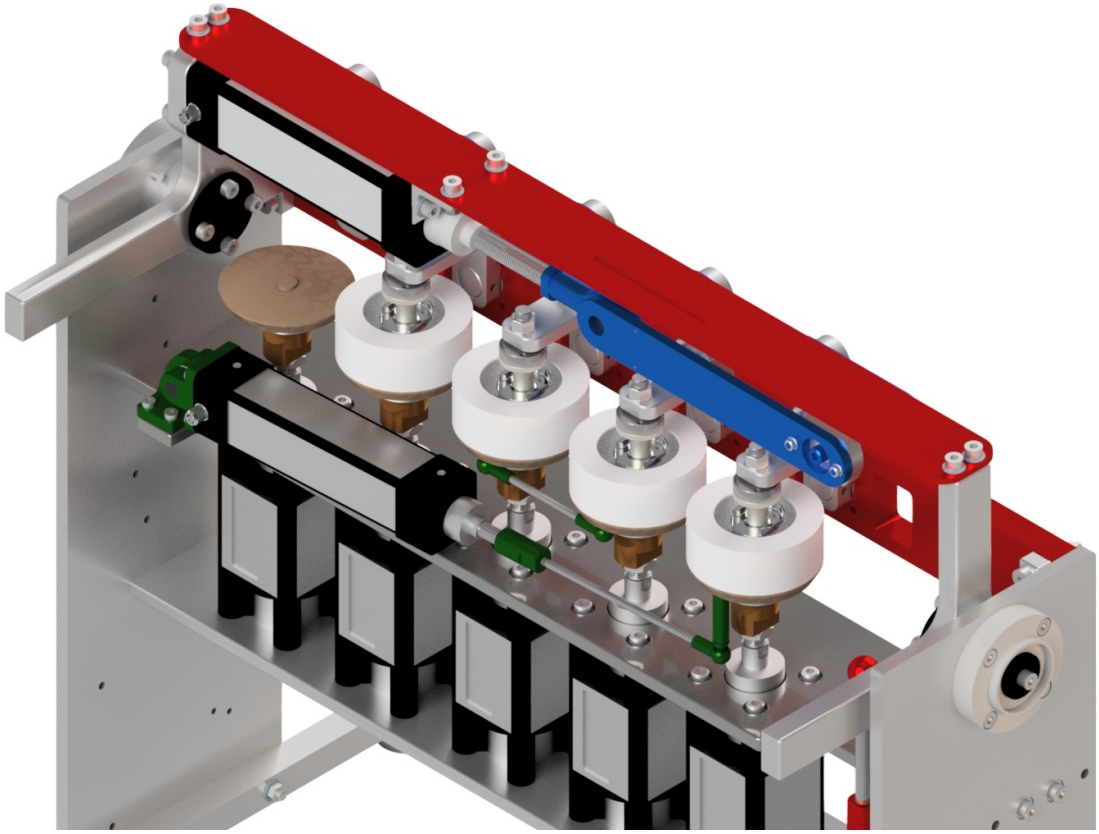

Figure 3.12 Schematic of the Newcastle Shoulder Wear Simulator located at Newcastle University, School of Engineering. Showing the test stations

This simulator is a fully programmable multi-station, three-axis machine capable of applying a wide range of motions and dynamic loads, so that *in vivo* adverse conditions can be replicated. In the ISO standard for artificial hip and knee joint testing, five million cycles were established as a total duration for the wear test.

The frequency applied by the Newcastle Shoulder Wear Simulator during the wear tests was 1 Hz which resulted in a sliding distance of 22.43 mm per cycle. The relationship between the test duration and the frequency of the simulator allows for the simulation of five years *in vivo* conditions in a period of no more than two months.

The simulator was running 'unattended' 24 hrs a day, 7 days a week, except for occasional lubrication checks (Section 3.3.3 Lubrication conditions) and periodic processing of the implants for cleaning (Section 3.2.1 Cleaning protocol) and measuring wear (Section 3.2.2 Gravimetric wear measurements).

3.3.4 Lubrication conditions

Newborn calf *serum* (Gibco®; Life Technologies Europe BV, Netherlands), was diluted with deionized water to give a lubricant for the shoulder wear simulator studies with an approximately protein concentration of 26 g/L using a 1:2 ratio mimicking synovial fluid; no additives were used with the lubricant.

Each graduated test chamber of the shoulder simulator was filled with approximately 120 mL of this lubricant and maintained at room temperature. During the wear testing, 5 mL of deionized water was added in each chamber every 24 hrs to replenish the water volume loss due to evaporation. This loss in lubricant was calculated using the graduation level in each test chamber. The *serum* was replaced with a freshly prepared batch at each clean interval (every 500,000 cycles) through the test.

This page intentionally left blank

Chapter 4. RESULTS

4.1 THE EFFECT OF COMBINED LOADING CYCLES ON THE WEAR OF REVERSE SHOULDER JOINT REPLACEMENTS

4.1.1 Summary

This study investigated, for the first time, the influence of a combination of clinically relevant daily activities on the ultra-high molecular weight polyethylene wear performance in a reverse total shoulder replacement (rTSR). This physiological combined motion and loading cycle, termed "repeated–motion–load" (RML), was applied on four new samples of a commercially available reverse shoulder prosthesis for five million cycles using the unique Newcastle Shoulder Wear Simulator.

The studied rTSR resulted in a polyethylene wear rate of 11.4 ± 3.7 mm^3/million cycles in combination with CoCr glenosphere components. The polyethylene surface roughness, S_a, became smoother, changing from 692 ± 132 nm to 42 ± 29 nm (Ramirez-Martinez *et al.*, 2019).

4.1.2 Effect of the RML wear test conditions on the wear rate of rTSR

As can be seen in **Figure 4.1**, over the 5 million cycles of testing, the wear rate of each UHMWPE humeral component against its respective CoCr glenosphere of a reverse total shoulder replacement was linear. The mean wear rate and standard deviation (SD) for the four test UHMWPE humeral components (H_1 to H_4) under RML test conditions was 11.4 ± 3.7 mm^3/million cycles. The total volumetric wear calculated in this study was 58.8 ± 5.8 mm^3 for the UHMWPE humeral components.

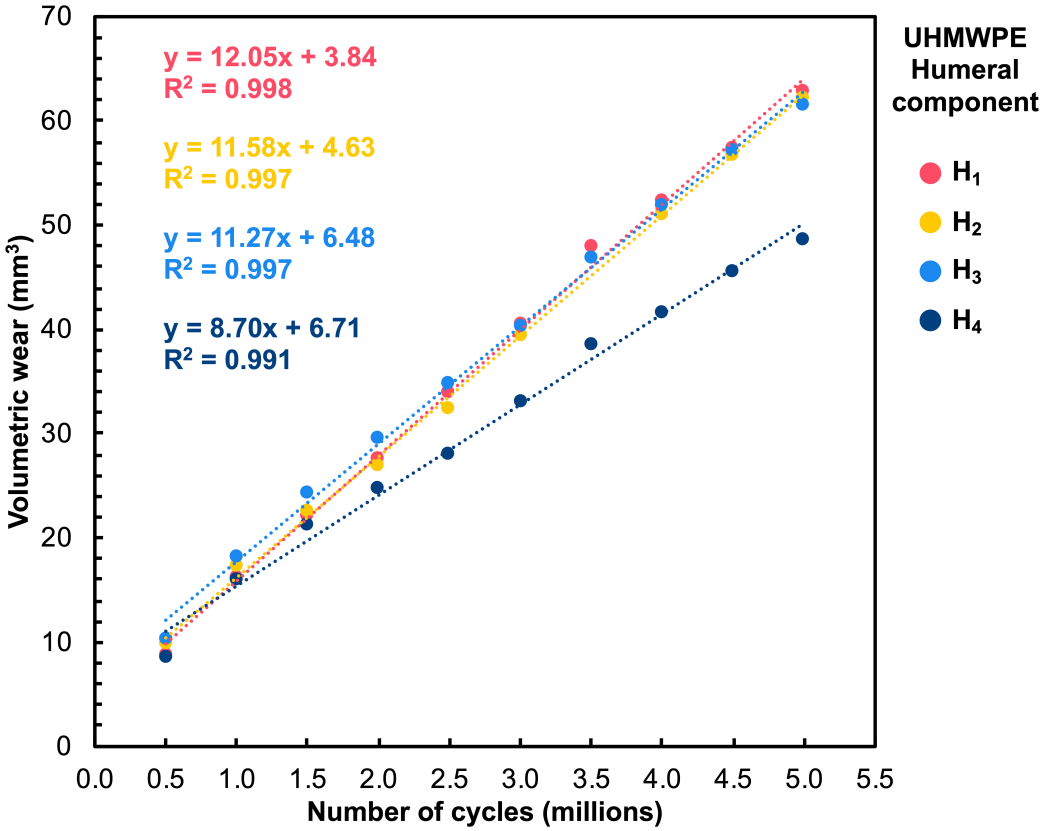

Figure 4.1 Volumetric wear rate of four UHMWPE humeral components (H_1–H_4) in mm^3 against the number of cycles (millions) of the wear test

The average mass of the four UHMWPE humeral components decreased by 0.052 ± 0.005 g at the end of the test. This compared with the humeral control component, which showed a mass increase of 0.003 g at the end of the test. Therefore, lubricant uptake had little overall influence.

The CoCr test components showed a wear rate over the test duration of 0.01 ± 0.02 mm^3/million cycles. At the control station, the CoCr glenosphere had no change in mass within the sensitivity (0.1 mg) of the balance.

4.1.3 Surface roughness analysis

Figure 4.2 shows the average roughness values of the articulating surfaces of the CoCr and UHMWPE components before and after the test. The change in the CoCr glenosphere's roughness decreased ($\rho = 0.017$), from 32 ± 8 nm S_a to 28 ± 8 nm S_a over the duration of the test. The UHMWPE humeral components became smoother ($\rho < 0.001$), from 692 ± 132 nm S_a to 42 ± 29 nm S_a.

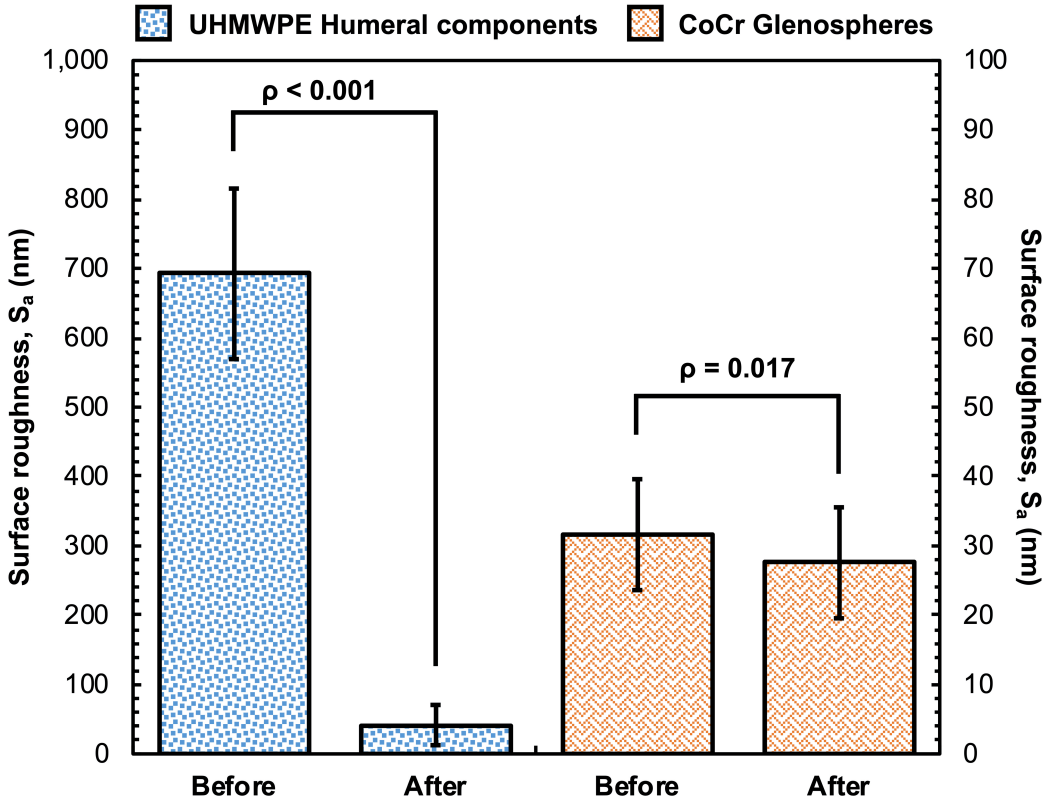

Figure 4.2 Surface roughness (S_a) before and after 5 million cycles for UHMWPE and CoCr components (mean +/– SD, $n = 4$)

A set of representative ZYGO images from UHMWPE humeral component (H_1) and CoCr glenosphere (G_1) are shown in **Figure 4.3** and **Figure 4.4**. As can be seen in **Figure 4.3**, the original concentric machining marks that were several microns in amplitude (*top*) were worn away over the duration of testing leaving a smoother surface (*bottom*) as a consequence of abrasive wear. This change in the surface topography was consistent among all the samples tested, with the exception of the UHMWPE humeral component used in the control station, which did not present a change in its surface roughness or evidence of wear.

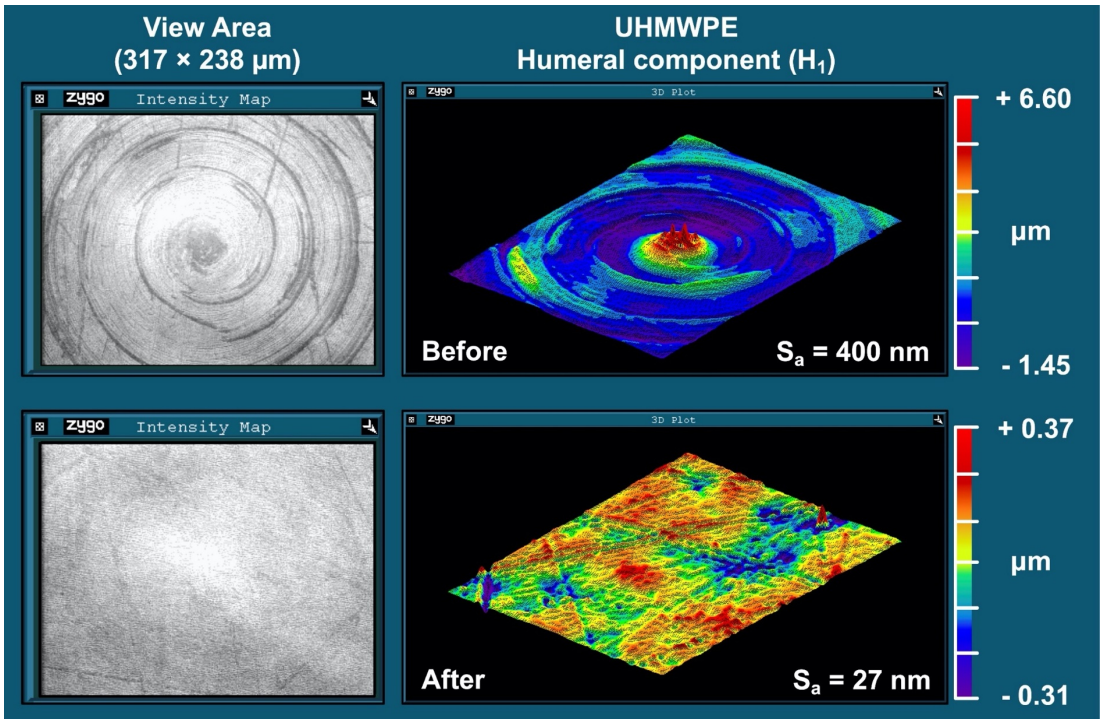

Figure 4.3 ZYGO images of the articulating surface of the UHMWPE humeral test component (H_1). Unworn surface with machining marks visible before (*top*) and resultant worn surface after 5 million cycles (*bottom*)

In **Figure 4.4** an image of the articulating surface of the CoCr glenosphere component from station one shows a change in the surface over the course of the wear test, where a Co-rich matrix with carbide blocks stands proud of the surface (*top*) can be observed (Sun *et al.*, 2011) in contrast with the presence of multi-directional scratches (*bottom*) and in some areas an increase of the surface roughness after the wear test. The changes observed on the surface topography were consistent among all the CoCr samples tested.

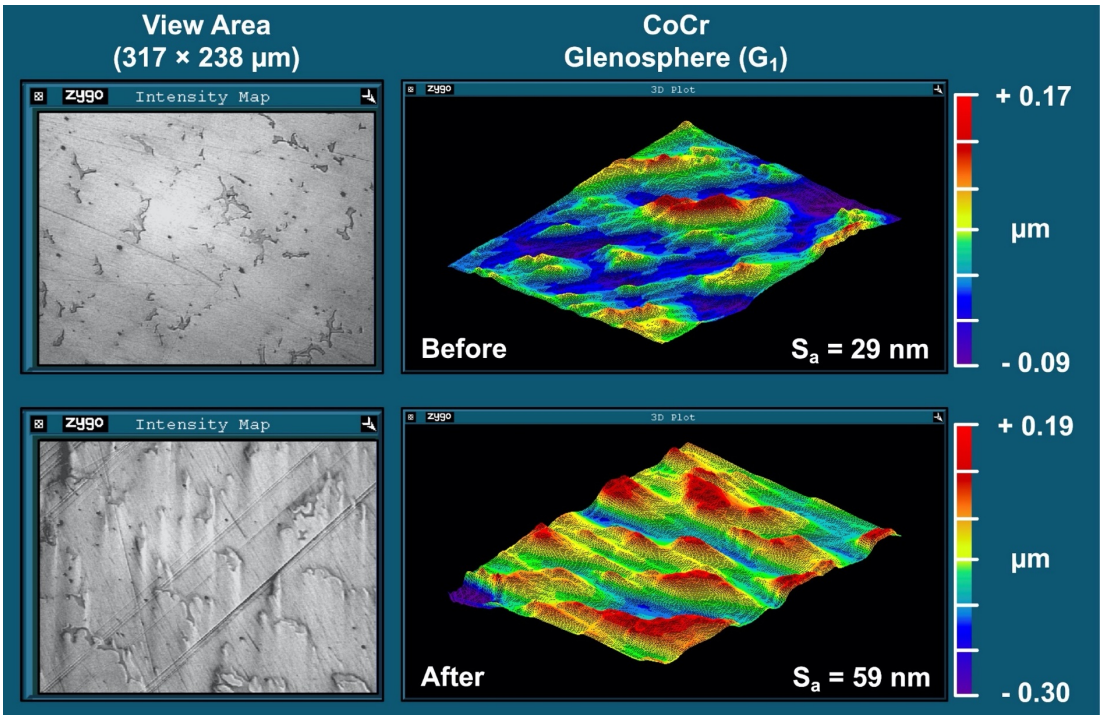

Figure 4.4 ZYGO images of the articulating surface of the CoCr glenosphere test component (G_1) before (*top*) and after 5 million cycles (*bottom*)

4.1.4 Surface morphology

The roughness of UHMWPE humeral components reduced by almost one order of magnitude after 5 million cycles wear test. However, the presence of distinct topographies on the UHMWPE articular surface appeared after the first 500,000 cycles when scratches were first observed on the test components.

After 1.5 million cycles a small indentation was visible to the naked eye in the polar region of each polymeric component. This “notch” in the humeral articular surfaces was inspected using a stereo microscope with a halogen ring light to improve the contrast with the reflective surface.

The pole region was divided into four quadrants (Q_1 to Q_4) to describe the location of it. **Figure 4.5** shows stereoscope images of the UHWMPE humeral component H_2 before and after the 5 million cycle wear test.

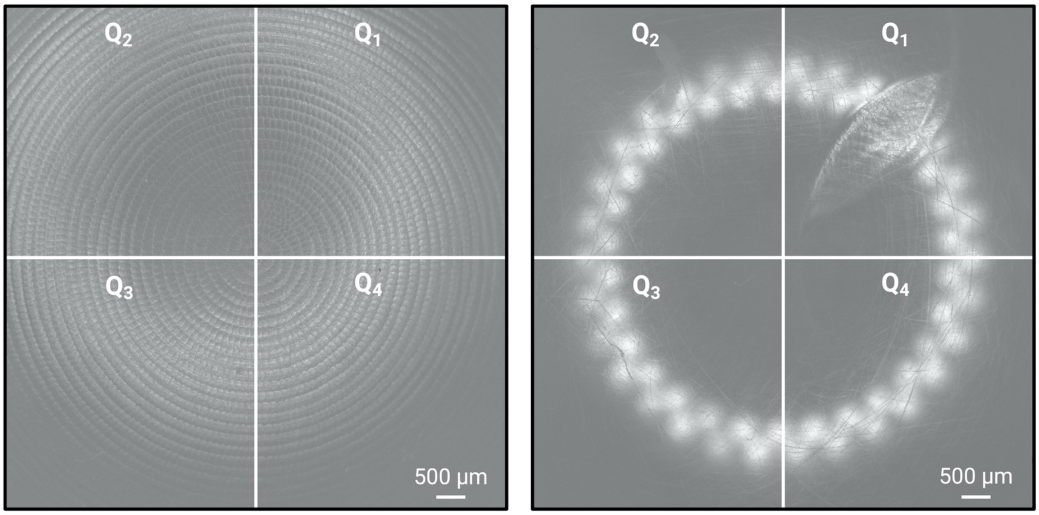

Figure 4.5 Representative stereoscopic images of the UHMWPE humeral component (H_2) before (*left*) and after (*right*) the wear test showing the pole zone; scale bar is 500 µm

A closer view of the indentation’s shape is presented in **Figure 4.6**. This shape was consistent among all the tested polymeric components with an average length of 4,174 ± 190 µm and may be the result of plastic deformation on the articulating surface during the wear test simulation which slowly deforms the original machining marks in combination with a 'dead zone' of motion between the components in contact.

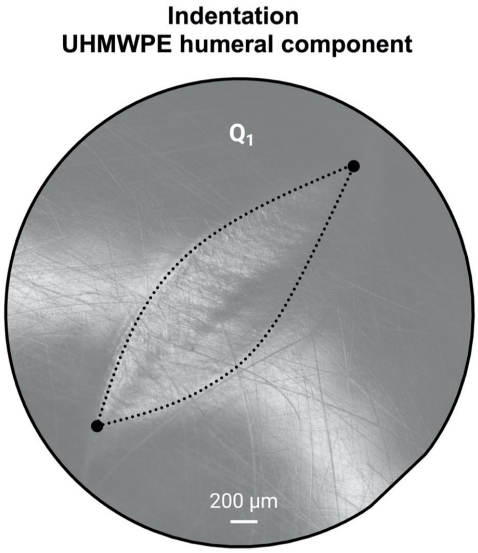

Figure 4.6 Magnified image of the indentation (scale bar is 200 µm

4.2 INFLUENCE OF HUMERAL HEAD MATERIAL ON WEAR PERFORMANCE IN ANATOMIC TOTAL SHOULDER JOINT ARTHROPLASTY

4.2.1 Summary

The main purpose of this study was to investigate, for the first time, the wear behaviour of a novel PyroCarbon–on–polyethylene bearings. The wear test was performed using PyroCarbon humeral heads, which were articulated against commercially available polyethylene glenoid insert components to form an anatomic total shoulder replacement (aTSR).

The wear assessment was performed using the Newcastle Shoulder Wear Simulator for five million cycles, wear was assessed gravimetrically, and the change of the surface roughness was measured with a non-contacting profilometer. Simulator parameters were match to real patient activity patterns of motion and loading using the newly repeated–motion–load protocol (Ramirez-Martinez *et al.*, 2019).

The studied aTSR resulted in a polyethylene wear rate of 19.3 ± 9.5 mm^3/million cycles in combination with PyroCarbon heads. The roughness value, S_a, of the UHMWPE glenoid inserts, reduced, changing from 296 ± 28 nm to 32 ± 8 nm. In contrast, the mean roughness of the PyroCarbon humeral heads remained in the same range (21 ± 2 nm S_a to 18 ± 5 nm S_a). There was no reduction in weight (no measurable wear) of the PyroCarbon humeral heads over the duration of testing (Ramirez-Martinez *et al.*, 2020a).

4.2.2 Gravimetric analysis

Figure 4.7 shows the cumulative volumetric wear (mm^3) from the four UHMWPE glenoid inserts tested (G_1 to G_4) under repeated–motion–load conditions and after being compensated by the loaded soak control component data. All glenoid inserts exhibited a linearly increasing relationship with increasing number of wear cycles. A mean volumetric wear rate of 19.3 ± 9.5 mm^3/million cycles was obtained using regression analysis for the UHMWPE glenoid inserts after the 5 million cycles against the PyroCarbon humeral head components. The total volumetric wear calculated in this study was 90.6 ± 5.0 mm^3 for the UHMWPE glenoid inserts.

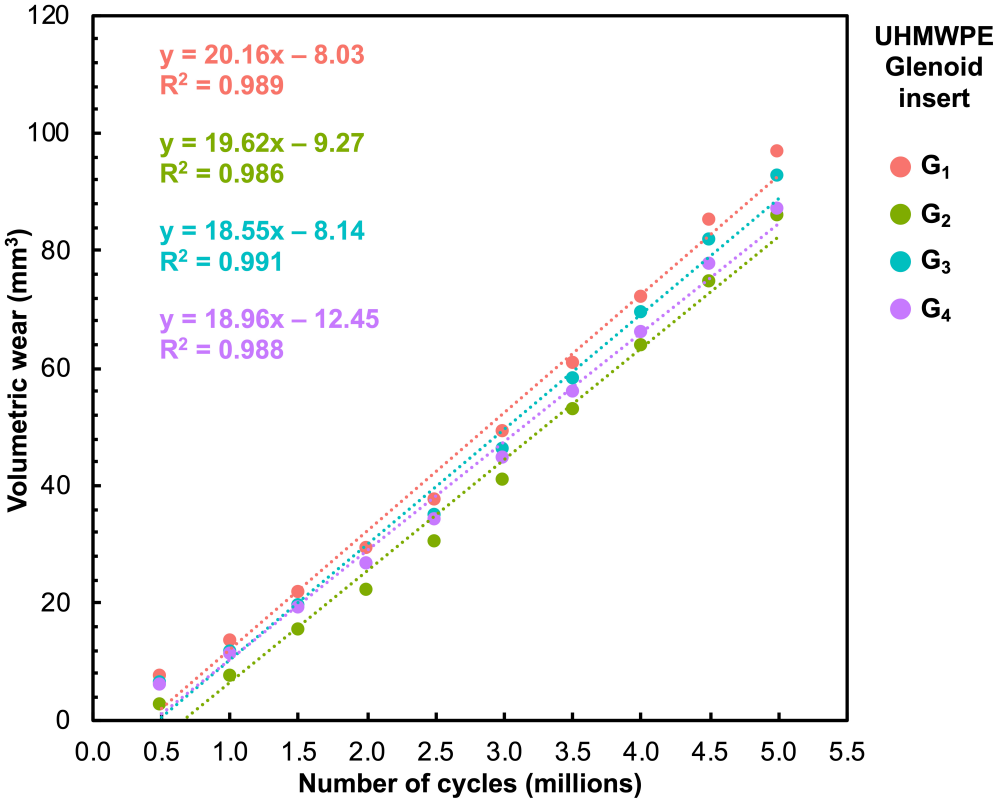

Figure 4.7 UHMWPE wear rate of the four glenoid insert components (G_1–G_4) in mm^3 against the number of cycles (millions) of the wear test

At the end of the test, the UHMWPE glenoid inserts showed an average decrease in mass of 84.95 ± 4.70 mg (range, 80.50 mg to 90.70 mg), while the glenoid control component exhibited a small mass increase of 1.40 mg. Therefore, there was little influence from lubricant uptake on mass change. The four PyroCarbon test humeral heads did not exhibit a measurable loss in mass throughout the 5 million cycles of wear testing; hence no wear rates have been presented in this thesis.

4.2.3 Surface roughness of the articulating surfaces

Prior to testing, the mean ± SD surface roughness, S_a, of the UHMWPE components was 296 ± 28 nm, while that on the PyroCarbon samples was 21 ± 2 nm. After 5 million cycles in the shoulder simulator, the surface roughness values of the UHMWPE glenoid inserts decreased to 32 ± 8 nm S_a ($\rho < 0.001$). In contrast, the PyroCarbon humeral head components did not show a significant change ($\rho = 0.402$) over the 5 million cycles, remaining in the range of 18 ± 5 nm S_a. **Figure 4.8** shows the change in the surface roughness of both components after 5 million cycles wear test.

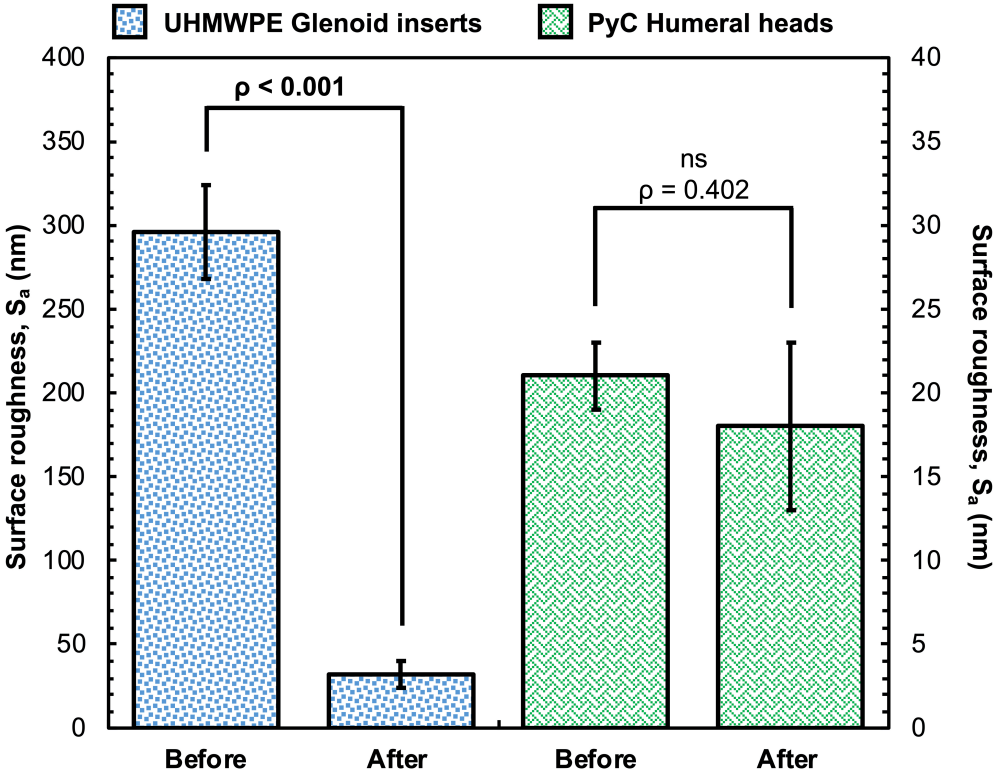

Figure 4.8 Change of the surface roughness (S_a) before and after the 5 million cycles wear testing (mean +/– SD, *n* = 4). *ns= non-statistical significance

During the first inspection at 500,000 cycles, a worn area was visible to the naked eye on the articulating surface of the polyethylene glenoid inserts. This area had a smooth elliptical shape. The rest of the surface was unworn. No visible change on the articulating surface topography was noted in the unworn area. During the course of the test, the worn area steadily increased in size, resulting in a length of 18 mm in the superior-inferior direction and 20 mm in the anterior-posterior direction both in the transverse plane.

In the case of the PyroCarbon humeral head components, a change of the surface appearance was noted at the same interval in the polar region, as a white-foggy coloured surface. This non-uniform surface did not increase in size, nor did it change shape through the test. White light interferometry microscopy images are given in **Figure 4.9** and **Figure 4.10**. **Figure 4.9** shows the surface topography of a representative UHMWPE glenoid insert (G_1) before and after 5 million cycles wear test, where concentric machining marks can be seen in the initially unworn area (*top*) in contrast with the later worn area where the presence of fine multidirectional scratches (*bottom*) could be observed. This change in the surface topography was consistent among all the samples tested, with the exception of the UHMWPE glenoid insert used in the control station, which did not present a change in its surface roughness or evidence of wear.

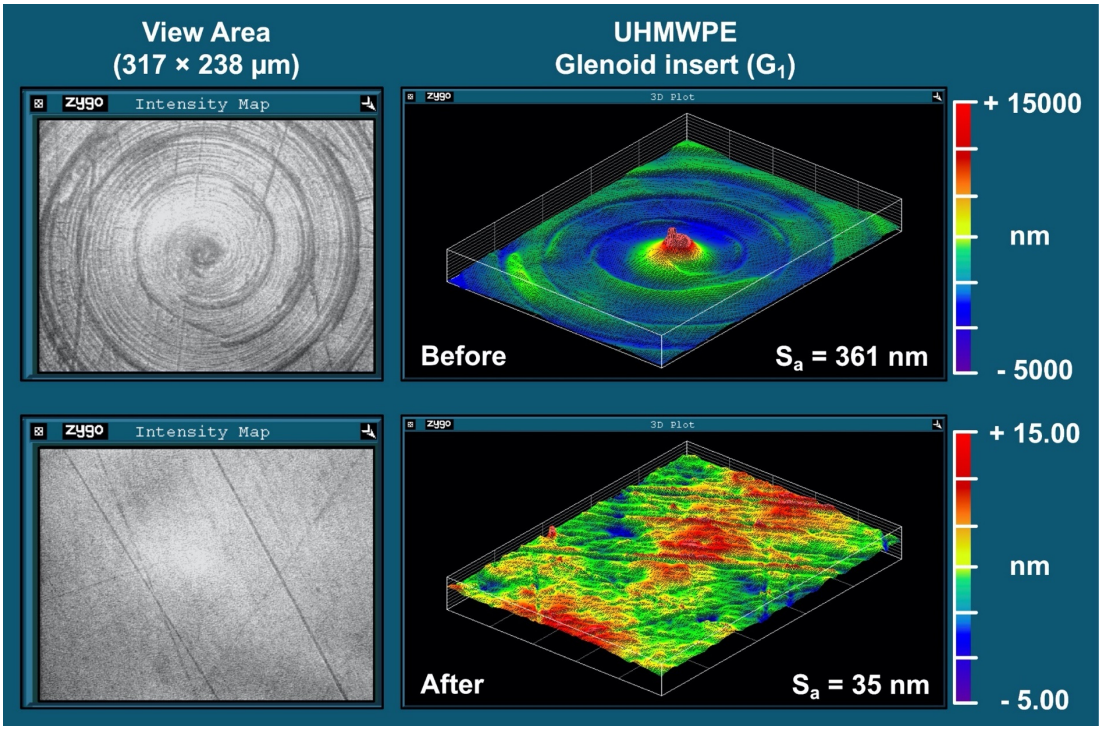

Figure 4.9 3D plot image taken on the Zygo profilometer of the UHMWPE glenoid insert (G_1) on the pole zone. Original concentric machining marks at zero cycles (*top*) and multidirectional scratches at 5 million cycles (*bottom*)

Figure 4.10 shows the representative surface topography of a PyroCarbon humeral head (H_1) characterized by having a microporous surface, which consist of sintered granules (1 to 10 µm) with many hollows among them (Carpenter *et al.*, 2016). No signs of wear, visible damage or unidirectional marks were observed before and after the test. While visible to the eye, the white-foggy coloured surface did not affect the surface roughness value. All wear tested PyroCarbon humeral heads showed to be consistent with a surface topography "undamaged" (no change in surface roughness) after five million cycles wear test.

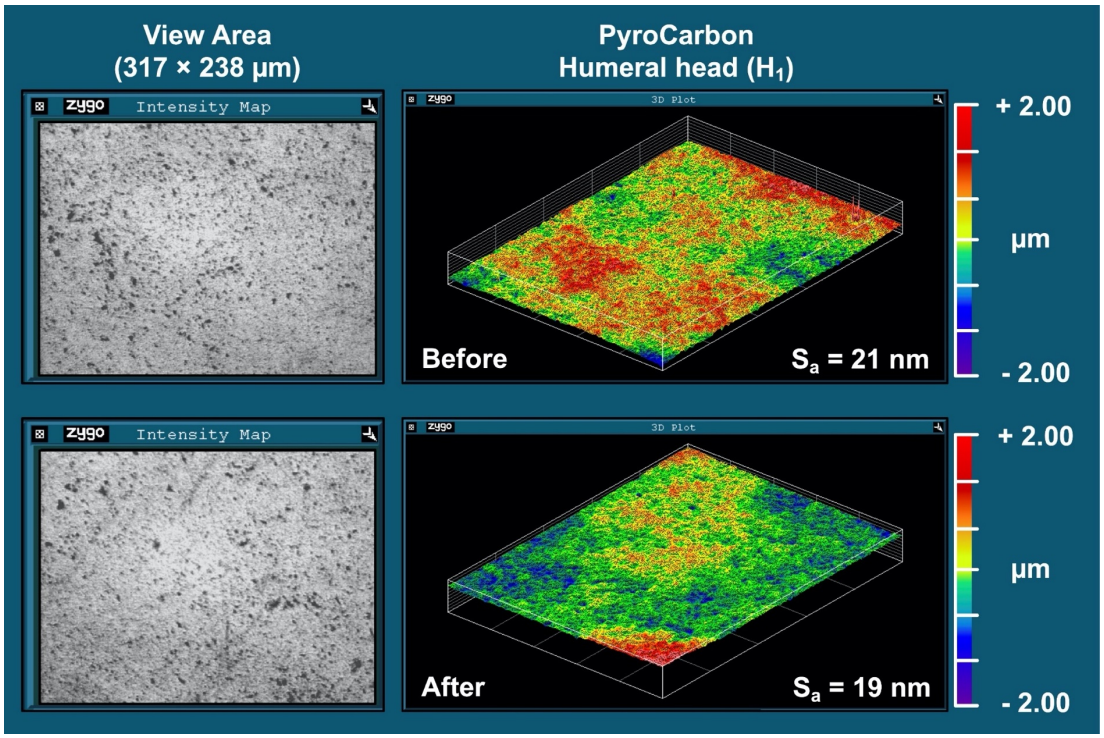

Figure 4.10 3D plot image taken on the Zygo profilometer of the PyroCarbon humeral head (H_1) on the pole zone. No visible surface damage was observed after 5 million cycles

4.3 Analysis of the surface topography of retrieved metal–on–polyethylene reverse total shoulder replacements

4.3.1 Summary

The main purpose of this study was to assess, for the first time, the surface roughness of thirteen retrieved metal–on–polyethylene reverse total shoulder replacements using a white light profilometer with nanometre resolution.

Although no significant relationship was observed between the surface roughness values and patient variables, it was noted that half of the polyethylene components still showed their original machining marks, indicating little change *in vivo*; and that the metallic humeral components in the reversed design configuration showed low values of surface roughness after their time *in vivo* (Ramirez-Martinez *et al*., 2020b).

4.3.2 Circumstance of retrieval

The reasons for primary surgery were fracture (31%, $n = 4$), revision (23%, $n = 3$), not specified (23%, $n = 3$), arthrosis (15%, $n = 2$), and dislocation (8%, $n = 1$). Eight of the patients were women and five were men. Seven surgical procedures were performed on the right shoulder and six on the left.

The shoulders were retrieved between October 2010 and April 2018. The mean ± standard deviation age of the 13 patients at their revision surgery was 72 ± 8 years (range, 50 to 82 years). All patients had multiple indications for revision procedures, with infection (septic loosening) the predominant reason in seven cases (54%), followed by dislocation in four cases (31%).

All of the rTSR revisions in this study occurred within 3 years of implantation (0 to ≤ 1 year, $n = 5$; ≥ 1 to ≤ 2 years, $n = 4$; ≥ 2 to ≤ 3 years, $n = 4$). The average time of implantation was 16 ± 11 months (range, 1 to 36 months). Of the 13 retrieved rTSR devices, five had an implantation time lower than 10 months.

4.3.3 Analysis of bearing surface roughness

4.3.3.1 Polymeric shoulder components

Table 4.1 shows the average surface roughness values (S_a, S_q and S_{sk}) for the analysed polymeric retrieved reverse total shoulder components. The humeral insert component from shoulder No. 6 (Lima Corporate) was excluded for the surface roughness analysis due to disassembly complications.

Table 4.1 Surface roughness (S_a, S_q and S_{sk}) results of the polymeric shoulder components divided by design type of rTSA replacement

	Shoulder No.	Manufacturer	S_a (µm) Mean ± SD	S_q (µm) Mean ± SD	S_{sk} Mean ± SD
Humeral insert	1	Aston Medical	1.379 ± 0.888	2.031 ± 1.580	0.313 ± 0.976
	2	DePuy Synthes	0.285 ± 0.129	0.470 ± 0.269	– 0.948 ± 1.572
	3	FX Solutions	0.215 ± 0.153	0.342 ± 0.256	– 0.262 ± 2.014
	4	Lima Corporate	0.918 ± 0.360	1.219 ± 0.471	0.312 ± 1.371
	5	Lima Corporate	0.962 ± 0.402	1.249 ± 0.588	– 0.897 ± 2.277
	7	Tornier	2.768 ± 0.862	3.580 ± 1.120	– 0.524 ± 0.438
	8	Zimmer Biomet	0.409 ± 0.183	0.533 ± 0.295	0.506 ± 1.205
	9	Zimmer Biomet	0.558 ± 0.416	0.844 ± 0.738	0.180 ± 1.367
		Mean ± SD	0.937 ± 0.838	1.288 ± 1.078	– 0.165 ± 0.575
Glenosphere	10	Lima Corporate	1.385 ± 0.806	1.784 ± 1.037	– 0.170 ± 0.787
	11	Lima Corporate	0.756 ± 0.435	1.018 ± 0.609	0.096 ± 1.198
	12	Lima Corporate	1.561 ± 0.887	2.009 ± 1.150	– 0.080 ± 0.739
	13	Mathys	1.224 ± 0.559	1.785 ± 0.891	– 0.878 ± 1.199
		Mean ± SD	1.232 ± 0.346	1.649 ± 0.438	– 0.258 ± 0.428
		ρ-value	0.413	0.426	0.761

SD: standard deviation.
The parameter value of S_{sk} is dimensionless.
Negative values of S_{sk} are coloured in red.

The surface roughness values from **Table 4.1** show that the overall mean ± SD of the surface skewness (S_{sk}) for both designs tended to a negative value (*conventional*, – 0.165 ± 0.575; n = 8 and *inverted*, – 0.258 ± 0.428; n = 4), which indicates an articulating surface dominated by the presence of valleys (i.e., scratches) rather than peaks (positive value) and thus indicated of a worn surface.

As can be seen in **Figure 4.11**, the surface roughness parameter S_a showed a wide range of values for the polymeric components. The red dotted line shows the maximum value according to the ASTM (ASTM F1378, 2018) guideline and the green dotted line the reference value according to previous *in vitro* studies (Smith *et al.*, 2015; Ramirez-Martinez *et al.*, 2019).

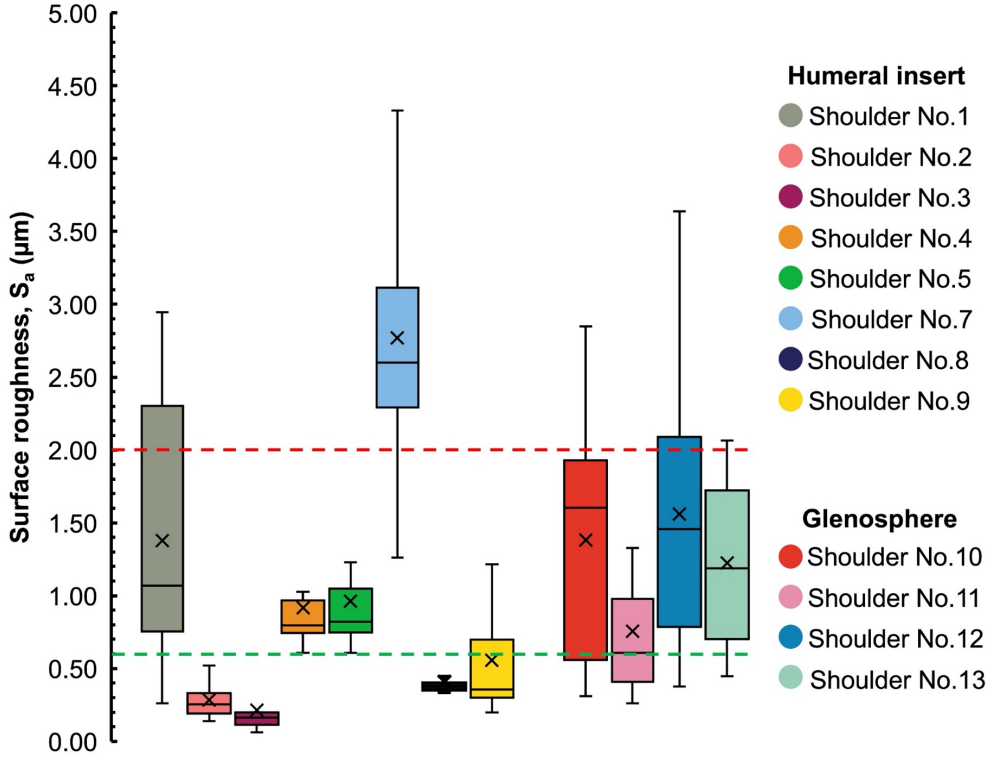

Figure 4.11 S_a surface roughness value among the polymeric components divided by design type of rTSA replacement

The highest value of S_a between the humeral inserts was found in sample 7 (Tornier; septic mobilization) with a value of 2.768 ± 0.862 µm and a time *in vivo* of 3 months. The lowest value was obtained for sample 3 (FX Solutions; recurrent dislocation) with a value of 0.215 ± 0.153 µm an *in vivo* time of 24 months. While the polymeric glenosphere components used in the *inverted* bearing design were in the range of 0.756 ± 0.435 µm to 1.561 ± 0.887 µm.

From **Figure 4.12** and **Figure 4.13** the roughness measurements of S_a compared to time *in vivo* indicated that after one year in use the polymeric components tended to decrease their S_a values (1.208 ± 0.950 µm; 1.093 ± 0.418 µm; 0.776 ± 0.611 µm) and increase their negative value in S_{sk} (0.061 ± 0.410; – 0.294 ± 0.530; – 0.444 ± 0.591). New components tend to have positive skewness, which indicates that the surfaces have more peaks than valleys. Worn/used surfaces, on the other hand, tend to have negative skewness, meaning that the surface profile contains more valleys than peaks (Scholes et al., 2013).

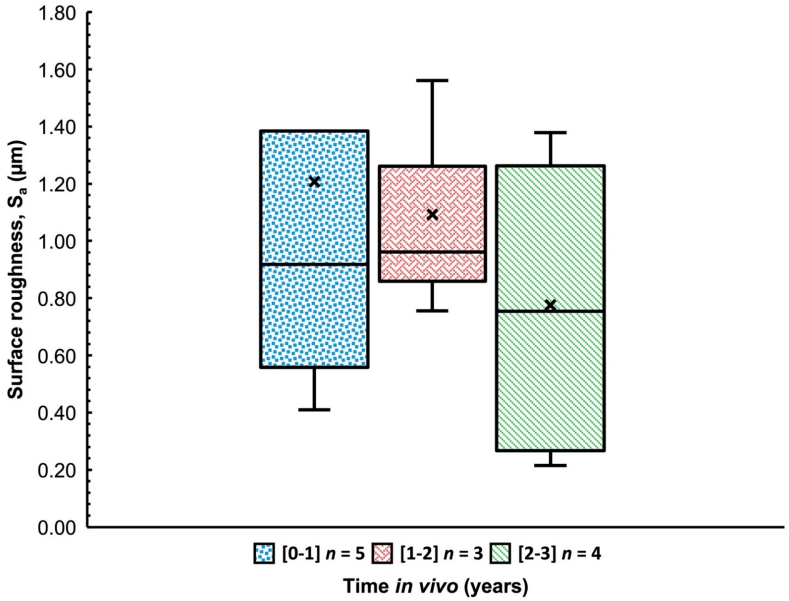

Figure 4.12 Variation of S_a with time *in vivo* among explanted polymeric components

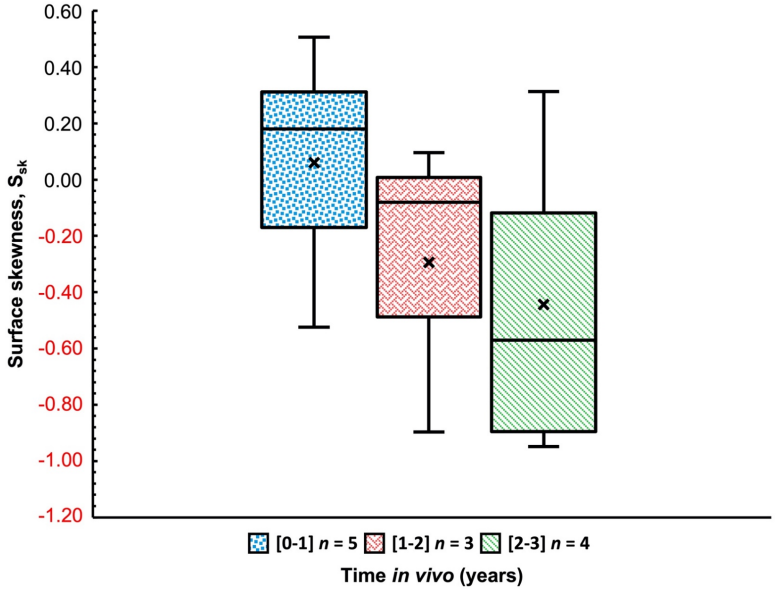

Figure 4.13 S_{sk} with time *in vivo* among explanted polymeric components

However, no correlation was found between the polymeric surface roughness (S_a) and their time *in vivo* (months) after a Pearson's correlation test; resulting in a ρ-value of 0.485 with a correlation coefficient of - 0.224 as shown in **Figure 4.14**.

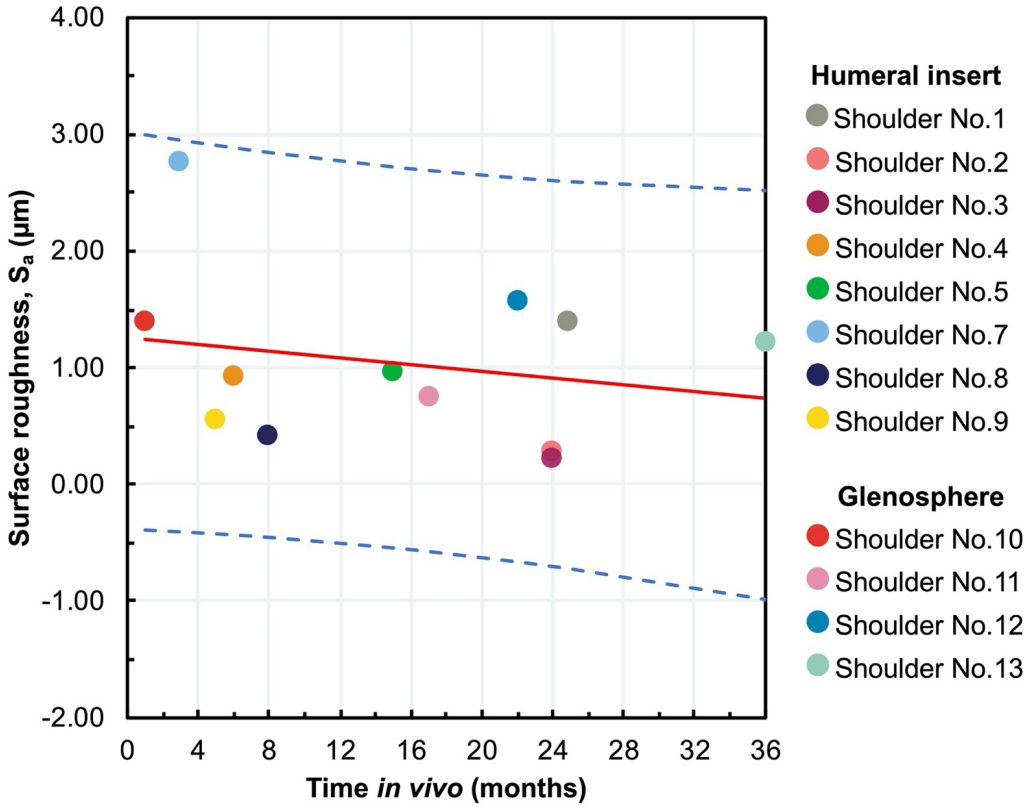

Figure 4.14 Surface roughness (S_a) plotted against the time the polymeric component was implanted. The red fitted line shows the predicted surface roughness for time *in vivo* up to 36 months. The blue dashed lines show the 95% prediction interval

There was not relationship between whether the implant was positioned on the right or left-hand side of the patient and the surface roughness (*right*, 1.068 ± 0.695 µm; $n = 6$ and *left*, 1.003 ± 1.076 µm; $n = 6$) (result not shown graphically).

Data were separated between the gender of the patients, and as can be seen in **Figure 4.15**, the surface roughness, S_a, values were not significantly different ($\rho = 0.228$) in male patients (1.369 ± 0.843µm; $n = 5$) than in females (0.796 ± 0.534 µm; $n = 7$) patients.

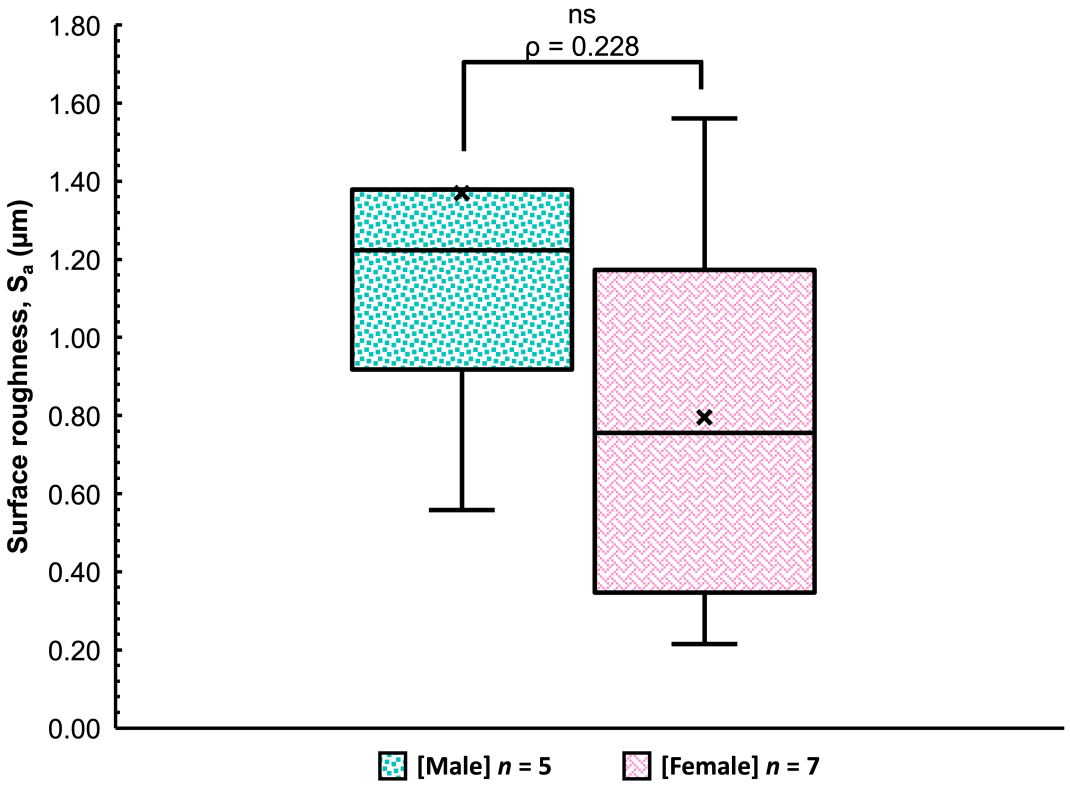

Figure 4.15 S_a surface roughness value of explanted polymeric components divided by gender

As shown in **Figure 4.16** and **Figure 4.17**, the polymeric humeral insert components used for the *conventional* reverse total shoulder arthroplasties showed no significant difference ($\rho = 0.413$) in the final surface roughness (S_a, 0.937 ± 0.838 µm; $n = 8$) in comparison when the bearing material was *inverted* and polymer material was used in the glenosphere components (S_a, 1.232 ± 0.346 µm; $n = 4$).

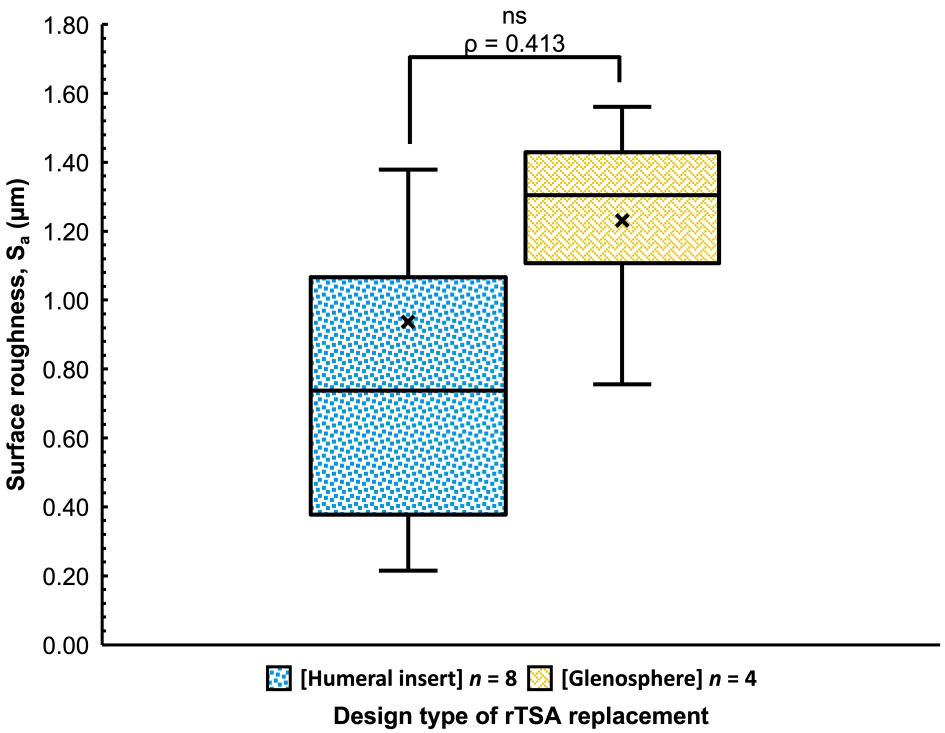

Figure 4.16 S_a surface roughness value of explanted polymeric components divided by design type of rTSA replacement

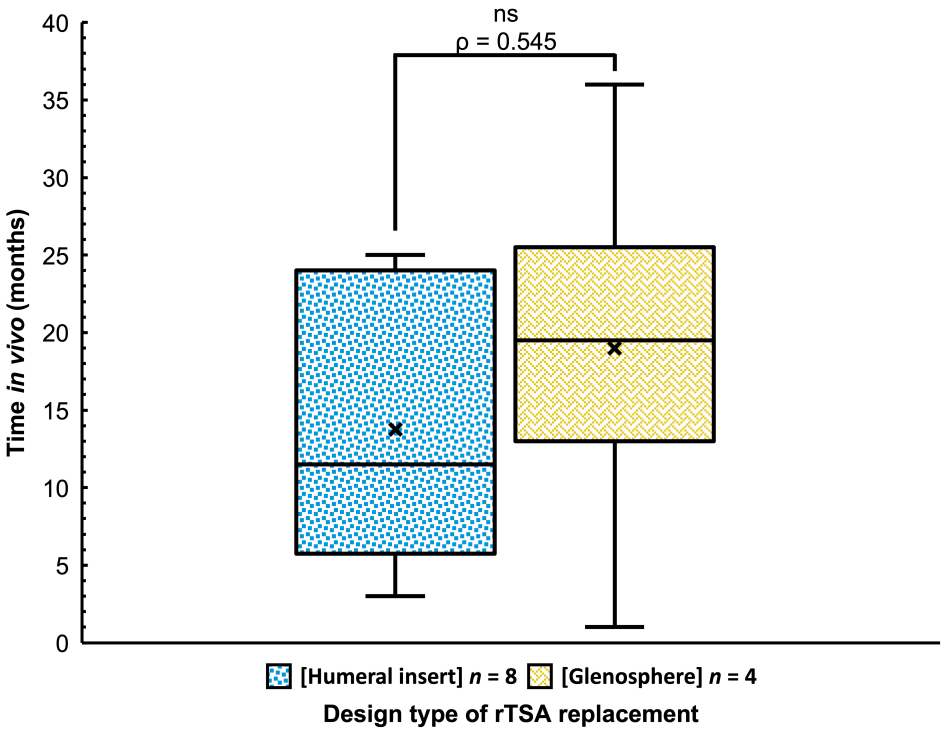

Figure 4.17 Time *in vivo* of explanted polymeric components divided by design type of rTSA replacement

Four of eight cases among the humeral inserts were revised due to infection, which represents 50% of the *conventional* reverse total shoulder arthroplasties cohort. These shoulder implants showed no significantly greater ($\rho = 0.369$) final surface roughness (S_a, 1.143 ± 1.118 µm; $n = 4$) in comparison when the reason for revision surgery was dislocation (S_a, 0.514 ± 0.363 µm; $n = 3$), as can be seen in **Figure 4.18**.

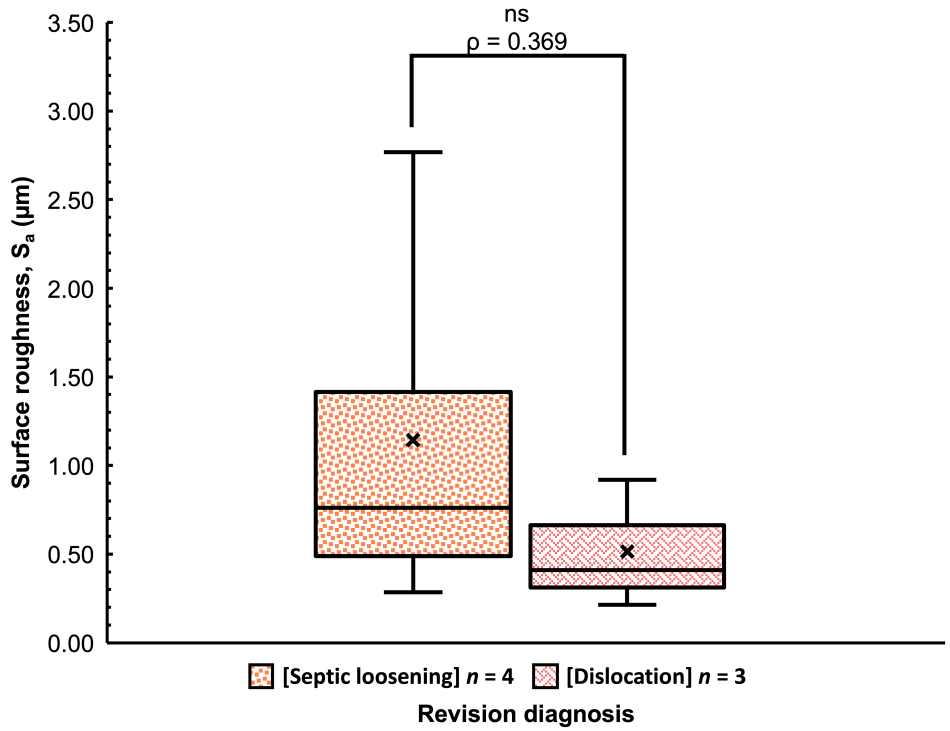

Figure 4.18 S_a surface roughness value of explanted polymeric components divided by main revision diagnosis

Retrieved polymeric rTSR components were also visually inspected macroscopically for the presence of different surface damage modes. The pole region at the centre of the humeral insert component was chosen, while in the glenosphere components a region at 25 degrees tilt from the pole region was selected. Scratching (abrasive wear), pitting and burnishing were the principal damage modes observed across the polyethylene *ex vivo* samples. **Figure 4.19** shows a comparison between the 3D surface roughness plot for the polymeric components.

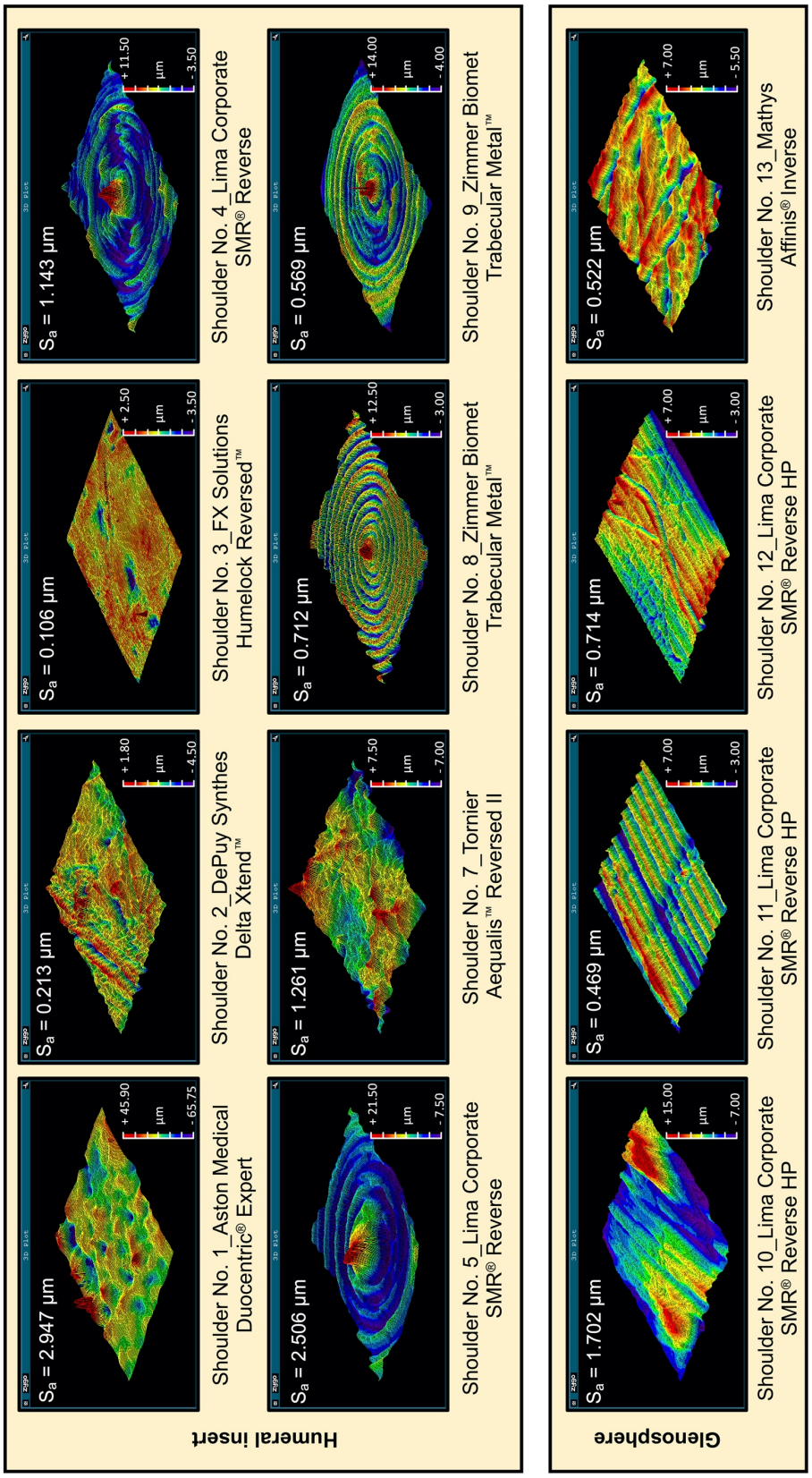

Figure 4.19 3D surface topography images of polyethylene components divided by design type of rTSA replacement. Field of view 634 × 475 µm

The polymeric humeral insert components used in *conventional* bearing design from Lima Corporate and Zimmer Biomet still showed the presence of machining marks on the pole region after an *in vivo* time of 9 ± 5 months (range, 5 to 15 months), while in other cases (Aston Medical, DePuy Synthes, FX Solutions, and Tornier) the concentric machining marks appeared to have been progressively worn away after 19 ± 11 months (range, 3 to 15 months), leaving a surface with the presence of multidirectional scratches, possibly as a consequence of an abrasive wear mechanism.

Surface damage was also found on the rim of certain polyethylene humeral inserts designs (**Figure 4.20**) as a possible result of mechanical impingement with the scapula and/or screw contact.

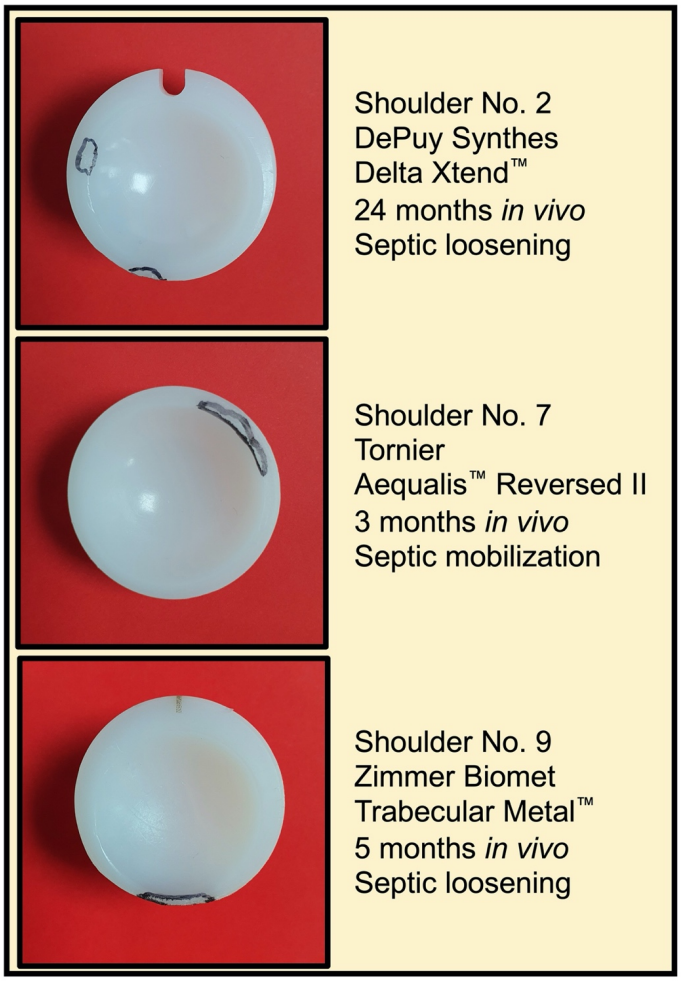

Figure 4.20 Surface damages observed on the polyethylene humeral insert of retrieved reverse shoulder replacements. Worn areas were outlined with dark marker to show the rim damage

4.3.3.2 Metallic shoulder components

The results of surface roughness measurements for the *ex vivo* metallic components are summarised in **Table 4.2**. In general, roughness parameters (S_a and S_q) were significantly greater in the glenosphere group than in the humeral insert group.

Table 4.2 Surface roughness (S_a, S_q and S_{sk}) results of the metallic shoulder components divided by design type of rTSA replacement

	Shoulder No.	Manufacturer	S_a (µm) Mean ± SD	S_q (µm) Mean ± SD	S_{sk} Mean ± SD
Glenosphere	1	Aston Medical	0.046 ± 0.024	0.128 ± 0.161	–0.869 ± 2.034
	2	DePuy Synthes	0.016 ± 0.004	0.022 ± 0.011	–1.486 ± 1.924
	3	FX Solutions	0.042 ± 0.055	0.071 ± 0.101	–0.529 ± 1.212
	4	Lima Corporate	0.050 ± 0.051	0.074 ± 0.069	–2.054 ± 2.287
	5	Lima Corporate	0.025 ± 0.021	0.039 ± 0.038	–1.453 ± 1.669
	6	Lima Corporate	0.056 ± 0.024	0.087 ± 0.049	–1.033 ± 1.248
	7	Tornier	0.260 ± 0.252	0.379 ± 0.394	–0.950 ± 1.322
	8	Zimmer Biomet	0.097 ± 0.070	0.129 ± 0.097	0.023 ± 0.666
	9	Zimmer Biomet	0.096 ± 0.093	0.128 ± 0.117	0.909 ± 1.790
		Mean ± SD	0.076 ± 0.074	0.117 ± 0.105	–0.827 ± 0.881
Humeral insert	10	Lima Corporate	0.006 ± 0.002	0.010 ± 0.006	–0.735 ± 1.205
	11	Lima Corporate	0.018 ± 0.005	0.024 ± 0.007	–1.369 ± 0.876
	12	Lima Corporate	0.008 ± 0.008	0.010 ± 0.009	–1.009 ± 1.269
	13	Mathys	0.016 ± 0.003	0.022 ± 0.004	–1.602 ± 1.149
		Mean ± SD	0.012 ± 0.006	0.016 ± 0.007	–1.179 ± 0.383
		ρ-value	**0.032**	**0.021**	0.340

SD: standard deviation.
The parameter value of S_{sk} is dimensionless.
Negative values of S_{sk} are coloured in red.
ρ-value of less than 0.05 was considered to show a significant difference (**in bold**).

As can be seen in **Figure 4.21**, the highest value of S_a between the glenosphere components was found in sample 7 (Tornier; septic mobilization) with a value of 0.260 ± 0.252 µm and a time *in vivo* of 3 months. The lowest value was obtained for sample 2 (DePuy Synthes; septic loosening) with a value of 0.016 ± 0.004 µm an *in vivo* time of 24 months. While the metallic humeral inserts components used in the *inverted* bearing design were in the range of 0.006 ± 0.002 µm to 0.018 ± 0.005 µm.

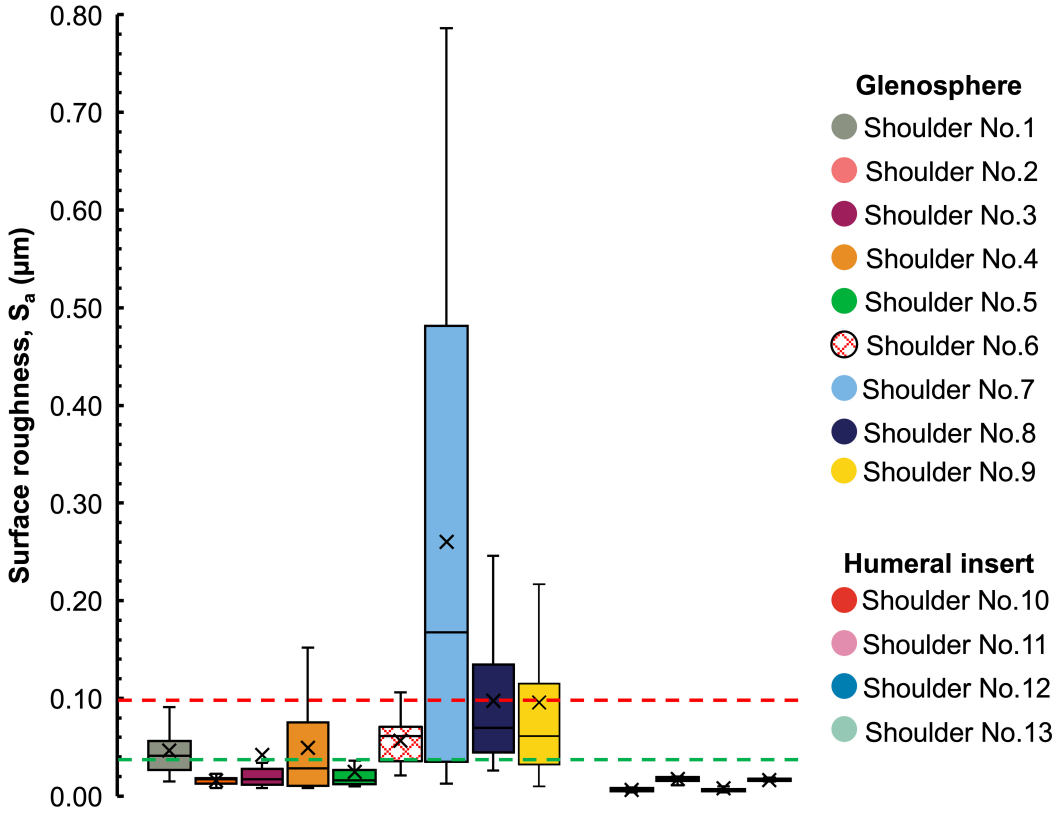

Figure 4.21 S_a surface roughness value among the metallic components divided by design type of rTSA replacement

Surface roughness values from explanted glenosphere shoulder number 1 to 5, and maybe even shoulder number 6, show a fairly good match with the *in vitro* tested CoCr glenosphere components (Ramirez-Martinez *et al.*, 2019), where virtually no change in roughness value over 5 million cycles was reported. In contrast, samples number 7, 8, and 9 definitely do not resemble the results obtained during the *in vitro* simulation, these last two are even three times larger in surface roughness value with a large standard deviation too. The explanation for this may be the moderate to severe scratches found in their surface.

As shown in **Figure 4.22**, significant difference (ρ = 0.032) in the final surface roughness was found between the metallic glenospheres (S_a, 0.076 ± 0.074 µm, n = 9) and the humeral insert components (S_a, 0.012 ± 0.006 µm, n = 4) used in the inverse arrangement.

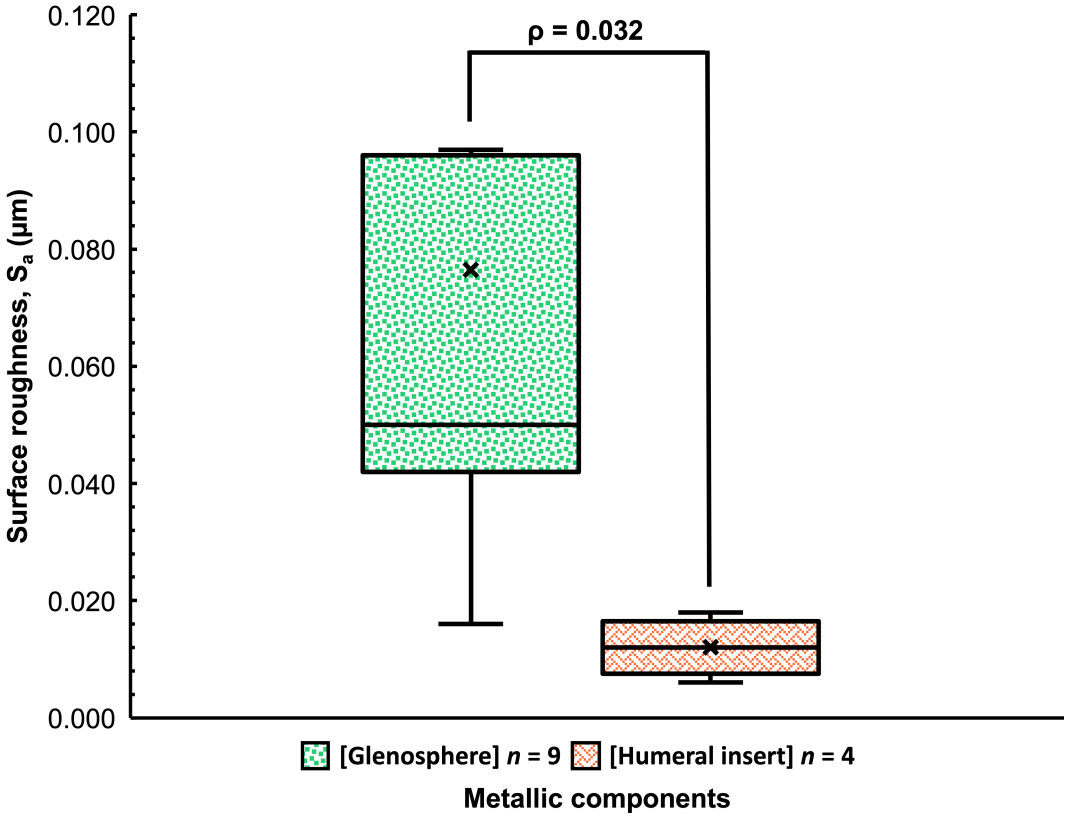

Figure 4.22 S_a surface roughness value type of metallic component divided by design type of rTSA replacement

Figure 4.23 shows representative 3D surface plot images for the retrieved metallic components, where abrasive wear is evident as a scratches and grooves with a concomitant increase of their surface roughness values.

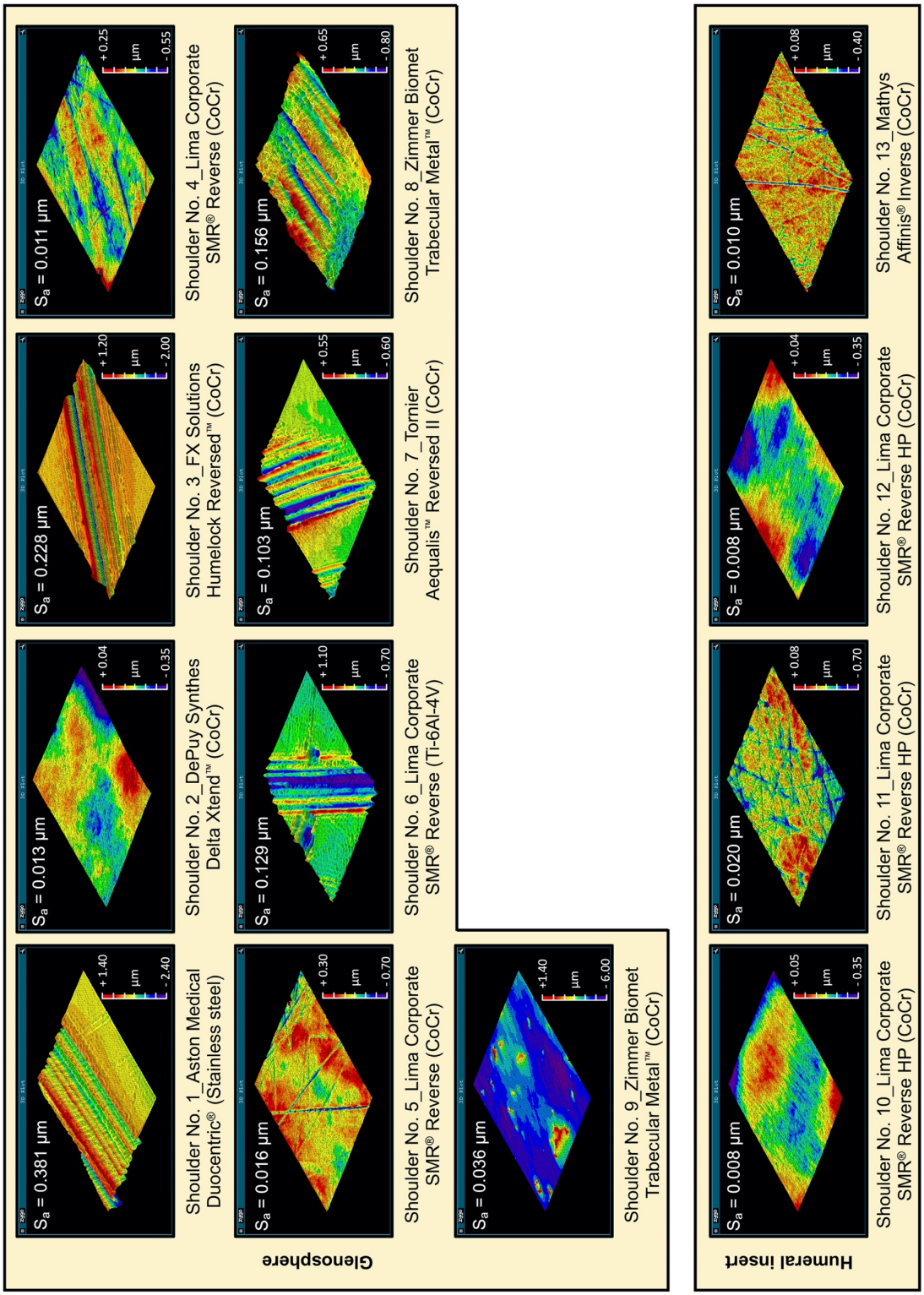

Figure 4.23 3D surface topography images of metallic components divided by design type of rTSA replacement. Field of view 317 × 238 µm

During the visual inspection, light scratching was seen on most of the metallic components, which resemble the "damage" of the original surface finish after the *in vitro* wear test simulation under RML protocol (Ramirez-Martinez *et al.*, 2019). However, on some shoulder glenospheres a more dulled appearance was seen, with the presence of multidirectional scratches as shown in **Figure 4.24**.

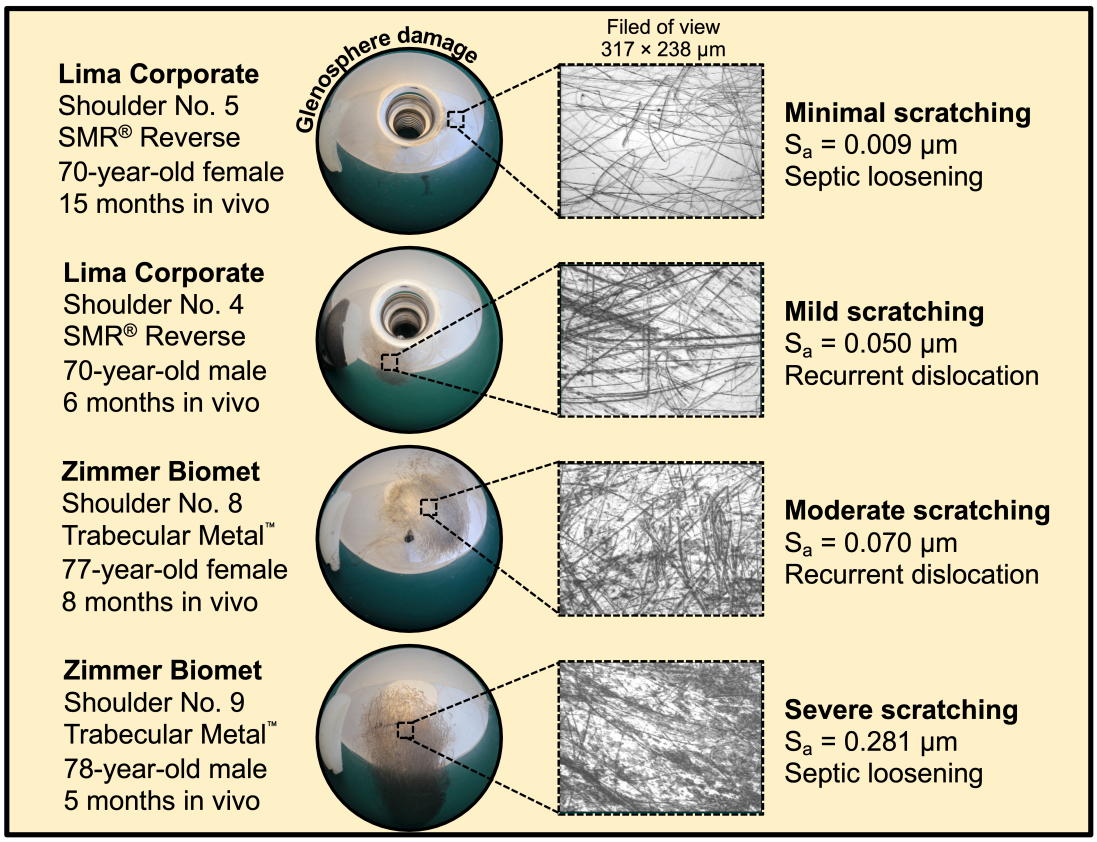

Figure 4.24 Changes in articulating surface topography on retrieved glenospheres. Field of view 317 × 238 µm

The change in the articulating surface roughness on retrieved glenospheres (observed mostly close to the polar area) can occur due to scratching of the metal bearing surface by third-body particles such as bone debris, or metal debris which become embedded in the polyethylene counterfaces surface (Davidson *et al.*, 1994; Que *et al.*, 2000). Or as a result of unintentional contact between the glenosphere components and the surrounding components in the case of dislocation events (Mai *et al.*, 2010).

This page intentionally left blank

Chapter 5. DISCUSSION

5.1 WEAR OF REVERSE SHOULDER REPLACEMENT UNDER REPEATED–MOTION–LOAD SIMULATOR PROTOCOL

This is the first *in vitro* study to investigate the effect of combined motion and static load cycles on the wear of reverse total shoulder implants. According to the Lancaster (1973) wear equation (**Equation 2.1**) where the volume of material removed (V, mm^3) is proportional to the total distance slid (x, m) and the load applied (P, N); the wear factor (k, mm^3/Nm) of the UHMWPE components was then calculated:

$$k = \frac{V}{Px} = 2.1 \pm 0.7 \times 10^{-6}\ mm^3/Nm$$

Equation 2.1 Lancaster wear equation

The wear factor obtained during this study shows good agreement with the 2.2×10^{-6} mm^3/Nm calculated by Mattei *et al.* (2016) during a set of computational numerical simulations for JRI reverse total shoulder components for 2 million cycles. The wear factor of this study is also similar to that found by Saikko (2017) of 2.0×10^{-6} mm^3/Nm for *conventional* UHMWPE rubbing against CoCr during a pin-on-disk wear study.

The UHMWPE wear rate was calculated as 12.0 ± 3.9 mm^3/million cycles for rTSR implants under RML conditions. This mean wear rate is statistically similar to those from Kohut *et al.* (2012) (14.1 mm^3/million cycles; ρ = 0.449, one-sample t-test) and Smith *et al.* (2015) (14.3 ± 1.6 mm^3/million cycles; ρ = 0.444). Smith *et al.* (2015) applied the "mug to mouth" ADL during a 4.5 million cycles test on rTSR using the same Newcastle Shoulder Wear Simulator.

The overall polyethylene wear in this study was of the order of 60 mm^3. This is a fairly good match to a recent study conducted by Lewicki *et al.* (2017) which determined the wear volumes on four retrieved polyethylene humeral components ranging from 40 to 90 mm^3, with an average time of 3.6 years *in vivo*.

Therefore, it has been shown that the addition of a static load during the wear test does not produce a statistically significant difference in the overall wear in comparison

with when only continuous motion was applied. It was hypothesized that the inclusion of an interval of "static load with no motion" into a wear test would increase *in vitro* wear, due to interruption of the squeeze film action retaining lubricant in the bearing during the "mug to mouth" cycle and depletion of the thickness of the squeeze film during the resting period, leading to sub-optimal lubricant conditions when motion re-starts. However, no significant increase in bearing wear was observed.

The mean wear rate of this study is significantly lower in comparison to Vaupel *et al.* (2012) (125.7 ± 28.2 mm^3/million cycles; $\rho = 0.020$) and Langohr *et al.* (2016) (42.0 mm^3/million cycles; $\rho = 0.006$ and 38.8 mm^3/million cycles; $\rho = 0.007$). This could be due to the differences in the prostheses used (femoral heads) and the higher load range applied (813 N to 914 N) in their tests.

A direct comparison of the roughness values (S_a) obtained by Smith *et al.* (2015) during rTSR "mug to mouth" wear test was made. Their UHMWPE components showed a non-statically significant change ($\rho = 0.112$) passed from 620 ± 220 nm to 258 ± 66 nm, while the implants in the current test became significantly smoother ($\rho < 0.001$) changed from 692 ± 132 nm to 42 ± 29 nm. Previous theoretical lubricant regime studies in joint replacements did not take in consideration the change in surface roughness for the components (composite R_a) and the increase of the curvature of the "cup" (UHMWPE humeral component in reverse total shoulder replacement) as a consequence of the wear process; factors which have a crucial impact on the lubrication regime that can be achieved. Assuming that R_a is approximately equivalent to S_a, the minimum effective film thickness (h_{min}) was calculated using the Hamrock and Dowson lubrication equation (**Equation 2.4**).

The adding of the central hole in the rTSR implants did not make a significant difference between this study and that of Smith *et al.* (2015) in terms of wear values ($\rho = 0.444$). However, the formation of the small indentation (**Figure 4.5**) could perhaps be explained as a result of localised stress as a consequence of the central hole's rim and the range of motion applied.

The lambda ratio (λ) was used to identify the lubrication regime before and after the RML wear test, which is a function of the surface roughness (S_a). The values of the parameters used to calculate the lubricant regime in a metal–on–polyethylene total reverse shoulder replacements are given in **Table 5.1**.

Table 5.1 Material properties and values used in the analysis

Parameter (symbol)	Value	
Load (L)	250 N	
Entraining velocity (u)	0.0261 m/s	
Viscosity of synovial fluid (η)	0.005 Pa s	
Young's modulus of CoCr (E_1)	210 GPa	
Young's modulus of UHMWPE (E_2)	1 GPa	
Poisson's ratio of CoCr (v_1)	0.30	
Poisson's ratio of UHMWPE (v_2)	0.40	
Glenosphere radius (R_1)	41.96 mm	
	Before	**After**
Radial clearance ($R_2 - R_1$)	40 μm	70 μm
CoCr glenosphere surface roughness (S_{a1})	32 nm	28 nm
UHMWPE humeral component surface roughness (S_{a2})	692 nm	42 nm

Using these values, the effective elastic modulus (E*) can be calculated to be 2.37 GPa, with an effective radius (R_x) of 11.02 before the test and 6.31 m after five million cycles. In turn, these quantities permit a lambda ratio of 1.80 and 16.11 to be calculating, indicating that such a metal–on–polyethylene reverse total shoulder prosthesis would transit from a mixed lubrication regime ($1 < \lambda < 3$) to fluid film ($\lambda > 3$) by the end of the test. Therefore, it may that the intermittent static load in this test caused a reduction in polyethylene roughness by compressing any localised peaks on the articulating surface, and also could both form and breakdown rapidly the lubrication film during intermittent motion.

From **Figure 4.1** "Volumetric wear rate of four UHMWPE humeral components (H1–H4) in mm^3 against the number of cycles (millions) of the wear test", it can be seen that the S_4 UHMWPE test component showed lower wear than the other components. All components were of the same size and made to the same specification, so there were no differences in this regard. In terms of CoCr component roughness, the component in H_4 did not show the highest roughness so again this does not provide an explanation. While no final explanation is currently available, it should be noted that

such differences in wear rates between stations have been seen in simulator studies of metal on polymer bearings (Smith *et al.*, 1999; Smith and Unsworth, 2001).

However, it has been shown that the wear mechanisms during an *in vitro* wear test can be affected by the protein degradation within the serum lubricant and the formation of precipitated protein, which forms a solid boundary between the articulating bearing surfaces and compromise the test results (e.g., low wear rate for UHMWPE) (Clarke *et al.*, 2000; Good *et al.*, 2000; Brandt *et al.*, 2012). Although the same phenomenon may occur *in vivo*, the accumulation of protein degradation products is effectively suppressed by the high-volume turnover rate of the body (Wang *et al.*, 2004).

The serum degradation during *in vitro* simulations is mainly caused by the rise in its temperature as a result of the high number of cycles, the continuous motion and loading, and the friction of the articulating bearing surfaces which can generate temperatures near to the point necessary to denature the protein (Liao *et al.*, 2003). For this reason, regular lubricant replacement during *in vitro* wear tests needs to be done, however, the disposal of actual wear particles within the tested lubricant can also camouflage the true effect of third-body wear (Scholes and Joyce, 2013). Saikko (2005) suggests that a preferable lubricant temperature for wear simulator studies should be 20°C with a high volume of lubricant present in an open chambers' configuration, this "low temperature" would eliminate the need for the use of external microbial growth agents which also affect the wear mechanisms.

The frequency in this study was set at 1 Hz (60 cycles/min) based on ISO standards, however, the number of cycles per year and frequency of activities varies among shoulder, hip, and knee replacements. For hip and knee replacements, it has been reported that approximately 5,000 to 7,000 steps are performed per day, which would result in about 2.2 million cycles per year (Kinkel *et al.*, 2009). In the case of shoulder replacements, approximately only 38 and 52 motions per hour for rTSA and aTSA have been reported respectively, which is equivalent of less than 1 cycle per minute, or the equivalent of 0.017 Hz (Langohr *et al.*, 2018). These values correspond to approximately 0.22 million cycles and 0.34 million cycles per year respectively (assuming 16 hours of activities per day (Matthews *et al.*, 2008)), which is far below the activity reported by patients with of hip and knee joints. However, undertaking an

in vitro shoulder simulator wear test with such slow speed would increase dramatically the time taken and the cost of the testing, hence the decision of increasing the frequency to that in line with the international standards for the hip and the knee replacements was taken.

This study has a number of limitations. First, as with any *in vitro* wear study there exists differences in the lubricant (rheology and biochemistry) used in place of the natural synovial fluid, which could have an impact on the wear rates in these studies compared to *in vivo* conditions. Second, any polymeric and metallic debris in the lubricant was not analysed from the RML wear test. This may have helped with understanding the origin of the wear and will be the subject of future work

5.2 COULD PYROCARBON SERVE AS AN ALTERNATIVE BEARING SURFACE IN ANATOMIC SHOULDER REPLACEMENT?

The present study is the first long-term shoulder simulator test to evaluate the wear of PyroCarbon humeral heads on polyethylene in an anatomic total shoulder joint arthroplasty. The UHMWPE wear rate obtained in this study was compared with previous *in vitro* wear tests, where *conventional* and alternative bearing material surfaces were used in the humeral heads of anatomic total shoulder arthroplasties (**Table 2.15**).

The UHMWPE wear rate over 5 million cycles against PyroCarbon humeral heads reported in this study was 19.3 ± 9.5 mm^3/million cycles, which is within the range shown in **Table 2.15** (9.9 mm^3/million cycles to 49.9 ± 1.4 mm^3/million cycles). While there will likely be differences between the simulators shown in **Table 2.15**, the key comparison of results will be with those of Smith *et al.* (2018) who used the same Newcastle Shoulder Wear Simulator. They reported a UHMWPE wear rate of 21.5 ± 5.4 mm^3/million cycles on glenoid inserts against CoCr humeral heads. There was no statistically significant difference ($\rho = 0.750$) between the wear of UHMWPE against PyroCarbon compared to CoCr. There was a slightly difference in this test. As Smith *et al.* (2018), applied only the loads and motion associated with "mug to mouth" and an sliding motion of 4 mm.

Even though the Newcastle Shoulder Wear Simulator was used in the previous experiment, and the wear testing conditions are assumed to be closely similar, the effect of the shoulder joints kinematics used as a simulator input (activities of daily living) should be taken into consideration for further comparisons as described by Braun *et al.* (2018) as it may also influence the wear performance of the polyethylene components.

Unfortunately, to date, there is no *ex vivo* data in terms of surface roughness for PyroCarbon shoulder components. During this *in vitro* test, the surface roughness (S_a) of the PyroCarbon humeral heads did not show a significant change (21 ± 2 nm to 18 ± 5 nm; $\rho = 0.402$). In contrast, the aTSR CoCr humeral head components tested by Smith *et al.* (2018), roughened over 5 million cycles (from 19 ± 3 nm to 43 ± 13 nm; $\rho = 0.013$). The metallic components showed macroscopic scratches, while the articulating surfaces of the PyroCarbon humeral heads showed no similar damage.

PyroCarbon bearings have some advantages over prior CoCr metal components in anatomical total shoulder arthroplasty system. As a ceramic-like bearing, PyroCarbon may have an increased wettability compared to metal, resulting in better boundary layer lubrication (Galetz *et al.*, 2010; Piconi *et al.*, 2017). In addition, they are resistant to the wear-promoting scratches that can develop in metal humeral heads (Urban *et al.*, 2001; Lee *et al.*, 2009). Both of these factors may have contributed to the lack of surface changes observed with PyroCarbon humeral heads when compared to the roughened CoCr components.

On the other hand, scratches may occur on metallic components in total joint replacements even if they articulate against a softer polyethylene. Furthermore, if the metallic material also takes part in the wear process, a release of metal particles may be expected during the *in vivo* time. The polyethylene wear might even be accelerated if the surface roughness of the metallic counterpart is increased. Thus, the humeral heads made of PyroCarbon material may also have the potential to eliminate the release of metal particles in aTSR and be useful where patients have a metal sensitivity.

The lack of change in roughness values of the PyroCarbon humeral heads is in agreement with an explant study on PyroCarbon finger implants by Bone *et al.* (2014), which noted no evidence of damage on the articulating surfaces of retrieved PyroCarbon components. The time *in vivo* for these explants was between 1 and 3 years, and the articulating surfaces had an average roughness value of 28 ± 11 nm. The PyroCarbon roughness values are also in good agreement with the results obtained by Naylor *et al.* (2015) during a 5 million cycles wear test on PyroCarbon–on–PyroCarbon finger replacements, where at the end of the test no change in the surface roughness values was observed on the test components (from 23 ± 9 nm to 29 ± 19 nm; $\rho = 0.244$).

5.3 SURFACE ROUGHNESS IN RETRIEVED REVERSE SHOULDER COMPONENTS

To the authors' best knowledge this is the first retrieval study of explanted metal–on–polyethylene reverse total shoulder replacements to report the surface topography of the two articulating counterfaces.

While each manufacturer may have their own guidance on values of surface finish, and these may be commercially confidential, international standards for the articulating surfaces of artificial shoulder joints states that two-dimensional (2D) roughness average values denoted with the capital letter "R" (R_a) should be no rougher than 2 µm for the polyethylene bearing surface and less than 0.10 µm for the metallic bearing component ASTM F1378 (2018) "Standard specification for shoulder prostheses".

Additionally, in previous *in vitro* wear studies on rTSR (Smith *et al.*, 2015; Ramirez-Martinez *et al.*, 2019) three-dimensional surface roughness were assessed on pristine JRI Reverse VAIOS® 42-mm articulating components (JRI Orthopaedics, Sheffield, United Kingdom; n = 11), having a mean ± standard deviation (S_a) values as-manufactured of 0.656 ± 0.051 µm for the *non-crosslinked* UHMWPE humeral inserts and 0.036 ± 0.006 µm for the CoCr glenospheres.

If this ASTM guidance is taken into consideration as one factor when deciding if an explanted component has roughened or not during *in vivo* time, and assuming that R_a is approximately equivalent to S_a, only the articulated bearing components from shoulder sample 7 (Tornier; septic mobilization) fell outside the ASTM guidance, and could therefore be assumed to have worn *in vivo*. After three months *in vivo*, the polymeric humeral insert roughened to 2.768 ± 0.862 µm S_a, and the metallic glenosphere increase its value in an order of magnitude to 0.260 ± 0.252 µm S_a. Alternatively, perhaps these components were out of specification.

However, if the surface roughness values from these studies are taken as a reference, four polyethylene humeral inserts and seven metallic glenosphere components among the *conventional* arrangement group get roughened over the time *in vivo*, in contrast with the *inverted* arrangement group where four polyethylene humeral inserts and two metallic glenosphere components became smoother. Therefore, a better understanding

of the surface roughness of the reverse total shoulder replacement bearing surfaces may help explain wear and damage that occur *in vivo*.

Machining marks are the principal sight of an unworn surface in polymeric components, previous rTSR *in vitro* wear study (Ramirez-Martinez *et al.*, 2019) has described the topography surface change on humeral inserts after being tested under activities of daily living over extended periods. Where the original machine marks worn away leaving a relatively smooth surface with the presence of multidirectional scratches. Among the retrieved polymeric components, the manufacturer's machining marks were still present on the polar region of the humeral inserts (4/8) and on the surface of the glenosphere components (2/4), indicating a lack of surface damage *in vivo*.

Nonetheless, this is not congruent with the visual and surface roughness assessment among the retrieved reverse total shoulder articulating components, which in most of the cases showed evidence of multidirectional scratches and burnishing on the bearing surfaces as a consequence of abrasive mechanism during the time *in vivo*. This wear mechanism affects the UHMWPE performance (Nam *et al.*, 2010b; Harman *et al.*, 2011; Day *et al.*, 2012) and is dominated by surface asperities on the harder surface (metallic component) of the bearing couple. Although third-body wear particles can also influence and cause abrasive wear, a key component is the roughness of the bearing material itself.

In addition, there was also evidence of rim damage on rTSR *conventional* bearing design, three of eight retrieved cases (38%) of humeral insert components showed damage around the rim as a possible consequence of bony scapular notching impingement (Sirveaux *et al.*, 2004) or contact with the inferior locking screw (Day *et al.*, 2012).

This damage was not present during the analysis of the metallic humeral inserts used in the *inverted* bearing design; suggesting that the inversion of the articulated bearing materials (humeral component made by highly polished metallic alloy) could eliminate the gradual erosion of the polymeric component implant against the scapular bone, and the subsequent generation of polyethylene wear debris in rTSR. The rim damage on these components did not affect the surface roughness analysis.

The skewness of height distribution (S_{sk}) appears to be a better 3D surface roughness parameter to discriminate the *in vivo* change of explanted shoulder replacements and should be included in the retrieved studies together with the arithmetic average height of the surface (S_a), which normally describes the absolutes values of the surface. Work carried out by Joyce *et al.* (2011a) on metal–on–metal hip replacements shown a significant change of the skewness distribution between the 'unworn' and 'worn' areas, where smooth surfaces have a positive skewness while surfaces with deep scratches exhibit a negative skewness.

The increase in roughness of the rTSR metallic components during the time *in vivo* is in agreement with other *ex vivo* studies on metal–on–polyethylene hip (Elfick *et al.*, 1999) and knee (Scholes *et al.*, 2013) replacements, where an increase in the surface roughness values has been observed between the "worn" and "unworn" regions of metallic femoral components. *In vitro* studies report abrasion and multidirectional scratches on the polyethylene humeral insert surface after been tested under activities of daily living over extender periods (Smith *et al.*, 2015; Ramirez-Martinez *et al.*, 2019).

While the sample size of four is small, that retrieved metallic humeral insert components used in the *inverted* agreement had a relatively low S_a value (mean of < .020 µm) is worthy of note and perhaps deserves further investigation in other retrieval studies.

In rTSR systems, long-term survival is influenced by multiple contributing factors that are a combination of the surgeon, patient, and implant variables. The surface roughness of the articulating surfaces is just one contributor to this larger picture. Data provided in this retrieval study can be added to clinical follow-up studies, *in vitro* wear analysis, and *in silico* simulations to help provide a clearer understanding of how the component variables could influence wear *in vivo*.

Infection is the second most common complication after reverse total shoulder arthroplasty (Australian Orthopaedic Association (AOA), 2020), in this study eight of the thirteen cases were revised due to infection which represents 62% of the rTSR explanted population. This high percentage of infections tallies with the results of

others (Farshad and Gerber, 2010; Boileau, 2016). Indeed, Farshad and Gerber (2010) talk of the 'extraordinarily high infection rate' associated with reverse shoulders.

The most common bacterial pathogens related to infected rTSR implants are *Propionibacterium acnes*, *Staphylococcus epidermidis* and *Staphylococcus aureus* (Franceschini and Chillemi, 2013; Jacquot *et al.*, 2015). The surface roughness of the implant plays a key role in the bacterial adhesion process, where a rougher surface with the presence of irregularities in its topography normally provide a more favourable site for adhesion and colonization than a smoother surface (Scheuerman *et al.*, 1998; Cheng *et al.*, 2019). However, the influence of the surface roughness on the bacterial adhesion in polymeric implants is not as evident (Kinnari *et al.*, 2010) in comparison with metallic components, where a surface roughness of 0.010 μm is recommended for medical implants (Mendonca *et al.*, 2008).

This study had several limitations. Compared to some retrieval studies, 13 may appear a small sample size, but it is the largest sample of reverse shoulders reported to date where roughness values have been offered. The sample size reduces further when different manufacturers, different implant designs and different bearing materials have been offered but is why this study has only stratified between *conventional* and *inverse* material arrangements.

It is also possible that different materials and sizes could be linked with roughness, but this cohort was not large enough to investigate this. In terms of the polyethylenes used by different manufacturers, it was unable to get full details. It is known that different polyethylenes show different wear characteristics (Harsha and Joyce, 2013). In addition, it is appreciated that reverse shoulders can be classified according to the design principle of medial glenosphere and medial humerus (MGMH), lateral glenosphere and medial humerus (LGMH), lateral glenosphere and lateral humerus (LGLH), and medial glenosphere and lateral humerus (MGLH). This design feature can affect the biomechanics of the reverse shoulder, so it is of importance. While this cohort was too small to investigate this area, it is an important consideration for future work. As a further limitation, the study lacked data on the *in vivo* positioning of the implants so such variables could not be investigated.

This page intentionally left blank

Chapter 6. THESIS CLOSURE

6.1 NOVELTY STATEMENT

The collection of results and findings obtained in this research at Newcastle University may help others who test artificial shoulder joints to validate the design of their simulators, improve mathematical wear model predictions, optimize the selection of bearing materials, and contribute to the ongoing efforts to produce the first international standard for *in vitro* wear testing of shoulder prostheses.

6.2 CONCLUSIONS

6.2.1 Influence of severe protocol on polyethylene wear in rTSR?

This is the first time a repeated–motion–load cycle has been applied to artificial total shoulder joints. Wear rates showed good agreement to those when motion without interspersed static load was applied. This result fits with the Lancaster wear equation, in which wear is proportional to sliding distance. Based on this result, it may be that, when wear testing metal–on–polyethylene shoulder implants, the application of a physiological motion and dynamic loading are sufficient.

However, the surface roughness of samples from repeated–motion–load (RML) wear test was found to be significantly lower than those from continuous motion test after a similar number of wear cycles. This was attributed to the more clinically relevant wear simulation method which can promote the breakdown of the protective lubricant film under the intermittent motion, clearly suggesting that further simulator testing should include an RML motion protocol.

6.2.2 PyroCarbon humeral head as an alternative bearing surface in aTSR?

For the first time, PyroCarbon humeral heads were *in vitro* wear tested against UHMWPE components. Wear rates were found to be similar to well-proven CoCr humeral heads on UHMWPE shoulder arthroplasties.

The lack of an appreciable reduction in wear of the UHMWPE component when articulated with an expensive and complex to manufacture PyroCarbon component likely means there is little clinical cost-benefit in the use of a PyroCarbon on UHMWPE shoulder implant.

However, the PyroCarbon heads showed no change in roughness after 5 million cycles. Should a patient have metal sensitivities, then a PyroCarbon component could be considered.

6.2.3 Retrieval analysis of rTSR

Thirteen retrieved metal–on–polyethylene reverse total shoulder implants from seven different manufactures were assessed for changes to their articulating surface roughness. Nine had a *conventional* arrangement of a metallic glenosphere component articulating against a polyethylene humeral insert. The other four explants *inverted* this configuration.

The polymeric humeral insert components used for the *conventional* reverse total shoulder arthroplasties showed no significant difference ($\rho = 0.413$) in the final surface roughness (S_a, 0.937 ± 0.838 μm; $n = 8$) in comparison when the bearing material was *inverted* and polymer was used in the glenosphere components (S_a , 1.231 ± 0.346 μm; $n = 4$). However, a significant finding from this study is that the inversion of the materials may avoid the accelerated polyethylene wear caused by scapular notching, and minimize the articular surface damage on metallic humeral components.

The most important finding in this first reported measurement of roughness of explanted reverse shoulders is that the metallic components used in the *conventional* arrangement (glenospheres) were significantly rougher than those in the inverse arrangement (humeral inserts). This quantitative finding was supported by visual

assessment, with none of the four retrieved humeral insert components showing the presence of mild to severe scratches, which was the case with some of the glenospheres. This could as a result of the effect of different sliding distances between the components depending on their bearing configuration.

In addition, predominant surface damage modes observed on most of the *conventional* reverse total shoulder arthroplasty implants during the analysis of the surface topography were similar to those obtained from the *in vitro* wear test, and consistent with previous observations on retrieved components; the similitude between these results helped to validate the Newcastle Shoulder Wear Simulator.

6.3 FUTURE DIRECTIONS

This research has achieved the specific aims outlined at the beginning of this thesis, however, there still exists the opportunity to further investigate the tribology of anatomic and reverse total shoulder replacements.

The current wear simulation strategy has established a clinically relevant protocol for testing shoulder replacements using a unique shoulder wear simulator, which has complemented those of previous researches, and contributed to extend the knowledge of the wear performance of artificial shoulder joint replacements. Nevertheless, future research work can be built upon the outcome of this and various improvements could be made in future studies, which are suggested below as:

- Evaluate the effect of the repeated–motion–load (RML) protocol on different bearing material combinations on implants with the same design and size.
- Isolate, analyse and report the size, morphonology, and concentration of the polyethylene wear particles from the *serum*.
- Detail the lubrication film thickness change through the wear test and confirm the suggested potential use of RML adverse protocol.

This work herein is also one of the first to examine the change of the surface roughness on explanted shoulder replacements, and therefore, the potential direction could be suggested as:

- One of the possible limitations of this explant study was the cohort size. Ideally, larger collections of shoulder explants of similar design should be analysed in order to identify correlations between change of surface roughness and patient factors, time *in vivo*, design factors, etc. Implant failures tend to be multi-factorial and therefore larger cohorts are required to identify trends in failure mechanisms. However, it is also important to make a start with what is available and the uniqueness of the roughness assessment of explanted rTSRs should be recognised.
- Develop a method to obtain the 3D geometry of a larger collection of shoulder explants and compared with unworn implants, in order to identify the correlation between the volumetric wear, change of surface roughness, patient factors, and time *in vivo*.

6.3.1 The perfect shoulder wear simulator

The perfect shoulder wear simulator would be the one that could exactly replicate the surrounding lubricants, the loading profiles, and the motion tracks experience by the shoulder implants during *in vivo* conditions.

The wear test protocol that takes place should subject the artificial shoulder joints to a range of motions and loads to reflect the various patients for whom they are intended. Examples of differences between patients might include the type of implant (aTSR or rTSR), age, weight, activities, and activity levels. This level of testing complexity would be both exhaustive and exhausting.

The temperature of the lubricant must be monitored throughout the test in order to avoid protein degradation and the creation of sedimentation between the articulating surfaces, which can promote different wear mechanisms and resulting in different wear rates.

REFERENCES

Ackland, D.C., Patel, M. and Knox, D. (2015) 'Prosthesis design and placement in reverse total shoulder arthroplasty', *J Orthop Surg Res*, *10*, p. 101.

Ackland, D.C., Roshan-Zamir, S., Richardson, M. and Pandy, M.G. (2010) 'Moment arms of the shoulder musculature after reverse total shoulder arthroplasty', *J Bone Joint Surg Am*, *92*(5), pp. 1221-1230.

Ackland, D.C., Roshan-Zamir, S., Richardson, M. and Pandy, M.G. (2011) 'Muscle and joint-contact loading at the glenohumeral joint after reverse total shoulder arthroplasty', *J Orthop Res*, *29*(12), pp. 1850-1858.

Affatato, S. (2014) 'The History of Biomaterials sed in Total Hip Arthroplasty (THA) ', in *Perspective inTotal Hip Arthroplasty*. Woodhead Publishing, pp. 19-36.

Affatato, S., Leardini, W. and Zavalloni, M. (2006) 'Hip joint simulators: State of the Art', in Benazzo, F., Falez, F. and Dietrich, M. (eds.) *Bioceramics and Alternative Bearings in Joint Arthroplasty*. Ceramics in Orthopaedics: Steinkopff, pp. 171-180.

Alexander, J.J., Bell, S.N., Coghlan, J., Lerf, R. and Dallmann, F. (2019) 'The effect of vitamin E-enhanced cross-linked polyethylene on wear in shoulder arthroplasty-a wear simulator study', *J Shoulder Elbow Surg*, *28*(9), pp. 1771-1778.

Amstutz, H.C., Campbell, P., Kossovsky, N. and Clarke, I.C. (1992) 'Mechanism and clinical significance of wear debris-induced osteolysis', *Clin Orthop Relat Res*, (276), pp. 7-18.

Anakwenze, O.A., Yehyawi, T., Dillon, M.T., Paxton, E., Navarro, R. and Singh, A. (2017) 'Effect of age on outcomes of shoulder arthroplasty', *Perm J*, *21*, pp. 16-056.

Anglin, C., Wyss, U.P. and Pichora, D.R. (2000) 'Glenohumeral contact forces', *Proc Inst Mech Eng H*, *214*(6), pp. 637-644.

Antunes, R.A. and de Oliveira, M.C. (2012) 'Corrosion fatigue of biomedical metallic alloys: mechanisms and mitigation', *Acta Biomater*, *8*(3), pp. 937-962.

ASTM F75 (2018) *Standard Specification for Cobalt-28Chromium-6Molybdenum Alloy Castings and Casting Alloy for Surgical Implants (UNS R30075)*. West Conshohocken, PA: ASTM International.

ASTM F138 (2019) *'Standard Specification for Wrought 18Chromium-14Nickel-2.5Molybdenum Stainless Steel Bar and Wire for Surgical Implants (UNS S31673)'*. West Conshohocken, PA: ASTM International.

ASTM F799 (2018) *'Standard Specification for Cobalt-28 Chromium-6 Molybdenum Alloy Forgings for Surgical Implants (UNS R31537, R31538, R31539)'*. West Conshohocken, PA: ASTM International.

ASTM F1108 (2014) *'Standard Specification for Titanium-6Aluminum-4Vanadium Alloy Castings for Surgical Implants (UNS R56406)'*. West Conshohocken, PA: ASTM International.

ASTM F1378 (2018) *'Standard Specification for Shoulder Prostheses'*. West Conshohocken, PA: ASTM International.

ASTM F2028 (2017) *'Standard Test Methods for Dynamic Evaluation of Glenoid Loosening or Disassociation'*. West Conshohocken, PA: ASTM International.

ASTM G40 (2017) *'Standard Terminology relating to Wear and Erosion'*. West Conshohocken, PA: ASTM International.

Australian Orthopaedic Association (AOA) (2020) *'National Joint Replacement Registry'*. [Online]. Available at: https://aoanjrr.sahmri.com (Accessed: October 2020).

Beckenbaugh, R.D., Klawitter, J. and Cook, S. (2006) 'Osseointegration and mechanical stability of pyrocarbon and titanium hand implants in a load-bearing in vivo model for small joint arthroplasty', *J Hand Surg Am*, *31*(7), pp. 1240-1241.

Bellemere, P. (2018) 'Pyrocarbon implants for the hand and wrist', *Hand Surg Rehabil*, *37*(3), pp. 129-154.

Bergmann, G., Graichen, F., Bender, A., Kaab, M., Rohlmann, A. and Westerhoff, P. (2007) 'In vivo glenohumeral contact forces--measurements in the first patient 7 months postoperatively', *J Biomech*, *40*(10), pp. 2139-2149.

Bergmann, G., Graichen, F., Bender, A., Rohlmann, A., Halder, A., Beier, A. and Westerhoff, P. (2011) 'In vivo gleno-humeral joint loads during forward flexion and abduction', *J Biomech*, *44*(8), pp. 1543-1552.

Berliner, J.L., Regalado-Magdos, A., Ma, C.B. and Feeley, B.T. (2015) 'Biomechanics of reverse total shoulder arthroplasty', *J Shoulder Elbow Surg*, *24*(1), pp. 150-160.

Bey, M.J., Kline, S.K., Zauel, R., Kolowich, P.A. and Lock, T.R. (2010) 'In Vivo Measurement of Glenohumeral Joint Contact Patterns', *EURASIP J Adv Signal Process*, *2010*.

Binazzi, R. (2014) 'Ceramic Articulations: (Much) More Benefits than Concerns', in Knahr, K. (ed.) *Tribology in Total Hip and Knee Arthroplasty*. Springer-Verlag Berlin, pp. 65-70.

Bohsali, K.I., Wirth, M.A. and Rockwood, C.A., Jr. (2006) 'Complications of total shoulder arthroplasty', *J Bone Joint Surg Am*, *88*(10), pp. 2279-2292.

Boileau, P. (2016) 'Complications and revision of reverse total shoulder arthroplasty', *Orthop Traumatol Surg Res*, *102*(1 Suppl), pp. S33-43.

Boileau, P. and Walch, G. (1997) 'The three-dimensional geometry of the proximal humerus. Implications for surgical technique and prosthetic design', *J Bone Joint Surg Br*, *79*(5), pp. 857-865.

Boileau, P., Watkinson, D., Hatzidakis, A.M. and Hovorka, I. (2006) 'Neer Award 2005: The Grammont reverse shoulder prosthesis: Results in cuff tear arthritis, fracture sequelae, and revision arthroplasty', *J Shoulder Elbow Surg*, *15*(5), pp. 527-540.

Boileau, P., Watkinson, D.J., Hatzidakis, A.M. and Balg, F. (2005) 'Grammont reverse prosthesis: design, rationale, and biomechanics', *J Shoulder Elbow Surg*, *14*(1 Suppl S), pp. 147S-161S.

Bokros, J.C. (1977) 'Carbon Biomedical Devices', *Carbon*, *15*(6), pp. 355-371.

Bokros, J.C. (1983) 'Carbon in medical devices', *Ceramics International*, *9*(1), pp. 3-7.

Bone, M.C., Giddins, G. and Joyce, T.J. (2014) 'An analysis of explanted pyrolytic carbon prostheses', *J Hand Surg Eur Vol*, *39*(6), pp. 666-667.

Braman, J.P., Falicov, A., Boorman, R. and Matsen, F.A., 3rd (2006) 'Alterations in surface geometry in retrieved polyethylene glenoid component', *J Orthop Res*, *24*(6), pp. 1249-1260.

Brandt, J.M., Charron, K., Zhao, L., MacDonald, S.J. and Medley, J.B. (2012) 'Calf serum constituent fractions influence polyethylene wear and microbial growth in knee simulator testing', *Proc Inst Mech Eng H*, *226*(6), pp. 427-440.

Braun, S., Schroeder, S., Mueller, U., Sonntag, R., Buelhoff, M. and Kretzer, J.P. (2018) 'Influence of joint kinematics on polyethylene wear in anatomic shoulder joint arthroplasty', *J Shoulder Elbow Surg*, *27*(9), pp. 1679-1685.

Brockett, C., Williams, S., Jin, Z., Isaac, G. and Fisher, J. (2007) 'Friction of total hip replacements with different bearings and loading conditions', *J Biomed Mater Res B Appl Biomater*, *81*(2), pp. 508-515.

Brockett, C., Williams, S., Jin, Z.M. and Fisher, J. (2012) 'Friction in Joint Replacements', in Wang, Q.J. and Chung, Y. (eds.) *Encyclopedia of Tribology*. Springer, pp. 1325-1330.

Brorson, S., Rasmussen, J.V., Olsen, B.S., Frich, L.H., Jensen, S.L. and Hrobjartsson, A. (2013) 'Reverse shoulder arthroplasty in acute fractures of the proximal humerus: A systematic review', *Int J Shoulder Surg*, *7*(2), pp. 70-78.

Brown, S.S. and Clarke, I.C. (2006) 'A Review of Lubrication Conditions for Wear Simulation in Artificial Hip Replacements', *Tribology Transactions*, *49*(1), pp. 72-78.

Bytyqi, D., Kafeloff, M. and Shabani, B. (2020) 'Biomechanics of rTSA', in Huri, G., Familiari, F., Moon, Y.L., Doral, M.N. and Marcheggiani Muccioli, G.M. (eds.) *Shoulder Arthroplasty-The Shoulder Club Guide*. Springer International Publishing, pp. 41-45.

Cann, P.M. (2013) 'Boundary Lubrication Mechanisms in Artificial Joints', in Wang, Q.J. and Chung, Y. (eds.) *Encyclopedia of Tribology*. Springer, pp. 259-262.

Carnes, K.J., Odum, S.M., Troyer, J.L. and Fehring, T.K. (2016) 'Cost Analysis of Ceramic Heads in Primary Total Hip Arthroplasty', *J Bone Joint Surg Am*, *98*(21), pp. 1794-1800.

Carpenter, S.R., Urits, I. and Murthi, A.M. (2016) 'Porous metals and alternate bearing surfaces in shoulder arthroplasty', *Curr Rev Musculoskelet Med*, *9*(1), pp. 59-66.

Chalmers, P.N., Kahn, T., Broschinsky, K., Ross, H., Stertz, I., Nelson, R., Yoo, M. and Tashjian, R.Z. (2019) 'An analysis of costs associated with shoulder arthroplasty', *J Shoulder Elbow Surg*, *28*(7), pp. 1334-1340.

Charlton, I.W. and Johnson, G.R. (2006) 'A model for the prediction of the forces at the glenohumeral joint', *Proc Inst Mech Eng H*, *220*(8), pp. 801-812.

Charnley, J. (1979) *'Low Friction Arthroplasty of the Hip'*. Springer-Verlag Berlin.

Cheng, Y., Feng, G. and Moraru, C.I. (2019) 'Micro- and nanotopography sensitive bacterial attachment mechanisms: A review', *Front Microbiol*, *10*, p. 191.

Chillemi, C. and Franceschini, V. (2013) 'Shoulder osteoarthritis', *Arthritis*, *2013*, pp. 1-7.

Choi, A.H., Conway, R.C., Cazalbou, S. and Ben-Nissan, B. (2018) 'Maxillofacial bioceramics in tissue engineering: Production techniques, properties, and applications', in Thomas, S., Balakrishnan , P. and Sreekala, M.S. (eds.) *Fundamental Biomaterials: Ceramics*. Woodhead Publishing, pp. 63-93.

Churchill, R.S., Brems, J.J. and Kotschi, H. (2001) 'Glenoid size, inclination, and version: an anatomic study', *J Shoulder Elbow Surg*, *10*(4), pp. 327-332.

Clarke, I.C., Good, V., Williams, P., Schroeder, D., Anissian, L., Stark, A., Oonishi, H., Schuldies, J. and Gustafson, G. (2000) 'Ultra-low wear rates for rigid-on-rigid bearings in total hip replacements', *Proc Inst Mech Eng H*, *214*(4), pp. 331-347.

Codsi, M. (2016) 'Glenoid Anatomy and Biomechanics', in Armstrong, A.D. and Murthi, A.M. (eds.) *Anatomic Shoulder Arthroplasty*. Springer International Publishing, pp. 67-95.

Coley, B., Jolles, B.M., Farron, A. and Aminian, K. (2008) 'Arm position during daily activity', *Gait Posture*, *28*(4), pp. 581-587.

Cooke, A.F., Dowson, D. and Wright, V. (1978) 'The Rheology of Synovial Fluid and Some Potential Synthetic Lubricants for Degenerate Synovial Joints', *Engineering in Medicine*, *7*(2), pp. 66-72.

Culham, E. and Peat, M. (1993) 'Functional anatomy of the shoulder complex', *J Orthop Sports Phys Ther*, *18*(1), pp. 342-350.

Daecke, W., Veyel, K., Wieloch, P., Jung, M., Lorenz, H. and Martini, A.K. (2006) 'Osseointegration and mechanical stability of pyrocarbon and titanium hand implants in a load-bearing in vivo model for small joint arthroplasty', *J Hand Surg Am*, *31*(1), pp. 90-97.

Davidson, J.A., Poggie, R.A. and Mishra, A.K. (1994) 'Abrasive wear of ceramic, metal, and UHMWPE bearing surfaces from third-body bone, PMMA bone cement, and titanium debris', *Biomed Mater Eng*, *4*(3), pp. 213-229.

Davis, J.R. (2003) 'Metallic Materials', in Davis, J.R. (ed.) *Handbook of Materials for Medical Devices*. Materials Park-Ohio: ASTM International, pp. 21-50.

Day, J.S., MacDonald, D.W., Olsen, M., Getz, C., Williams, G.R. and Kurtz, S.M. (2012) 'Polyethylene wear in retrieved reverse total shoulder components', *J Shoulder Elbow Surg*, *21*(5), pp. 667-674.

Day, J.S., Paxton, E.S., Lau, E., Gordon, V.A., Abboud, J.A. and Williams, G.R. (2015) 'Use of reverse total shoulder arthroplasty in the Medicare population', *J Shoulder Elbow Surg*, *24*(5), pp. 766-72.

De Wilde, L. (2017) 'Unresolved questions in reverse total shoulder arthroplasty', *Obere Extremität*, *12*(1), pp. 4-5.

Deshmukh, A.V., Koris, M., Zurakowski, D. and Thornhill, T.S. (2005) 'Total shoulder arthroplasty: long-term survivorship, functional outcome, and quality of life', *J Shoulder Elbow Surg*, *14*(5), pp. 471-479.

Di Puccio, F. and Mattei, L. (2015) 'Biotribology of artificial hip joints', *World J Orthop*, *6*(1), pp. 77-94.

Dickson, D.R., Nuttall, D., Watts, A.C., Talwalkar, S.C., Hayton, M. and Trail, I.A. (2015) 'Pyrocarbon proximal interphalangeal joint arthroplasty: Minimum five-year follow-up', *J Hand Surg Am*, *40*(11), pp. 2142-2148.

Dieckmann, R., Liem, D., Gosheger, G., Henrichs, M.P., Holl, S., Hardes, J. and Streitburger, A. (2013) 'Evaluation of a reconstruction reverse shoulder for tumour surgery and tribological comparision with an anatomical shoulder arthroplasty', *Int Orthop*, *37*(3), pp. 451-456.

Diop, A., Maurel, N., Grimberg, J. and Gagey, O. (2006) 'Influence of glenohumeral mismatch on bone strains and implant displacements in implanted glenoids. An in vitro experimental study on cadaveric scapulae', *J Biomech*, *39*(16), pp. 3026-3035.

Dorozhkin, S.V. (2018) 'Calcium-orthophosphate-based bioactive ceramics', in Thomas, S., Balakrishnan , P. and Sreekala, M.S. (eds.) *Fundamental Biomaterials: Ceramics*. Woodhead Publishing, pp. 297-405.

Downson, D. (2014) 'Hip replacement: tribological properties, materials and engineering', in Revell, P.A. (ed.) *Joint Replacement Technology*. Woodhead Publishing, pp. 431-461.

Dowson, D. and Wright, V. (1981) *Introduction to the Biomechanics of Joints and Joint Replacements*. London: Mechanical Engineering Publications.

Drake, G.N., O'Connor, D.P. and Edwards, T.B. (2010) 'Indications for reverse total shoulder arthroplasty in rotator cuff disease', *Clin Orthop Relat Res*, *468*(6), pp. 1526-1533.

Drake, R., Vogl, W. and Mitchell, A.W.M. (2019) 'Upper Limb', in *Gray's Anatomy for Students*. 4th edn. Elsevier, pp. 673-818.

Elfick, A.P., Hall, R.M., Pinder, I.M. and Unsworth, A. (1999) 'The influence of femoral head surface roughness on the wear of ultrahigh molecular weight polyethylene sockets in cementless total hip replacement', *J Biomed Mater Res*, *48*(5), pp. 712-718.

Fang, H.-W., Shih, M.-L., Zhao, J.-H., Huang, H.-T., Lin, H.-Y., Liu, H.-L., Chang, C.-H., Yang, C.-B. and Liu, H.-C. (2007) 'Association of polyethylene friction and thermal unfolding of interfacial albumin molecules', *Applied Surface Science*, *253*(16), pp. 6896-6904.

Farshad, M. and Gerber, C. (2010) 'Reverse total shoulder arthroplasty-from the most to the least common complication', *Int Orthop*, *34*(8), pp. 1075-1082.

Favre, P., Snedeker, J.G. and Gerber, C. (2009) 'Numerical modelling of the shoulder for clinical applications', *Philos Trans A Math Phys Eng Sci*, *367*(1895), pp. 2095-2118.

Fortune Businnes Insights (2019) *'Orthopedic Joint Replacement Market Size, Share and Industry Analysis By Product (Knee, Hip, Shoulder, Ankle, Others), By Procedure (Total Replacement, Partial Replacement, Others), By End User (Hospital, Ambulatory Surgical Centers, Orthopedic Clinics, Others), and Regional Forecast 2019-2026'.* [Online]. Available at: www.fortunebusinessinsights.com/industry-reports/orthopedic-joint-replacement-market-100314.

Fox, T.J., Foruria, A.M., Klika, B.J., Sperling, J.W., Schleck, C.D. and Cofield, R.H. (2013) 'Radiographic survival in total shoulder arthroplasty', *J Shoulder Elbow Surg*, *22*(9), pp. 1221-1227.

Franceschini, V. and Chillemi, C. (2013) 'Periprosthetic shoulder infection', *Open Orthop J*, *7*, pp. 243-249.

Franklin, J.L., Barrett, W.P., Jackins, S.E. and Matsen, F.A., 3rd (1988) 'Glenoid loosening in total shoulder arthroplasty. Association with rotator cuff deficiency', *J Arthroplasty*, *3*(1), pp. 39-46.

Galetz, M.C., Seiferth, S.H., Theile, B. and Glatzel, U. (2010) 'Potential for adhesive wear in friction couples of UHMWPE running against oxidized zirconium, titanium nitride coatings, and cobalt-chromium alloys', *J Biomed Mater Res B Appl Biomater*, *93*(2), pp. 468-475.

Gazielly, D.F., Scarlat, M.M. and Verborgt, O. (2015) 'Long-term survival of the glenoid components in total shoulder replacement for arthritis', *Int Orthop*, *39*(2), pp. 285-289.

Geary, C., O'Donnell, G.E., Jones, E., FitzPatrick, D. and Birkinshaw, C. (2010) 'Automated in-vitro testing of orthopaedic implants: a case study in shoulder joint replacement', *Proc Inst Mech Eng H*, *224*(11), pp. 1297-1309.

Geraldes, D.M., Hansen, U., Jeffers, J. and Amis, A.A. (2017) 'Stability of small pegs for cementless implant fixation', *J Orthop Res*, *35*(12), pp. 2765-2772.

Gerber, C., Pennington, S.D. and Nyffeler, R.W. (2009) 'Reverse total shoulder arthroplasty', *J Am Acad Orthop Surg*, *17*(5), pp. 284-295.

Good, V.D., Clarke, I.C., Gustafson, G.A., Downs, B., Anissian, L. and Sorensen, K. (2000) 'Wear of ultra-high molecular weight polyethylene and polytetrafluoroethylene in a hip simulator: a dose-response study of protein concentration', *Acta Orthop Scand*, *71*(4), pp. 365-369.

Goodman, S.B., Gomez Barrena, E., Takagi, M. and Konttinen, Y.T. (2009) 'Biocompatibility of total joint replacements: A review', *J Biomed Mater Res A*, *90*(2), pp. 603-618.

Graichen, H., Hinterwimmer, S., von Eisenhart-Rothe, R., Vogl, T., Englmeier, K.H. and Eckstein, F. (2005) 'Effect of abducting and adducting muscle activity on glenohumeral translation, scapular kinematics and subacromial space width in vivo', *J Biomech*, *38*(4), pp. 755-760.

Grammont, P.M., Trouilloud, P., Laffay, J. and Deries, X. (1987) 'Concept study and realization of a new total shoulder prosthesis', *Rhumatologie*, *39*, pp. 407-418.

Green, T. (1998) 'Polyethylene particles of a 'critical size' are necessary for the induction of cytokines by macrophages in vitro', *Biomaterials*, *19*(24), pp. 2297-2302.

Green, T.R., Fisher, J., Matthews, J.B., Stone, M.H. and Ingham, E. (2000) 'Effect of size and dose on bone resorption activity of macrophages by in vitro clinically relevant ultra high molecular weight polyethylene particles', *J Biomed Mater Res*, *53*(5), pp. 490-497.

Grobbelaar, C.J., du Plessis, T.A. and Marais, F. (1978) 'The radiation improvement of polyethylene prostheses. A preliminary study', *J Bone Joint Surg Br*, *60-B*(3), pp. 370-374.

Guery, J., Favard, L., Sirveaux, F., Oudet, D., Mole, D. and Walch, G. (2006) 'Reverse total shoulder arthroplasty. Survivorship analysis of eighty replacements followed for five to ten years', *J Bone Joint Surg Am*, *88*(8), pp. 1742-1747.

Gunther, S.B., Graham, J., Norris, T.R., Ries, M.D. and Pruitt, L. (2002) 'Retrieved glenoid components: A classification system for surface damage analysis', *The Journal of Arthroplasty*, *17*(1), pp. 95-100.

Haider, H., Sperling, J. and Throckmorton, T. (2013) 'A method for wear testing or reverse shoulder arthroplasty systems', *J Bone Joint Surg Am*, *95-B*, p. 607.

Hallab, N.J., McAllister, K., Brady, M. and Jarman-Smith, M. (2012) 'Macrophage reactivity to different polymers demonstrates particle size- and material-specific reactivity: PEEK-OPTIMA((R)) particles versus UHMWPE particles in the submicron, micron, and 10 micron size ranges', *J Biomed Mater Res B Appl Biomater*, *100*(2), pp. 480-492.

Hamrock, B.J. and Dowson, D. (1978) 'Elastohydrodynamic Lubrication of Elliptical Contacts for Materials of Low Elastic-Modulus I - Fully Flooded Conjunction. Transactions of the American Society of Mechanical Engineers.', *J Lubric Technol*, *100*(2), pp. 236-245.

Hanawa, T. (2010) 'Overview of Metals and Applications', in Niinomi, M. (ed.) *Metals for Biomedical Devices*. Woodhead Publishing, pp. 3-24.

Harman, M., Cristofolini, L., Erani, P., Stea, S. and Viceconti, M. (2011) 'A pictographic atlas for classifying damage modes on polyethylene bearings', *J Mater Sci Mater Med*, *22*(5), pp. 1137-1146.

Harris, W.H. (2001) 'Wear and periprosthetic osteolysis: the problem', *Clin Orthop Relat Res*, (393), pp. 66-70.

Harsha, A.P. and Joyce, T.J. (2013) 'Comparative wear tests of ultra-high molecular weight polyethylene and cross-linked polyethylene', *Proc Inst Mech Eng H*, *227*(5), pp. 600-608.

Hasan, S.S., Leith, J.M., Campbell, B., Kapil, R., Smith, K.L. and Matsen, F.A., 3rd (2002) 'Characteristics of unsatisfactory shoulder arthroplasties', *J Shoulder Elbow Surg*, *11*(5), pp. 431-441.

Hasirci, V. and Hasirci, N. (2018a) 'Ceramics as Biomaterials', in *Fundamentals of Biomaterials*. Springer-New York, pp. 51-64.

Hasirci, V. and Hasirci, N. (2018b) 'Metals as Biomaterials', in *Fundamentals of Biomaterials*. Springer-New York, pp. 35-50.

Hasirci, V. and Hasirci, N. (2018c) 'Polymers as Biomaterials', in *Fundamentals of Biomaterials*. Springer-New York, pp. 65-82.

Hasler, A., Meyer, D.C., Tondelli, T., Dietrich, T. and Gerber, C. (2020) 'Radiographic performance depends on the radial glenohumeral mismatch in total shoulder arthroplasty', *BMC Musculoskelet Disord*, *21*(1), p. 206.

Hastings, G., Gair, I. and Daily, D. (2016) 'Ceramic Materials Testing and Fracture Mechanics', in Murphy, W., Black, J. and Hastings, G. (eds.) *Handbook of Biomaterials Properties*. Springer-Verlag New York, pp. 353-445.

Henry, G. (1918) *'Anatomy of the human body'*. 20th edn. Philadelphia: Lea & Febiger.

Hess, S.A. (2000) 'Functional stability of the glenohumeral joint', *Man Ther*, *5*(2), pp. 63-71.

Hosseini, S. (2012) 'Fatigue of Ti-6Al-4V', in Hudak, R., Penhaker, M. and Majernik, J. (eds.) *Biomedical Engineering—Technical Applications in Medicine*. Rijeka, Croatia: InTech, pp. 75-92.

Hutchings, I.M. (2016) 'Leonardo da Vinci′s studies of friction', *Wear*, *360-361*, pp. 51-66.

Illgen, R.L., 2nd, Bauer, L.M., Hotujec, B.T., Kolpin, S.E., Bakhtiar, A. and Forsythe, T.M. (2009) 'Highly crosslinked vs conventional polyethylene particles: relative in vivo inflammatory response', *J Arthroplasty*, *24*(1), pp. 117-124.

Ingham, E. and Fisher, J. (2000) 'Biological reactions to wear debris in total joint replacement', *Proc Inst Mech Eng H*, *214*(1), pp. 21-37.

Inman, V.T., Saunders, J.B. and Abbott, L.C. (1944) 'Observations on the function of the shoulder joint', *J Bone Joint Surg Am*, *26*(1), pp. 1-30.

Irlenbusch, U., Kaab, M.J., Kohut, G., Proust, J., Reuther, F. and Joudet, T. (2015) 'Reversed shoulder arthroplasty with inversed bearing materials: 2-year clinical and radiographic results in 101 patients', *Arch Orthop Trauma Surg*, *135*(2), pp. 161-169.

ISO 14242 (2014) *'Implants for surgery - wear of total hip-joint prostheses - Part1: Loading and displacement parameters for wear-testing machines and corresponding enviromental conditions for test'*. Geneva, Switzerland: International Organization for Standardization (ISO).

ISO 14242 (2016) *'Implants for surgery - wear of total hip-joint prostheses - Part 2: Methods of measurement'*. Geneva, Switzerland: International Organization for Standardization (ISO).

ISO 14243 (2009) *'Implants for surgery - wear of total knee-joint prostheses - Part1: Loading and displacement parameters for wear-testing machines with load control and corresponding enviromental conditions for test'*. Geneva, Switzerland: International Organization for Standardization (ISO).

ISO 25178 (2012) *'Geometric product speficications (GPS) - Surface texture: Areal - Part 2: Terms, definitions and surface texture parameters'*. Geneva, Switzerland: International Organization for Standardization (ISO).

Jacquot, A., Sirveaux, F., Roche, O., Favard, L., Clavert, P. and Mole, D. (2015) 'Surgical management of the infected reversed shoulder arthroplasty: a French multicenter study of reoperation in 32 patients', *J Shoulder Elbow Surg*, *24*(11), pp. 1713-1722.

Jin, Z.M., Stone, M., Ingham, E. and Fisher, J. (2006) '(v) Biotribology', *Curr Orthop*, *20*(1), pp. 32-40.

Joyce, T.J., Grigg, H., Langton, D.J. and Nargol, A.V.F. (2011a) 'Quantification of self-polishing in vivo from explanted metal-on-metal total hip replacements', *Tribol Int*, *44*(5), pp. 513-516.

Joyce, T.J., Langton, D.J., Jameson, S.S. and Nargol, A.V.F. (2009) 'Tribological analysis of failed resurfacing hip prostheses and comparison with clinical data', *Proc Inst Mech Eng H*, *223*, pp. 317-323.

Joyce, T.J., Langton, D.J. and Nargol, A.V.F. (2011b) 'A study of the wear of explanted metal-on-metal resurfacing hip prostheses', *Tribol Int*, *44*(5), pp. 517-522.

Keurentjes, J.C., Kuipers, R.M., Wever, D.J. and Schreurs, B.W. (2008) 'High incidence of squeaking in THAs with alumina ceramic-on-ceramic bearings', *Clin Orthop Relat Res*, *466*(6), pp. 1438-1443.

Kiet, T.K., Feeley, B.T., Naimark, M., Gajiu, T., Hall, S.L., Chung, T.T. and Ma, C.B. (2015) 'Outcomes after shoulder replacement: Comparison between reverse and anatomic total shoulder arthroplasty', *J Shoulder Elbow Surg*, *24*(2), pp. 179-185.

Kinkel, S., Wollmerstedt, N., Kleinhans, J.A., Hendrich, C. and Heisel, C. (2009) 'Patient activity after total hip arthroplasty declines with advancing age', *Clin Orthop Relat Res*, *467*(8), pp. 2053-2058.

Kinnari, T.J., Esteban, J., Zamora, N., Fernandez, R., Lopez-Santos, C., Yubero, F., Mariscal, D., Puertolas, J.A. and Gomez-Barrena, E. (2010) 'Effect of surface roughness and sterilization on bacterial adherence to ultra-high molecular weight polyethylene', *Clin Microbiol Infect*, *16*(7), pp. 1036-1041.

Kitano, T., Ateshian, G.A., Mow, V.C., Kadoya, Y. and Yamano, Y. (2001) 'Constituents and pH changes in protein rich hyaluronan solution affect the biotribological properties of artificial articular joints', *J Biomech*, *34*(8), pp. 1031-1037.

Klemt, C., Prinold, J.A., Morgans, S., Smith, S.H.L., Nolte, D., Reilly, P. and Bull, A.M.J. (2018) 'Analysis of shoulder compressive and shear forces during functional activities of daily life', *Clin Biomech*, *54*, pp. 34-41.

Klimkiewicz, J.J., Iannotti, J.P., Rubash, H.E. and Shanbhag, A.S. (1998) 'Aseptic loosening of the humeral component in total shoulder arthroplasty', *J Shoulder Elbow Surg*, *7*(4), pp. 422-426.

Kluess, D., Mittelmeier., W. and Bader, R. (2014) 'Ceramics for Joint Replacement', in Revell, P. (ed.) *Joint Replacement Technology*. Woodhead Publishing, pp. 163-175.

Kohut, G., Dallmann, F. and Irlenbusch, U. (2012) 'Wear-induced loss of mass in reversed total shoulder arthroplasty with conventional and inverted bearing materials', *J Biomech*, *45*(3), pp. 469-473.

Konttinen, Y.T., Milosev, I., Trebse, R., Rantanen, P. and Linden, R. (2014) 'Metals for Joint Replacement', in Revell, P. (ed.) *Joint Replacement Technology*. Woodhead Publishing, pp. 115-162.

Kurdziel, M.D., Newton, M.D., Hartner, S., Baker, K.C. and Wiater, J.M. (2018) 'Quantitative evaluation of retrieved reverse total shoulder arthroplasty liner surface deviation and volumetric wear', *J Orthop Res*, *36*(7), pp. 2007-2014.

Kurtz, S.M. (2016) 'A Primer on UHMWPE', in Kurtz, S.M. (ed.) *UHMWPE Biomaterials Handbook*. William Andrew Publishing, pp. 1-6.

Kurtz, S.M., Gawel, H.A. and Patel, J.D. (2011) 'History and systematic review of wear and osteolysis outcomes for first-generation highly crosslinked polyethylene', *Clin Orthop Relat Res*, *469*(8), pp. 2262-277.

Labek, G., Thaler, M., Janda, W., Agreiter, M. and Stockl, B. (2011) 'Revision rates after total joint replacement: cumulative results from worldwide joint register datasets', *J Bone Joint Surg Br*, *93*(3), pp. 293-297.

Labriola, J.E., Lee, T.Q., Debski, R.E. and McMahon, P.J. (2005) 'Stability and instability of the glenohumeral joint: the role of shoulder muscles', *J Shoulder Elbow Surg*, *14*(1 Suppl S), pp. 32S-38S.

Lam, F., Bhatia, D.N., Mostofi, S.B., van Rooyen, K. and de Beer, J.F. (2007) 'Biomechanical considerations of the normal and rotator cuff deficient shoulders and the reverse shoulder prosthesis', *Current Orthopaedics*, *21*(1), pp. 40-46.

Lancaster, J.K. (1973) 'Dry bearings: A survey of materials and factors affecting their performance', *Tribology 6*(6), pp. 219-251.

Langohr, G.D., Athwal, G.S., Johnson, J.A. and Medley, J.B. (2016) 'Wear simulation strategies for reverse shoulder arthroplasty implants', *Proc Inst Mech Eng H*, *230*(5), pp. 458-469.

Langohr, G.D.G., Haverstock, J.P., Johnson, J.A. and Athwal, G.S. (2018) 'Comparing daily shoulder motion and frequency after anatomic and reverse shoulder arthroplasty', *J Shoulder Elbow Surg*, *27*(2), pp. 325-332.

Lee, R., Essner, A., Wang, A. and Jaffe, W.L. (2009) 'Scratch and wear performance of prosthetic femoral head components against crosslinked UHMWPE sockets', *Wear*, *267*(11), pp. 1915-1921.

Lerf, R., Reimelt, I., Dallmann, F. and Delfosse, D. (2016) 'Tribological behaviour of the reverse inverse shoulder prosthesis: shoulder simulator study with four different material pairings', *Orthopaedic Proceedings 98-B:SUPP_8*, pp. 150-150.

Lewicki, K.A., Bell, J.E. and Van Citters, D.W. (2017) 'Analysis of polyethylene wear of reverse shoulder components: A validated technique and initial clinical results', *J Orthop Res*, *35*(5), pp. 980-987.

Lewis, P.R. and McCutchen, C.W. (1959) 'Experimental evidence for weeping lubrication in mammalian joints', *Nature*, *184*, p. 1285.

Liao, Y.S., McKellop, H., Lu, Z., Campbell, P. and Benya, P. (2003) 'The effect of frictional heating and forced cooling on the serum lubricant and wear of UHMW polyethylene cups against cobalt-chromium and zirconia balls', *Biomaterials*, *24*(18), pp. 3047-3059.

Lugli, T. (1978) 'Artificial shoulder joint by Pean (1893): The facts of an exceptional intervention and the prosthetic method', *Clin Orthop Relat Res*, *133*(133), pp. 215-218.

Luo, Y., Yang, L. and Tian, M. (2013) 'Application of biomedical-grade titanium alloys in trabecular bone and artificial joints', in Davim, J.P. (ed.) *Biomaterials and Medical Tribology*. Woodhead Publishing, pp. 181-216.

Mabrey, J.D., Afsar-Keshmiri, A., Engh, G.A., Sychterz, C.J., Wirth, M.A., Rockwood, C.A. and Agrawal, C.M. (2002) 'Standardized analysis of UHMWPE wear particles from failed total joint arthroplasties', *J Biomed Mater Res*, *63*(5), pp. 475-483.

Mai, K.T., Verioti, C., D'Lima, D., Colwell, C.W.J. and Ezzet, K.A.J. (2010) 'Surface roughness of femoral head prostheses after dislocation', *Am J Orthop 39*(10), pp. 495-500.

Mall, N.A., Nunley, R.M., Zhu, J.J., Maloney, W.J., Barrack, R.L. and Clohisy, J.C. (2011) 'The incidence of acetabular osteolysis in young patients with conventional versus highly crosslinked polyethylene', *Clin Orthop Relat Res*, *469*(2), pp. 372-381.

Mani, G. (2016) 'Metallic Biomaterials: Cobalt-Chromium Alloys', in Murphy, W., Black, J. and Hastings, G. (eds.) *Handbook of Biomaterials Properties*. Springer-Verlag New York, pp. 159-166.

Marqual IT Solutions Pvt. Ltd (KBV Research) (2019) *'Global Shoulder Arthroplasty Market (2018-2024)'*. [Online]. Available at: www.researchandmarkets.com/reports/4752501/global-shoulder-arthroplasty-market-2018-2024.

Marshall, A., Ries, M.D., Paprosky, W. and Implant Wear Symposium Clinical Work, G. (2008) 'How prevalent are implant wear and osteolysis, and how has the scope of osteolysis changed since 2000?', *J Am Acad Orthop Surg*, *16 Suppl 1*, pp. S1-6.

Masjedi, M. and Johnson, G.R. (2010) 'Glenohumeral contact forces in reversed anatomy shoulder replacement', *J Biomech*, *43*(13), pp. 2493-2500.

Matsen, F.A., 3rd, Clinton, J., Lynch, J., Bertelsen, A. and Richardson, M.L. (2008) 'Glenoid component failure in total shoulder arthroplasty', *J Bone Joint Surg Am*, *90*(4), pp. 885-896.

Matsen, F.A. and Lippitt, S.B. (2003) *'Shoulder Surgery: Principles and Procedures'*. WB Saunders.

Matsuki, K., Matsuki, K.O., Yamaguchi, S., Ochiai, N., Sasho, T., Sugaya, H., Toyone, T., Wada, Y., Takahashi, K. and Banks, S.A. (2012) 'Dynamic in vivo glenohumeral kinematics during scapular plane abduction in healthy shoulders', *J Orthop Sports Phys Ther*, *42*(2), pp. 96-104.

Mattei, L., Di Puccio, F., Joyce, T.J. and Ciulli, E. (2016) 'Numerical and experimental investigations for the evaluation of the wear coefficient of reverse total shoulder prostheses', *J Mech Behav Biomed Mater*, *55*, pp. 53-66.

Matthews, C.E., Chen, K.Y., Freedson, P.S., Buchowski, M.S., Beech, B.M., Pate, R.R. and Troiano, R.P. (2008) 'Amount of time spent in sedentary behaviors in the United States, 2003-2004', *Am J Epidemiol*, *167*(7), pp. 875-881.

Mazzucco, D., McKinley, G., Scott, R.D. and Spector, M. (2002) 'Rheology of joint fluid in total knee arthroplasty patients', *J Orthop Res*, *20*(6), pp. 1157-1163.

McGeough, J. (2013a) 'Anatomy of Joints', in McGeough, J. (ed.) *The Engineering of Human Joint Replacements*. John Wiley & Sons, pp. 25-59.

McGeough, J. (2013b) 'Materials in Human Joint Replacement', in McGeough, J. (ed.) *The Engineering of Human Joint Replacements*. John Wiley & Sons, pp. 71-101.

Mendonca, G., Mendonca, D.B., Aragao, F.J. and Cooper, L.F. (2008) 'Advancing dental implant surface technology -from micron- to nanotopography', *Biomaterials*, *29*(28), pp. 3822-3835.

Merolla, G., Tartarone, A., Sperling, J.W., Paladini, P., Fabbri, E. and Porcellini, G. (2017) 'Early clinical and radiological outcomes of reverse shoulder arthroplasty with an eccentric all-polyethylene glenosphere to treat failed hemiarthroplasty and the sequelae of proximal humeral fractures', *Int Orthop*, *41*(1), pp. 141-148.

Middernacht, B., Van Tongel, A. and De Wilde, L. (2016) 'A critical review on prosthetic features available for reversed total shoulder arthroplasty', *Biomed Res Int*, *2016*, pp. 1-9.

Montoya, F., Magosch, P., Scheiderer, B., Lichtenberg, S., Melean, P. and Habermeyer, P. (2013) 'Midterm results of a total shoulder prosthesis fixed with a cementless glenoid component', *J Shoulder Elbow Surg*, *22*(5), pp. 628-635.

Moore, D.D., Moravek, J.E., Baker, E.A., Salisbury, M.R., Baker, K.C. and Wiater, J.M. (2017) 'Exploring failure of total shoulder arthroplasty systems through implant retrieval, radiographic, and clinical data analyses', *Journal of Shoulder and Elbow Arthroplasty*, *1*, pp. 1-10.

Moore, K.L., Dalley, A.F. and Agur, A.M. (2018) 'Upper Limb', in *Clinically Oriented Anatomy*. 8th edn. Wolters Kluwer, pp. 392-716.

Mueller, U., Braun, S., Schroeder, S., Schroeder, M., Sonntag, R., Jaeger, S. and Kretzer, J.P. (2017) 'Influence of humeral head material on wear performance in anatomic shoulder joint arthroplasty', *J Shoulder Elbow Surg*, *26*(10), pp. 1756-1764.

Nam, D., Kepler, C.K., Neviaser, A.S., Jones, K.J., Wright, T.M., Craig, E.V. and Warren, R.F. (2010a) 'Reverse total shoulder arthroplasty: current concepts, results, and component wear analysis', *J Bone Joint Surg Am*, *92 Suppl 2*, pp. 23-35.

Nam, D., Kepler, C.K., Nho, S.J., Craig, E.V., Warren, R.F. and Wright, T.M. (2010b) 'Observations on retrieved humeral polyethylene components from reverse total shoulder arthroplasty', *J Shoulder Elbow Surg*, *19*(7), pp. 1003-1012.

National Joint Registry (NJR) for England Wales Northern Ireland and the Isle of Man (2020) *'17th Annual Report'*. [Online]. Available at: www.njrreports.org.uk (Accessed: October 2020).

Naylor, A., Bone, M.C., Unsworth, A., Talwalkar, S.C., Trail, I.A. and Joyce, T.J. (2015) 'In vitro wear testing of the PyroCarbon proximal interphalangeal joint replacement: Five million cycles of flexion and extension', *Proc Inst Mech Eng H*, *229*(5), pp. 362-368.

Neer, C.S., 2nd (1955) 'Articular replacement for the humeral head', *J Bone Joint Surg Am*, *37-A*(2), pp. 215-228.

Neer, C.S., 2nd (1974) 'Replacement arthroplasty for glenohumeral osteoarthritis', *J Bone Joint Surg Am*, *56*(1), pp. 1-13.

Neer, C.S., 2nd (1990) *'Shoulder reconstruction'*. Philadelphia: WB Saunders.

Neu, C.P., Komvopoulos, K. and Reddi, A.H. (2008) 'The interface of functional biotribology and regenerative medicine in synovial joints', *Tissue Eng Part B Rev*, *14*(3), pp. 235-247.

New Zealand Orthopaedic Association (NZOA) (2019) *'The New Zealand Joint Registry'*. [Online]. Available at: https://nzoa.org.nz/nzoa-joint-registry (Accessed: October 2020).

Nho, S.J., Ala, O.L., Dodson, C.C., Figgie, M.P., Wright, T.M., Craig, E.V. and Warren, R.F. (2008) 'Comparison of conforming and nonconforming retrieved glenoid components', *J Shoulder Elbow Surg*, *17*(6), pp. 914-920.

Nho, S.J., Nam, D., Ala, O.L., Craig, E.V., Warren, R.F. and Wright, T.M. (2009) 'Observations on retrieved glenoid components from total shoulder arthroplasty', *J Shoulder Elbow Surg*, *18*(3), pp. 371-378.

Niinomi, M. (2007) 'Fatigue characteristics of metallic biomaterials', *International Journal of Fatigue*, *29*(6), pp. 992-1000.

Niinomi, M. (2008) 'Mechanical biocompatibilities of titanium alloys for biomedical applications', *J Mech Behav Biomed Mater*, *1*(1), pp. 30-42.

Oates, K.M.N., Krause, W.E. and Colby, R.H. (2002) 'Using rheology to probe the mechanism of joint lubrication: Polyelectrolyte/protein interactions in synovial fluid', *Mat Res Soc Syrnp Proc*, *711*, pp. 53-58.

OBrien, S.J., Allen, A.A. and Fealy, S. (1998) 'Developmental Anatomy of The Shoulder and Anatomy of The Glenohumeral Joint', in Rockwood, C.A. and Matsen, F.A. (eds.) *The Shoulder*. WB Saunders.

Peat, M. (1986) 'Functional anatomy of the shoulder complex', *Phys Ther*, *66*(12), pp. 1855-1865.

Pharmaceutical Management Agency (PHARMAC) for New Zealand (2017). New Zealand. [Online]. Available at: www.pharmac.govt.nz.

Piconi, C., De Santis, V. and Maccauro, G. (2017) 'Clinical outcomes of ceramicized ball heads in total hip replacement bearings: a literature review', *J Appl Biomater Funct Mater*, *15*(1), pp. e1-e9.

Pijl, A.J., Swieszkowski, W. and Bersee, H.E.N. (2004) 'Design of a wear simulator for in vitro shoulder prostheses testing', *Experimental Techniques*, *28*(5), pp. 45-48.

Pokorny, A. and Knahr, K. (2012) 'Fracture and Squeaking in Ceramic-on-Ceramic Bearings: Is It Really a Concern?', in Knahr, K. (ed.) *Total Hip Arthroplasty*. Springer-Verlag Berlin, pp. 127-144.

Ponce, B.A., Oladeji, L.O., Rogers, M.E. and Menendez, M.E. (2015) 'Comparative analysis of anatomic and reverse total shoulder arthroplasty: In-hospital outcomes and costs', *J Shoulder Elbow Surg*, *24*(3), pp. 460-467.

Poppen, N.K. and Walker, P.S. (1978) 'Forces at the glenohumeral joint in abduction', *Clin Orthop Relat Res*, *58*, pp. 165-170.

Purdue, P.E., Koulouvaris, P., Potter, H.G., Nestor, B.J. and Sculco, T.P. (2007) 'The cellular and molecular biology of periprosthetic osteolysis', *Clin Orthop Relat Res*, *454*, pp. 251-261.

Que, L., Topoleski, L.D. and Parks, N.L. (2000) 'Surface roughness of retrieved CoCrMo alloy femoral components from PCA artificial total knee joints', *J Biomed Mater Res*, *53*(11), pp. 111-118.

Quillen, D.M., Wuchner, M. and Hatch, R.L. (2004) 'Acute shoulder injuries', *Am Fam Physician*, *70*(10), pp. 1947-1954.

Ramirez-Martinez, I., Smith, S.L. and Joyce, T.J. (2019) 'The effect of combined loading cycles on the wear of reverse shoulder joint replacements', *J Mech Behav Biomed Mater*, *94*, pp. 201-206.

Ramirez-Martinez, I., Smith, S.L., Trail, I.A. and Joyce, T.J. (2020a) 'Wear behaviour of polyethylene glenoid inserts against PyroCarbon humeral heads in shoulder arthroplasties', *J Mech Behav Biomed Mater*, *103*, p. 103553.

Ramirez-Martinez, I., Stea, S. and Joyce, T.J. (2020b) 'Analysis of the surface topography of retrieved metal-on-polyethylene reverse shoulder prostheses', *Proc Inst Mech Eng H*, *234*(12), pp. 1353-1362.

Rittmeister, M. and Kerschbaumer, F. (2001) 'Grammont reverse total shoulder arthroplasty in patients with rheumatoid arthritis and nonreconstructible rotator cuff lesions', *J Shoulder Elbow Surg*, *10*(1), pp. 17-22.

Roche, C.P. and Crosby, L. (2006) 'Kinematics and Biomechanics of Reverse Total Shoulder Arthroplasty', in Nocholson, G.P. (ed.) *Orthopaedic Knowledge Update Shoulder and Elbow 4*. AAOS, pp. 45-54.

Ross, M., James, C., Couzens, G. and Klawitter, J. (2014) 'Pyrocarbon small joint arthroplasty of the extremities', in Revell, P.A. (ed.) *Joint Replacement Technology*. Woodhead Publishing, pp. 628-673.

Sabesan, V.J., Ackerman, J., Sharma, V., Baker, K.C., Kurdziel, M.D. and Wiater, J.M. (2015) 'Glenohumeral mismatch affects micromotion of cemented glenoid components in total shoulder arthroplasty', *J Shoulder Elbow Surg*, *24*(5), pp. 814-822.

Sahoo, P., Das, S.K. and Paulo Davim, J. (2019) 'Tribology of materials for biomedical applications', in Paulo Davim, J. (ed.) *Mechanical Behaviour of Biomaterials*. Woodhead Publishing, pp. 1-45.

Saikko, V. (1998) 'A multidirectional motion pin-on-disk wear test method for prosthetic joint materials', *J Biomed Mater Res*, *41*(1), pp. 58-64.

Saikko, V. (2005) 'A hip wear simulator with 100 test stations', *Proc Inst Mech Eng H*, *219*(5), pp. 309-318.

Saikko, V. (2006) 'Effect of contact pressure on wear and friction of ultra-high molecular weight polyethylene in multidirectional sliding', *Proc Inst Mech Eng H*, *220*(7), pp. 723-731.

Saikko, V. (2017) 'Effect of contact area on the wear of ultrahigh molecular weigh tpolyethylene in noncyclic pin-on-disk tests', *Tribol Int*, *114*, pp. 84-87.

Saikko, V. and Ahlroos, T. (1999) 'Type of motion and lubricant in wear simulation of polyethylene acetabular cup', *Proc Inst Mech Eng H*, *213*(4), pp. 301-310.

Saikko, V., Calonius, O. and Keranen, J. (2001) 'Effect of counterface roughness on the wear of conventional and crosslinked ultrahigh molecular weight polyethylene studied with a multi-directional motion pin-on-disk device', *J Biomed Mater Res*, *57*(4), pp. 506-512.

Saikko, V. and Kostamo, J. (2011) 'RandomPOD--a new method and device for advanced wear simulation of orthopaedic biomaterials', *J Biomech*, *44*(5), pp. 810-814.

Scarlat, M.M. and Matsen, F.A., 3rd (2001) 'Observations on retrieved polyethylene glenoid components', *J Arthroplasty*, *16*(6), pp. 795-801.

Scheuerman, T.R., Camper, A.K. and Hamilton, M.A. (1998) 'Effects of substratum topography on bacterial adhesion', *J Colloid Interface Sci*, *208*(1), pp. 23-33.

Schoch, B., Abboud, J., Namdari, S. and Lazarus, M. (2017) 'Glenohumeral mismatch in anatomic total shoulder arthroplasty', *JBJS Rev*, *5*(9), pp. 1-8.

Schoch, B.S., Wright, T.W., Zuckerman, J.D., Flurin, P.H., Bolch, C., Roche, C.P. and King, J.J. (2019) 'The effect of radial mismatch on radiographic glenoid loosening', *JSES Open Access*, *3*(4), pp. 287-291.

Scholes, S.C. and Joyce, T.J. (2013) 'In vitro tests of substitute lubricants for wear testing orthopaedic biomaterials', *Proc Inst Mech Eng H*, *227*(6), pp. 693-703.

Scholes, S.C., Kennard, E., Gangadharan, R., Weir, D., Holland, J., Deehan, D. and Joyce, T.J. (2013) 'Topographical analysis of the femoral components of ex vivo total knee replacements', *J Mater Sci Mater Med*, *24*(2), pp. 547-554.

Schwarz, I.M. and Hills, B.A. (1998) 'Surface-active phospholipid as the lubricating component of lubricin', *Br J Rheumatol*, *37*(1), pp. 21-26.

Simovitch, R.W., Friedman, R.J., Cheung, E.V., Flurin, P.H., Wright, T., Zuckerman, J.D. and Roche, C. (2017) 'Rate of improvement in clinical outcomes with anatomic and reverse total shoulder arthroplasty', *J Bone Joint Surg Am*, *99*(21), pp. 1801-1811.

Sirveaux, F., Favard, L., Oudet, D., Huquet, D., Walch, G. and Mole, D. (2004) 'Grammont inverted total shoulder arthroplasty in the treatment of glenohumeral osteoarthritis with massive rupture of the cuff. Results of a multicentre study of 80 shoulders', *J Bone Joint Surg Br*, *86*(3), pp. 388-395.

Sivasundaram, L., Heckmann, N., Pannell, W.C., Alluri, R.K., Omid, R. and Hatch, G.F., 3rd (2016) 'Preoperative risk factors for discharge to a postacute care facility after shoulder arthroplasty', *J Shoulder Elbow Surg*, *25*(2), pp. 201-206.

Smith, S.L., Burgess, I.C. and Unsworth, A. (1999) 'Evaluation of a hip joint simulator', *Proc Inst Mech Eng H*, *213*(6), pp. 469-473.

Smith, S.L., Kennard, E. and Joyce, T.J. (2018) 'Shoulder simulator wear test of five contemporary total shoulder prostheses with three axes of rotation and sliding motion', *Biotribology*, *13*, pp. 36-41.

Smith, S.L., Li, B.L., Buniya, A., Lin, S.H., Scholes, S.C., Johnson, G. and Joyce, T.J. (2015) 'In vitro wear testing of a contemporary design of reverse shoulder prosthesis', *J Biomech*, *48*(12), pp. 3072-3079.

Smith, S.L., Li, L. and Joyce, T.J. (2016) 'Engineering of a multi-station shoulder simulator', *Proc Inst Mech Eng H*, *230*(5), pp. 470-480.

Smith, S.L. and Unsworth, A. (2001) 'A five-station hip joint simulator', *Proc Inst Mech Eng H*, *215*(1), pp. 61-64.

Stauffer, R.N. (1982) 'Ten-year follow-up study of total hip replacement', *The Journal of Bone & Joint Surgery*, *64*(7), pp. 983-990.

Strauss, E.J., Roche, C., Flurin, P.H., Wright, T. and Zuckerman, J.D. (2009) 'The glenoid in shoulder arthroplasty', *J Shoulder Elbow Surg*, *18*(5), pp. 819-833.

Subrata, P. (2014) 'The Shoulder Joint and its Artificial Replacement', in Subrata, P. (ed.) *Design of Artificial Human Joints & Organs*. Springer US, pp. 123-148.

Sun, D., Wharton, J.A. and Wood, R.J.K. (2011) 'Micro- and Nano-scale Tribo-Corrosion of Cast CoCrMo', *Tribology Letters*, *41*(3), pp. 525-533.

Sweets, T.M. and Stern, P.J. (2011) 'Pyrolytic carbon resurfacing arthroplasty for osteoarthritis of the proximal interphalangeal joint of the finger', *J Bone Joint Surg Am*, *93*(15), pp. 1417-1425.

Tamer, T.M. (2013) 'Hyaluronan and synovial joint: function, distribution and healing', *Interdiscip Toxicol*, *6*(3), pp. 111-125.

Teoh, S.H., Tang, Z.G. and Hastings, G. (2016) 'Thermoplastic Polymers In Biomedical Applications: Structures, Properties and Processing', in Murphy, W., Black, J. and Hastings, G. (eds.) *Handbook of Biomaterials Properties*. Springer-Verlag New York, pp. 261-291.

Terrier, A., Merlini, F., Pioletti, D.P. and Farron, A. (2009) 'Comparison of polyethylene wear in anatomical and reversed shoulder prostheses', *J Bone Joint Surg Br*, *91*(7), pp. 977-982.

Terrier, A., Reist, A., Merlini, F. and Farron, A. (2008) 'Simulated joint and muscle forces in reversed and anatomic shoulder prostheses', *J Bone Joint Surg Br*, *90*(6), pp. 751-756.

The Norwegian Arthroplasty Register (NAR) (2020) *'Norwegian National Advisory Unit on Arthroplasty and Hip Fractures'*. [Online]. Available at: http://nrlweb.ihelse.net/ (Accessed: October 2020).

The Swedish Shoulder Arthroplasty Registry (SSAR) (2020). [Online]. Available at: www.ssar-rapport.se/SAAR_web/publicReport.html?category=skulder (Accessed: October 2020).

Torborg, L. (2014) *Tuesday Q and A: Reverse shoulder arthroplasty may be best option for patient with torn rotator cuff and arthritis*. Mayo Clinic. [Online]. Available at: www.mayoclinic.org.

Traina, F., De Fine, M., Di Martino, A. and Faldini, C. (2013) 'Fracture of ceramic bearing surfaces following total hip replacement: a systematic review', *Biomed Res Int*, *2013*, p. 157247.

Triplet, J.J., Everding, N.G., Levy, J.C., Formaini, N.T., O'Donnell, K.P., Moor, M.A. and Virraroel, L.D. (2015) 'Anatomic and Reverse Total Shoulder Arthroplasty in Patients Older Than 80 Years', *Orthopedics*, *38*(10), pp. e904-10.

United Nations (2019a) *'Department of Economic and Social Affairs, Population Division. World Population Ageing: Highlights'*. [Online]. Available at: https://population.un.org/wpp/.

United Nations (2019b) *'Department of Economic and Social Affairs, Population Division. World Population Prospects: Highlights'*. [Online]. Available at: https://population.un.org/wpp/.

Urban, J.A., Garvin, K.L., Boese, C.K., Bryson, L., Pedersen, D.R., Callaghan, J.J. and Miller, R.K. (2001) 'Ceramic-on-polyethylene bearing surfaces in total hip arthroplasty. Seventeen to twenty-one-year results', *J Bone Joint Surg Am*, *83*(11), pp. 1688-1694.

van der Helm, F.C. (1994) 'Analysis of the kinematic and dynamic behavior of the shoulder mechanism', *J Biomech*, *27*(5), pp. 527-550.

Vaupel, Z.M., Baker, K.C., Kurdziel, M.D. and Wiater, J.M. (2012) 'Wear simulation of reverse total shoulder arthroplasty systems: Effect of glenosphere design', *J Shoulder Elbow Surg*, *21*(10), pp. 1422-1429.

Versus Arthritis (2018) *'Osteoarthritis arthritis'*. [Online]. Available at: www.versusarthritis.org/.

Walch, G., Bacle, G., Ladermann, A., Nove-Josserand, L. and Smithers, C.J. (2012) 'Do the indications, results, and complications of reverse shoulder arthroplasty change with surgeon's experience?', *J Shoulder Elbow Surg*, *21*(11), pp. 1470-1477.

Walch, G., Edwards, T.B., Boulahia, A., Boileau, P., Mole, D. and Adeleine, P. (2002) 'The influence of glenohumeral prosthetic mismatch on glenoid radiolucent lines: results of a multicenter study', *J Bone Joint Surg Am*, *84*(12), pp. 2186-2191.

Wall, B., Nove-Josserand, L., O'Connor, D.P., Edwards, T.B. and Walch, G. (2007) 'Reverse total shoulder arthroplasty: A review of results according to etiology', *J Bone Joint Surg Am*, *89*(7), pp. 1476-1485.

Wang, A., Essner, A. and Schmidig, G. (2004) 'The effects of lubricant composition on in vitro wear testing of polymeric acetabular components', *J Biomed Mater Res B Appl Biomater*, *68*(1), pp. 45-52.

Wang, S.B. and Ge, S.R. (2007) 'The mechanical property and tribological behavior of UHMWPE: Effect of molding pressure', *Wear*, *263*, pp. 949-956.

Wange, M., Rao, R.D., Yogonandan, N. and Pintar, F.A. (2015) 'Upper Extremity Injury Biomechanics', in Yoganandan, N., Nahum, A.M. and Melvin, J.W. (eds.) *Accidental Injury*. Springer-Verlag New York, pp. 309-329.

Warner, J.J., Deng, X.H., Warren, R.F. and Torzilli, P.A. (1992) 'Static capsuloligamentous restraints to superior-inferior translation of the glenohumeral joint', *Am J Sports Med*, *20*(6), pp. 675-685.

Westerhoff, P., Graichen, F., Bender, A., Halder, A., Beier, A., Rohlmann, A. and Bergmann, G. (2009) 'In vivo measurement of shoulder joint loads during activities of daily living', *J Biomech*, *42*(12), pp. 1840-1849.

Wiater, B.P., Baker, E.A., Salisbury, M.R., Koueiter, D.M., Baker, K.C., Nolan, B.M. and Wiater, J.M. (2015) 'Elucidating trends in revision reverse total shoulder arthroplasty procedures: a retrieval study evaluating clinical, radiographic, and functional outcomes data', *J Shoulder Elbow Surg*, *24*(12), pp. 1915-1925.

Williams, G.R. and Abboud, J.A. (2005) 'Total shoulder arthroplasty: Glenoid component design', *J Shoulder Elbow Surg*, *14*(1), pp. 122s-128s.

Williams, S., Schepers, A., Isaac, G., Hardaker, C., Ingham, E., van der Jagt, D., Breckon, A. and Fisher, J. (2007) 'The 2007 Otto Aufranc Award. Ceramic-on-metal hip arthroplasties: a comparative in vitro and in vivo study', *Clin Orthop Relat Res*, *465*, pp. 23-32.

Wimmer, M.A. and Laurent, M.P. (2012) 'Simulation of Physiological Conditions: An Overview', in Wang, Q.J. and Chung, Y. (eds.) *Encyclopedia of Tribology*. Springer, pp. 3099-3104.

Wirth, M.A., Agrawal, C.M., Mabrey, J.D., Dean, D.D., Blanchard, C.R., Miller, M.A. and Rockwood, C.A., Jr. (1999) 'Isolation and characterization of polyethylene wear debris associated with osteolysis following total shoulder arthroplasty', *J Bone Joint Surg Am*, *81*(1), pp. 29-37.

Wirth, M.A., Klotz, C., Deffenbaugh, D.L., McNulty, D., Richards, L. and Tipper, J.L. (2009) 'Cross-linked glenoid prosthesis: A wear comparison to conventional glenoid prosthesis with wear particulate analysis', *J Shoulder Elbow Surg*, *18*(1), pp. 130-137.

Wright, V. and Dowson, D. (1976) 'Lubrication and cartilage', *J Anat*, *121*(Pt 1), pp. 107-118.

Zhang, L.C. and Chen, L.Y. (2019) 'A Review on Biomedical Titanium Alloys: Recent Progress and Prospect', *Adv Eng Mater*, *21*(4), p. 1801215.

Zumstein, V., Kraljevic, M., Hoechel, S., Conzen, A., Nowakowski, A.M. and Muller-Gerbl, M. (2014) 'The glenohumeral joint - a mismatching system? A morphological analysis of the cartilaginous and osseous curvature of the humeral head and the glenoid cavity', *J Orthop Surg Res*, *9*(34), pp. 1-6.

APPENDIX A. PUBLICATIONS AND PRESENTATIONS

JOURNAL PUBLICATIONS

- **Ramírez-Martínez, I.**, Stea, S. and Joyce, T.J. (July 2020) 'Analysis of the surface topography of retrieved metal–on–polyethylene reverse shoulder prostheses', *Proceedings of the Institution of Mechanical Engineers, Part H: Journal of Engineering in Medicine*, 24(12), pp. 1353–1362
- **Ramírez-Martínez, I.**, Smith, S.L., Ian, A.T. and Joyce, T.J. (March 2020) 'Wear behaviour of polyethylene glenoid inserts against PyroCarbon humeral heads in shoulder arthroplasties', *Journal of the Mechanical Behaviour of Biomedical Materials,* 103, p. 103553.
- **Ramírez-Martínez, I.**, Smith, S.L. and Joyce, T.J. (June 2019) 'The effect of combined loading cycles on the wear of reverse shoulder joint replacements', *Journal of the Mechanical Behaviour of Biomedical Materials*, 94, pp. 201–206.

ABSTRACT PUBLICATIONS

- **Ramírez-Martínez, I.**, Smith, S.L., Ian, A.T. and Joyce, T.J. (2020) 'Tribological performance of PyroCarbon component against polyethylene counterpart in anatomic total shoulder arthroplasty', *Journal of Bone and Joint Surgery. Orthopaedic Proceedings*, 102–B: Supp_2, pp.77–77.
- **Ramírez-Martínez, I.**, Smith, S.L. and Joyce, T.J. (2019) 'First in vitro motion–load–motion wear test of reverse shoulder arthroplasties', *Journal of Bone and Joint Surgery. Orthopaedic Proceedings*,101–B: Supp_5, pp.15–15.

AWARDS

- Young Investigator. *International Society for Technology in Arthroplasty (ISTA)*, October 2019 | $ 500 USD
- Travel Fund. *Peter Jost Foundation*, June 2018 and 2019 | £1,500 GBP
- Best Poster. *4th Annual London Shoulder Meeting*, May 2018 | £300 GBP
- Best Oral. *Postgraduate Research (PGR) Conference*, March 2017 | £50 GBP

CONFERENCE PROCEEDINGS

- 'Could PyroCarbon serve as an alternative bearing surface in anatomic total shoulder replacement?' **Ramírez-Martínez, I.**, Smith, S.L., Trail, I. A. and Joyce, T.J., *British Elbow & Shoulder Society (BESS)*, Virtual Conference, 14th October 2020.
- 'Tribological performance of PyroCarbon component against polyethylene counterpart in anatomic total shoulder arthroplasty' **Ramírez-Martínez, I.**, Smith, S.L., Trail, I. A. and Joyce, T.J., *International Society for Technology in Arthroplasty (ISTA) 32nd Annual Congress*, Hilton, Toronto, Canada, 2nd – 5th October 2019.
- 'Tribological wear behaviour of polyethylene humeral inserts against PyroCarbon glenospheres in reverse shoulder arthroplasties' **Ramírez-Martínez, I.**, Smith, S.L., Trail, I. A. and Joyce, T.J., *5th Annual London Shoulder Meeting*, Orthopaedic Research UK, Bush House, London, England, 17th May 2019.
- 'First *in vitro* motion–load–motion wear test of reverse shoulder arthroplasties' **Ramírez-Martínez, I.**, Smith, S.L. and Joyce, T.J., *International Society for Technology in Arthroplasty (ISTA) 31st Annual Congress*, Queen Elizabeth II Conference Centre, London, England, 10th – 13th October 2018.
- 'First motion–load–motion wear test of reverse shoulder replacements' **Ramírez-Martínez, I.**, Smith, S.L. and Joyce, T.J., *4th Annual London Shoulder Meeting*, Orthopaedic Research UK, UCL Institute of Child Health, London, England, 18th May 2018.
- '*In vitro* wear testing of shoulder prostheses' **Ramírez-Martínez, I.**, Smith, S.L. and Joyce, T.J., *Postgraduate Research (PGR) Conference*, Newcastle University, Newcastle upon Tyne, England, 29th and 30th March 2017.

BESS Excellence through knowledge

ISTA

orthopaedic research UK

ABOUT THE AUTHOR

Mr. Israel Ramírez Martínez was born on the 1st of June 1990 in Colima, México, as a firstborn of two children. Soon after his birth, the family moved to Monterrey, Nuevo León - México where he has raised and completed his basic education.

In San Nicolas de los Garza, Nuevo León - México, he studied Mechatronics Engineering from 2008 until 2014 at the "Universidad Autónoma de Nuevo León" from which he earned his Bachelor's degree in Engineering. During this time, he started working as a Research and development engineer with Dr. Arturo Juárez Hernández and Dr. Marco A. L. Hernández Rodríguez at the "Centro de Investigación y Desarrollo Tecnológico". This time and experience work with Biomaterials, Biomechanics and Medical Technologies, encouraged him to pursue a higher degree. In 2016 he obtained his Master's degree in Materials Science and Engineering at "Universidad Autónoma de Nuevo León".

His interest in the tribology of total joint replacements was triggered by the enthusiasm of Prof. Tom J. Joyce, under whose supervision this Ph.D. thesis commenced in late 2016. For this practical term, he moved to Newcastle upon Tyne, United Kingdom, and work in the *"Tribological evaluation of total shoulder arthroplasty implants: Advanced in vitro wear testing and Retrieval analysis*" within the Bioengineering Group of the School of Engineering at Newcastle University.

His research work on total shoulder replacements was successfully finished in September 2020 under the supervision of Prof. Tom J. Joyce and Dr. Simon L. Smith, and with the economic support of The National Council of Science and Technology (CONACYT) of México and The Institute of Innovation and Technology Transfer (I2T2) of Nuevo León in Monterrey, México.

Tribological evaluation of total shoulder arthroplasty implants.